SYNTHETICALLY TARGETING COMPOSTABILITY AS THE END-OF-LIFE FATE FOR POLYMERIC MATERIALS

by

ETHAN JACOB STINCHCOMB

(Under the Direction of Jason Locklin)

ABSTRACT

The end-of-life fate for plastic waste has become a major social, economic, and environmental problem that requires widespread changes to fix. One avenue for addressing the increase in plastic waste is to produce materials that are compostable, and therefore biodegrade at the end of their useful life. One hurdle to synthetically producing novel compostable materials is the difficulty in measuring compostability throughout the new product pipeline. To address this issue, a high-throughput enzymatic degradation assay was developed as a guiding tool for the synthesis of industrially compostable polyurethanes. The assay was applied to the screening of aliphatic polyesters as the highly degradable prepolymer for the produced polyester polyurethanes. The inclusion of three biobased crosslinkers and the impact of isocyanate indexing was probed and tracked using the enzymatic degradation assay. The pathway to compostability was confirmed using respirometry analysis on a set of prepared polyurethanes. Targeting compostability as the final disposal mechanism through the synthesis of novel materials is challenging when balancing the material property demands with biodegradation needs. Furthermore, the need for a home compostable food contact safe pressure sensitive adhesive was addressed through the synthesis of a branched polymeric material from potentially biobased monomers. Pressure sensitive adhesives are viscoelastic materials that require tight control of adhesive and cohesive properties through synthesis and formulation. The pressure

sensitive adhesive has been produced and characterized in the laboratory setting, shown proof of concept in a pilot scale reactor, coated onto films using an industrial hot melt coating line, and converted into labels.

INDEX WORDS: Biodegradable polymers, polymer chemistry, green chemistry, polyesters, polyurethane, polymer synthesis, polymer characterization

SYNTHETICALLY TARGETING COMPOSTABILITY AS THE END-OF-LIFE FATE FOR POLYMERIC MATERIALS

by

ETHAN JACOB STINCHCOMB

B.S., Mercer University. 2014

M.S., Georgia State University, 2018

A Dissertation Submitted to the Graduate Faculty of The University of Georgia in Partial Fulfillment of the Requirements for the Degree

DOCTOR OF PHILOSOPHY

ATHENS, GEORGIA

2023

SYNTHETICALLY TARGETING COMPOSTABILITY AS THE END-OF-LIFE FATE FOR POLYMERIC MATERIALS

by

ETHAN JACOB STINCHCOMB

Major Professor:	Jason Locklin
Committee:	Branson Ritchie
	Tina Salguero

Electronic Version Approved:

Ron Walcott
Vice Provost for Graduate Education and Dean of the Graduate School
The University of Georgia
August 2023

DEDICATION

This dissertation is dedicated to my son, Theodore Walker Stinchcomb.

ACKNOWLEDGEMENTS

I want to thank my family for their continual love and support in all of my pursuits. To my amazing wife Kathryn for putting up with my continual late nights and early mornings, for supporting me in my time of need, and for always being my best friend. To my parents for instilling a strong drive to be successful and a work ethic that far exceeds my capabilities. And to my brother for being one of my greatest supporters.

I would like to acknowledge my advisor, Jason Locklin, for his guidance and continual support. Thank you for giving me nearly free reign to conduct the research that I found most enjoyable and for giving me the opportunity to grow as a researcher. To my doctoral committee Branson Ritchie and Tina Salguero, thank you for your advice and guidance.

To my lab mates I want to give you all a special thank you for making this journey more enjoyable.

TABLE OF CONTENTS

Page

LIST OF TABLES

Page

LIST OF FIGURES

Page

LIST OF SCHEMES

Page

LIST OF EQUATIONS

Page

CHAPTER 1

INTRODUCTION AND LITERATURE REVIEW

Plastic Production and End of Life Destinations

Global plastic production has steadily grown over the last 50 years, reaching 370 metric tons produced in 2019.[1-5] The high level of plastic production is due to its vast area of applications, its light-weight, high-strength characteristics, and its low cost to produce. The vast majority of plastic products are nondegradable and produced from nonrenewable feedstocks.[6-14] With this increase in production, a heightened focus has been placed on the end of-life destination for these plastics (Figure 1.1). Estimates show only 12% of manufactured plastic packaging being recyclable with the majority being captured in inert landfills (40%) or leaked into the natural environment (32%).[6, 11-13, 15]

Recycling has long been regarded as a beneficial end-of-life destination for plastic waste generated, but recycling rates have remained low, especially in the United States where only 7% of recyclable materials are recycled.[16-22] Unfortunately, in most cases recycling only delays the final disposal of these persisting products rather than avoiding landfilling. Therefore, the impact of recycling on the continual production and disposal of plastic products is only possible if the new material produced from recycled post-consumer waste displaces newly manufactured plastic products from virgin feedstocks. Furthermore, determining the reduction of plastic produced from the substitution to secondary recycling stream materials has been difficult to quantify. Plastic recycling collected is also not a singular waste stream and contains a multitude of plastic types,

which can become intertwined during recycling, significantly impacting the material properties of the recycled secondary materials. Additionally, most plastic waste is not a monomaterial, and instead contains additives, colorants, and plasticizers, which cause issues during reprocessing. Recycling can be successfully applied to certain waste streams and certain materials but is not a catch all solution for all plastic waste.

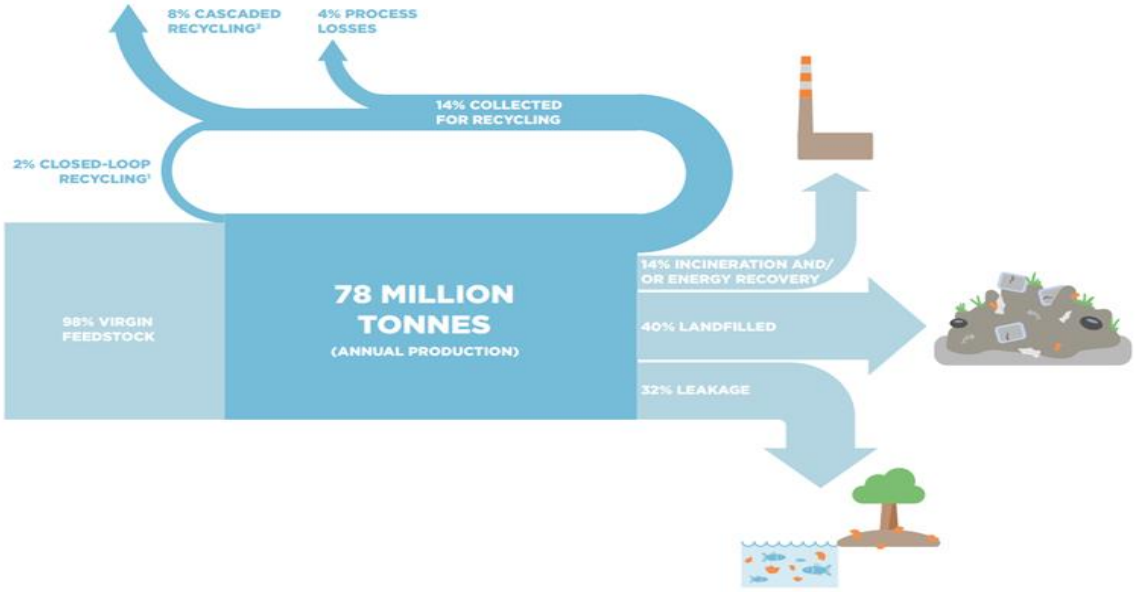

Figure 1.1 End-of-life fate for nonfibrous post-consumer waste broken down by waste stream. Reprinted with permission from Ellen MacArthur Foundation.[23] Copyright 2016 Ellen MacArthur Foundation.

The incineration of plastic waste has risen in prominence in certain countries, particularly in the European Union. Incineration is the burning of waste to generate heat allowing for the production of energy, this is considered a waste to energy process. Incineration of plastic waste has found appeal because the main waste plastics polyethylene (43.3 – 47.7 MJ/kg), polypropylene (42.6 – 46.5 MJ/kg) and polystyrene (41.6 – 43.7 MJ/kg) possess similar calorific values as conventional fuels, such as

gasoline (46 MJ/kg) and petroleum (42.3 MJ/kg) allowing them to produce similar energy.[24, 25] Additionally, the main incineration products are carbon dioxide and water, similar to conventional fuels. As with all energy production facilities, the environmental and health impacts depend heavily on the design and operation of the facility, as well as the emission control technology applied. From a sociopolitical viewpoint, incinerators have been under heavy scrutiny, as they have been predominately placed near lower income housing and developments raising concerns. The continued investment in incineration technology can also be seen as a stopgap solution for meaningful change of plastic production and waste practices. The locations where incineration is used most heavily also have the lowest recycling rates, with studies showing that recyclable materials are being diverted to incineration plants to meet capacity needs. Incineration allows for the reduction of landfilling of plastic waste, especially those items that could not go through a recycling process, but it comes at a cost.

The final destination for most post-consumer waste is through the capture and containment within an inert landfill.[26-29] This destination, while not ideal, allows for the management of waste that would otherwise leach into the natural environment and wreak havoc on plants, animals and the overall ecosystem. While landfill is the final destination of most plastic waste, these materials are still under constant stress within this environment. They can be degraded through physical, chemical, and biological processes which produce leachate and gas. Typical municipal waste solid waste landfills follow a five-stage waste treatment schedule to safely maintain the waste. For plastics this includes the initial aerobic degradation of the landfilled plastics which then transitions to anerobic conditions as it is fully encapsulated in tertiary materials. Under these anerobic

conditions the degradation products include the formation of acids from the hydrolysis of the polymeric material and methane gas from organic solid waste. Once the final maturation and stabilization of the landfill pile is completed these materials continue to break down into microplastics and nanoparticles. This occurs as a result of a combination of conditions including the reduced pH (4.5-9), the heightened temperature (60 – 90°C) physical stress, compaction, and limited microbial activity. It is important that these materials be encapsulated in a managed landfill to minimize their impact on the natural environment.

The worst end-of-life fate for any plastic material would be loss or disposal into marine or terrestrial biomes. Plastic waste that does enter the natural environments comes from a multitude of sources including application of films in agriculture, natural disasters, loss of fishing gear, and debris from product waste, such as tire degradation and textile fiber wear. Initially, the concern for maintaining plastic waste in landfills was spurred by the impact that litter and plastic waste has on the aesthetic of the natural environment. This has, however, been overtaken by the plethora of studies showing the negative impact of large plastic on marine and terrestrial environments.[26, 30-34] The collection of materials that are discarded into the natural environment is difficult. These plastic waste products do undergo significant degradation into the natural environment due to photodegradation, hydrolysis, and physical damage. The degradation products can include micro and nanoplastics which will continue to persist. Microplastics and their impact on the environment, agricultural products, and human health have been a growing area of concern in polymer research.

To address the issue of ever increasing plastic production, the types of plastic that are being produced, the rate of production, and the application for these materials must be understood in order to find solutions.[6, 26-29, 31, 32, 35-37] The majority of nonfibrous plastics produced each year are polyolefins, which contain only a carbon-carbon backbone.[7, 8] This molecular architecture provides strong resistance to degradation leading to materials that will persist for decades. Polyolefins account for 50% of all produce plastic each year including polypropylene (19.7%), low-density polyethylene (17.4%), and high-density polyethylene (12.9%). Including these three polyolefins, there are only seven types of plastics that account for 92% of all plastic ever produced. This includes polyvinyl chloride (9.6%), polyethylene terephthalate (8.4%), polyurethanes (7.8%), and polystyrene (6.1%). Understanding the types of plastics that are being produced is important, so that new waste streams can be produced for the most produced plastics.

Another facet of plastic production is the feed stocks that are being used to make these materials.[38-42] Predominately, these materials are produced from petroleum sources, owing to the availability and low source cost for the monomers. Fossil fuels are a finite resource on this planet, and alternative sources for plastic starting materials must be found. One avenue to divert from the usage of petroleum feedstocks is to use biobased monomers that can be derived from natural products to produce new biobased materials. Additionally, finding biobased sourcing for these monomers can improve the environmental impact that these plastic materials have over their entire life cycle.[8, 10, 43] The term “biobased” for a polymer signifies the constituent carbon within its makeup is entirely from biological sources and has no impact or indication for it being biodegradable. When considering biobased sourcing for monomers, it is important to not

compete with feed stocks, but instead to use waste products. Several commodity plastics can currently be produced using biobased monomers including biopolyethylene and biopolypropylene.[6, 8] Biopolyethylene is produced from bioethanol which can be dehydrated to produce ethylene. The biobased feed stocks for this product include sugar cane, sugar beet and wheat grain. Biopolypropylene is being pushed forward as a financially viable alternative to petroleum-based materials and is produced using bioethanol from the fermentation of soybeans. Biobased monomer sourcing can improve the environmental impact of these plastics, but it does not improve the end-of-life fate for the produced material.

Plastics are applied in a variety of sectors with the top three accounting for 70% of all plastics produced each year; this includes packaging (40.5%), construction (20.4%), and automotive (8.8%). Packaging consists of a massive number of different products including coated paperboard, plastic bags, and plastic clamshells as examples. Polyethylene, polypropylene, and polyethylene terephthalate are the plastics predominately used in packaging applications which coincides the top used plastics.[6, 8, 44] In the European Union, 67 million tons of packaging waste is produced annually, about one-third of all solid waste produced. The environmental impact of applying plastic to packaging of certain goods, even with the consideration of its disposal streams has been shown to be positive. The barrier properties, light weight nature, and cost efficiency of plastics make their application in packaging materials readily apparent. Unfortunately, this has also led to the application of these persistent materials into single-use plastics packaging. Single use plastics are a major source of plastic waste that should be addressed.

The useful lifespan of these plastic products is important to understand when determining the types of plastic, as well as the sectors, that are producing waste at the fastest rate (Figure 1.2).[1, 6, 45] For packaging applications, the mean lifespan of use for a plastic package is less than one year. This timescale is in stark contrast to construction plastic which has a mean lifespan of 35 years. Comparing these plastic lifespans and production data shows that the amount of plastic waste produced for packaging applications was much higher than for construction applications. In 2015, 54% of plastic waste was due to packaging applications, while only 42% of plastic produced was in plastics that are used in packaging applications. Only 5% of plastic waste produced was from construction applications, while over 10% of the plastic produced was applied in the construction sector. Therefore, to make the largest impact on the plastic waste issue, packaging applications should be targeted for alternative waste streams and alternative primary plastic materials.

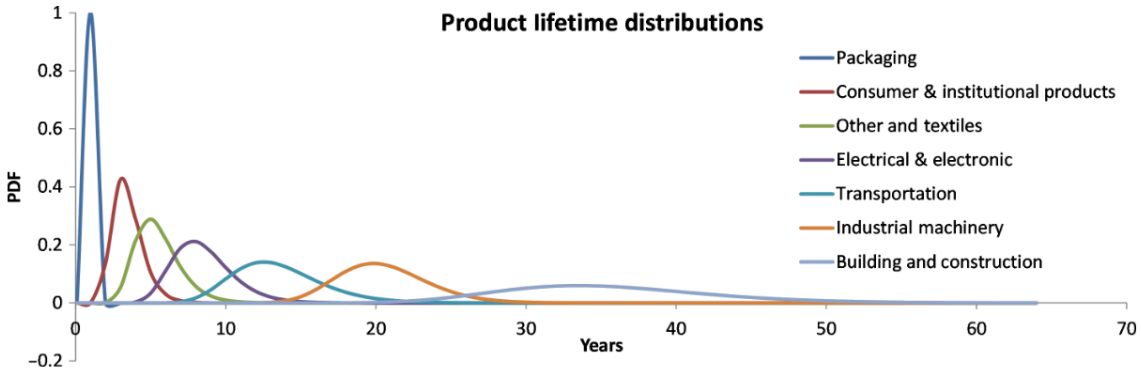

Figure 1.2 Product lifetime distributions for plastics determined from the production of the product to the time of disposal separated by application sector. Reprinted with permission from Science Advances.[1] Copyright 2017.

Biodegradable Plastics

One alternative route for plastic waste is to produce biodegradable commodity plastics that can supplant the current persisting products.[7-9] Biodegradable polymers are materials that are capable of undergoing mineralization into carbon dioxide, water, methane, biomass, or inorganics through the action of microorganisms. This mineralization must be measurable through standardized testing over a specified time period accurately reflecting the disposal conditions for the materials. Subsets of biodegradable are compostable, soil degradable, and marine degradable.[24, 46-48] Compostable can be divided into two categories – industrially compostable and home compostable. Industrially composting conditions include a higher temperature, more diverse microbiome, and a professionally maintained environment. Home compostable has a lower composting temperature of 22 – 25°C and a less diverse microbiome, which is highly varied based on location, maintenance, and environment. Soil and marine degradable focuses on the mineralization in the natural environment. When considering biodegradable products, it is important to understand the conditions in which the plastic will degrade.

Composting as an end-of-life fate for certain plastics, especially those used in packaging applications, is seen as highly advantageous. Being a compostable plastic can be broadly defined by the ASTM standard D6400, where the material must undergo degradation by a biological process under composting conditions to yield water, inorganic compounds, CO_2, and biomass. This degradation must occur at a rate that is consistent with known compostable materials and must leave no visible trace after degradation or toxic residue. If the entire composite material is compostable, then the

issues of a mixed-waste-stream, which plagues the recycling infrastructure, do not exist. Additionally, external contaminates, such as food waste, oils, and fats that would otherwise ruin recycling, even recycling of paper and paperboard products, would not be an issue during composting. The mineralization of the compostable materials would give rise to the regeneration of some of the energy expended to produce the plastic through sequestration of micronutrients in the produced compost.

Several industrially compostable polymers are currently available commercially, with polyesters being the most populace material owing to ease of hydrolyzing the ester linkage. The main compostable polyesters are polyhydroxyalkanoate (PHA), poly(butylene succinate) (PBS), poly(butylene adipate-co-butylene terephthalate) (PBAT), and polylactic acid (PLA) (Figure 1.3).

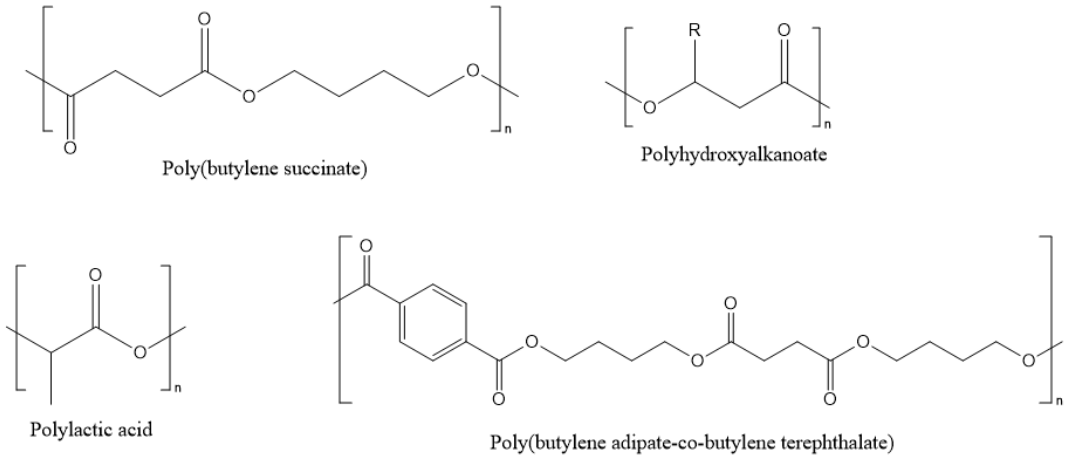

Figure 1.3 Structures for commodity compostable polymers poly(butylene succinate) (PBS), polyhydroxyalkanoate (PHA), polylactic acid (PLA), and poly(butylene adipate-co-butylene terephthalate) (PBAT).

PLA is the most price competitive aliphatic homopolymer currently commercially available with a production of approximately 250,000 tonnes per year. PLA is also a

biobased polymer being produced from the polycondensation of lactic acid sourced from the fermentation of sugars. Due to its optically clear nature, it is useful in packaging applications. However, while PLA is currently a highly used biopolymer that is industrially compostable, due to its high crystallinity, it has little ability to become home compostable. The elevated temperatures found within industrial composting conditions are needed for the initial breakdown of the long chains of PLA prior to enzymatic degradation being a possibility.

PBS is an aliphatic polyester that has a flexible molecular structure with a low glass transition temperature and high elongation at break similar to that of polyolefins. Succinic acid and 1,4 butanediol are the monomers for the synthesis of PBS and can be made from biosources. Succinic acid can be produced through the fermentation of different biomass sources, including lignocellulosic. Butanediol can be sourced from the hydrocracking of starches and sugars.

PHA is a rapidly developing group of aliphatic polyesters that are biodegradable, with the goal of these materials being soil degradable, marine degradable, and compostable. They are made from a variety of bacteria and algae through biofermentation processing. The materials properties of PHA are tuned through varying the side chain functionality, main chain length, and copolymerization. Depending on the PHA variety and processing, they can have very favorable materials properties for packaging applications with the end goal of supplanting polypropylene and polyethylene. The applications of these materials are widespread with use in paperboard coating, adhesives, and cutlery as a possibility. The main downsides with PHA currently are the cost to produce and the manufacturing process being susceptible to many issues.

The current marketplace for biodegradable polymers is growing, and the need for additional materials to fill market demands is present. Additional biodegradable polymers are needed to meet the material requirements that the current commodity biodegradable polymers do not meet.

Polyurethanes: Applications and Synthesis

Polyesters account for the majority of biodegradable polymers that are commercially available with continued research investment to develop novel biobased and biodegradable materials. The ester linkage is the key component of these materials that allows them to be easily hydrolyzable and also available for microorganism interaction. It is well understood that under degradation conditions, long polymer chains are broken apart at linkages along the chain that are susceptible to breakage. These linkages, for the majority of biodegradable polymers, are ester bonds. Once the long chains are fragmented into shorter chains with higher mobility, they can be more easily be digested by microorganisms and acted upon by enzymes to completely mineralize the remaining polymer chains (Figure 1.4).

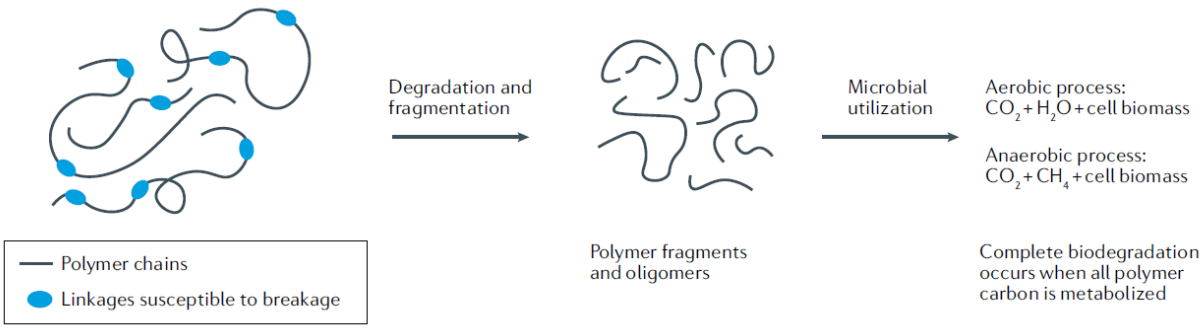

Figure 1.4 Degradation pathway of polymeric materials from long chains to oligomers and finally though microbial breakdown. Reprinted with permission from Nature Reviews.[44] Copyright 2021, Springer Nature Limited.

The ester linkage is, therefore, a good addition to any copolymer that is being synthesized with degradability as an integral material property. The degradability of the ester linkage has long been studied in the application of polyester polyurethanes.[24, 49-52] Polyester polyurethanes are found to be degradable when their soft segment has labile linkages in it. The soft segment is predominately composed of the polyol, which would be the polyester prepolymer used for the synthesis of the polyurethane.[53-57] The hard segment includes the more rigid urethane bond produced by the isocyanate reaction.

The standard synthesis of the urethane bond follows a typical addition mechanism where a hydroxy group can react with an isocyanate group to produce the urethane bond.[49-51, 58-63] Therefore, the production of polyurethanes follows a similar mechanism in polyaddition, where di substituted or multifunctional hydroxy molecules react with molecules with at least two isocyanate functionalities. One issue that arises during the synthesis of polyurethanes is the side reactions that can occur between the isocyanate and multiple functional groups (Figure 1.5). These sides reactions can have a huge negative impact on the mechanical properties of the produced polyurethanes. Additionally, when concerned with producing a biodegradable polyurethane, the side reactions are even more important, as the inclusion of some of these functional groups along the polymer chain can kill degradation – for example, the urea bond, which is a highly polar bond that is very strong and resistant to breaking. The allophanate and biuret produce a point of branching or crosslinking within the polyurethane that can dramatically change the mechanical properties, and the crosslinking point will be very difficult to break through typical abiotic and enzymatic degradation mechanisms.

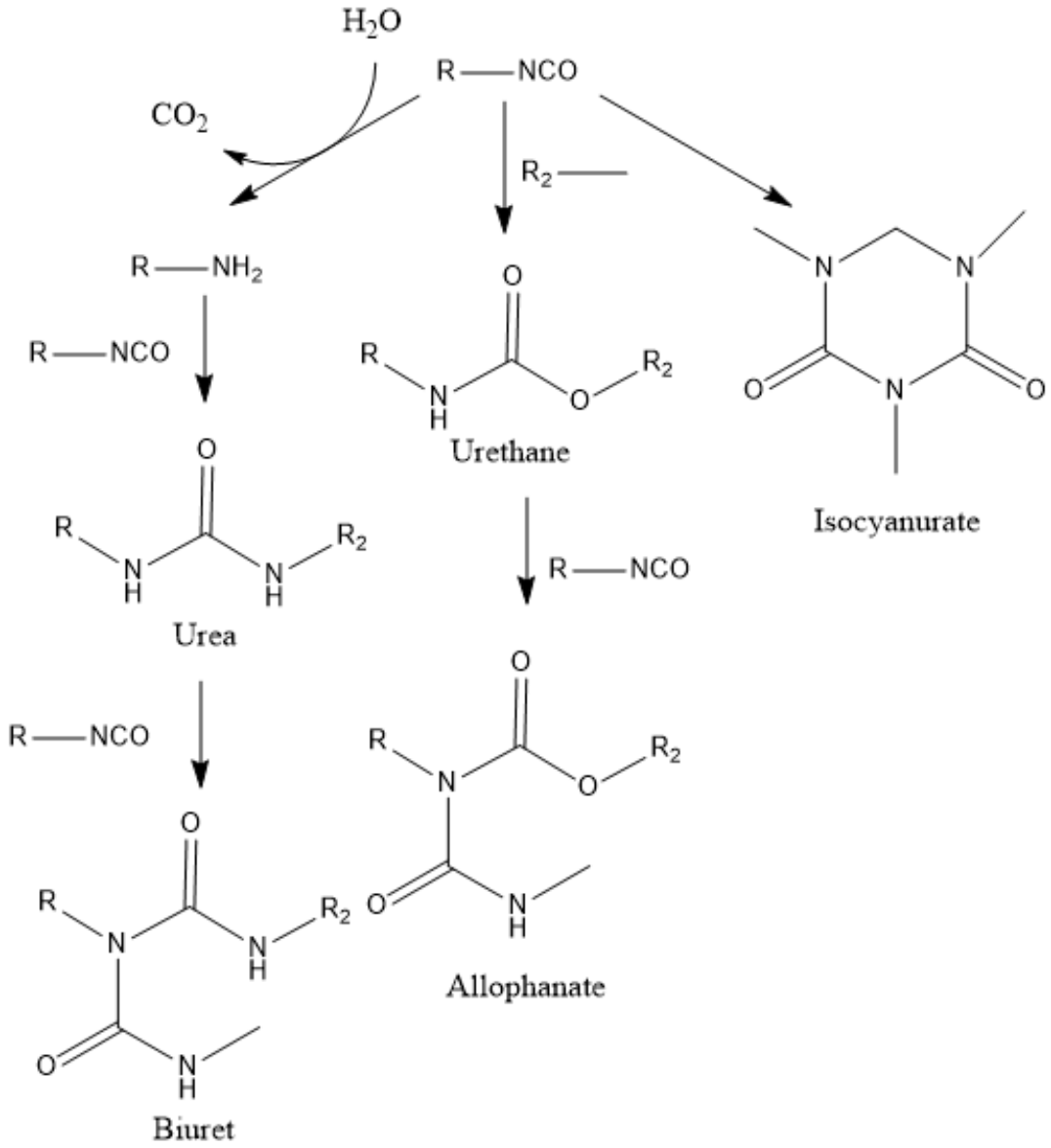

Figure 1.5 Side reactions of isocyanate functionality with various molecular architectures present during the polyaddition reaction to produce polyurethanes.

These side reactions can be controlled through the control of the isocyanate indexing value (Equation 1.1).[59, 60, 64] The isocyanate is a ratio of the molar equivalency between the hydroxy functionalities and the isocyanate functionalities within the polyurethane reaction. Controlling this value is important in controlling the molecular

weight of the produced polyurethane, but also to reduce these side reactions that can occur when the isocyanate content is much higher than the hydroxy content within a reaction. This indexing does a good job of controlling the side reactions because the reaction of the isocyanate with primary hydroxy groups is kinetically favored over the reaction of the isocyanate with other functionalities.

$$Index = \frac{n_{eq_{iso}}\, x\, m_{iso}}{(n_{eq_{crosslinker}}\, x\, m_{crosslinker}) + (n_{eq_{polyester}}\, x\, m_{polyester})}$$

Equation 1.1 Isocyanate indexing value determined using hydroxy and isocyanate functionality during the synthesis of polyurethanes.

Determining Biodegradability

The production of novel biodegradable polymers is made more difficult due to the difficulty associated with measuring the degradation of the products during the initial synthesis and formulation stage.[65-68] It is during this stage that changes are constantly being made to improve the physical and chemical properties of materials, but small changes can negatively impact its ability to degrade. The ideal method for measuring biodegradation under different conditions is respirometry analysis, but it is not a good choice for early material testing due to its high cost and extended testing times.[69-71]

Polymer degradation assays have been developed for use within the laboratory using chemical degradation and hydrolysis through the application of strong acids and bases. These methods use a variety of detection techniques, such as mass loss, nuclear magnetic resonance spectroscopy, molecular weight changes via size exclusion chromatography, and changes mechanical properties.[72-75] These methods can be readily completed in any chemistry lab during the initial synthesis and formulation of a new

material. The main issue with using strong acids and bases to degrade the polymers is that in the natural environment these materials will never be subjected to these extreme conditions. Therefore, such digestion techniques are not ideal to understand how the materials will truly biodegrade.

Adhesives

Adhesives are a ubiquitous product class that are applied to join two surfaces together through permanent or temporary bonding. Pressure sensitive adhesives (PSAs) have found widespread application in bonding dissimilar surfaces through the application of a slight force to encourage bonding. All commercial PSAs are based on a polymeric base with various additives to modify the physical properties of the bulk material. These polymers are predominately acrylics, natural rubbers, styrenic block copolymers, and niche application of silicone or polyurethanes (Figure1.6).

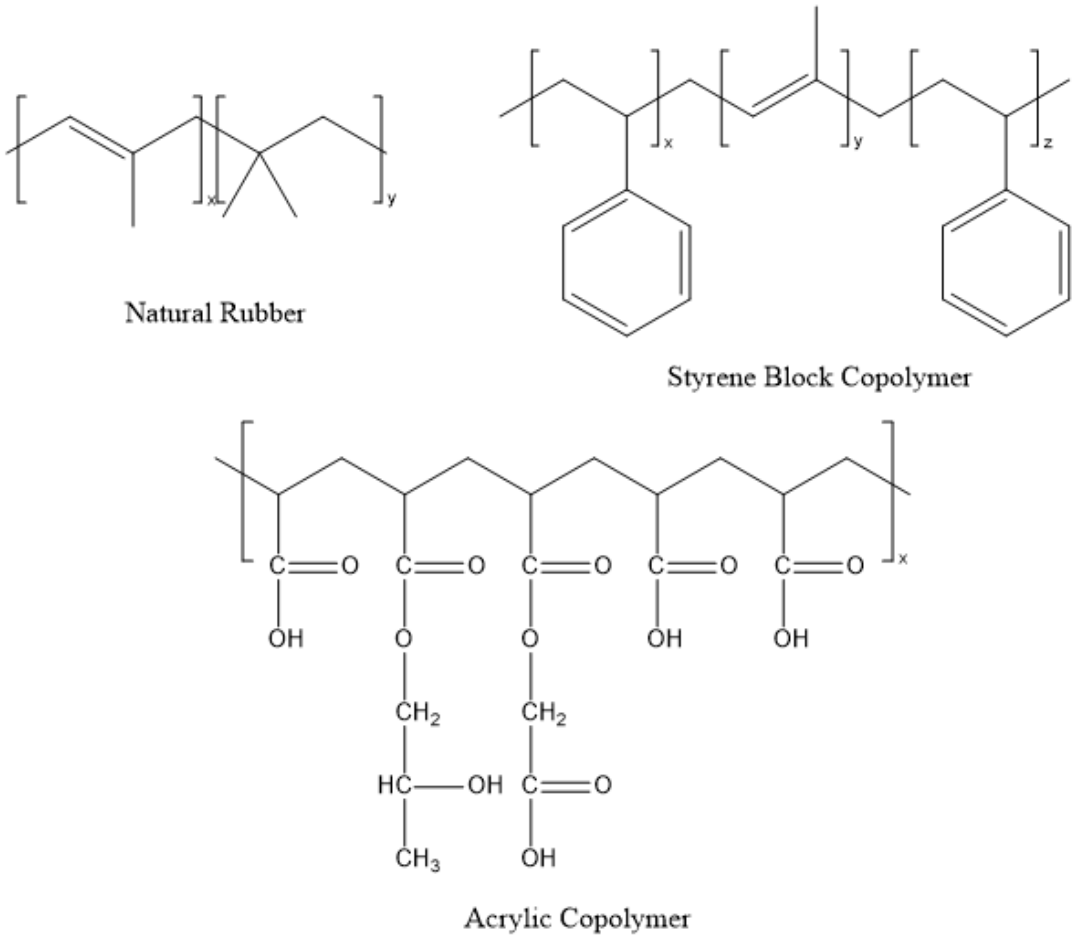

Figure 1.6 Structures of the three most common pressure sensitive adhesives: natural rubber, styrene block copolymer, and acrylic copolymer.

Natural rubber PSAs were the first to be developed and are still applied today because of their low cost to produce. These PSAs generally include natural rubber and a low molecular weight tackifier resin to improve the tack. Crosslinking has become more common in these natural rubber PSAs to address the high flow state of the natural product.

Acrylic PSAs are more tunable synthetically which allows for more optimization and formulation than natural rubber PSAs. These acrylic PSAs are traditionally composed

of a long side chain acrylate, for example 2-ethyhexyl acrylate or n-butyl acrylate, which provides a low glass transition temperature. To modulate the glass transition short side chain acrylates, such as methyl acrylate, are copolymerized. Acrylic acid can also be added to help improve adhesion and modify tensile properties, specifically to improve their deformation under uniaxial extension. Finally, small molecule additives can be formulated into acrylic PSAs to improve tack, modulate dissipative forces, and adjust glass transition temperature. Similarly, to natural rubber PSAs, crosslinking can be applied to modify the flow state of the final material to improve coating performance and creep compliance.

Styrenic block copolymers consist of a blend of triblock copolymers, typically styrene-isoprene-styrene, and deblock copolymers, typically styrene-isoprene. The deblock copolymer has a high glass transition temperature but a low molecular weight that is immiscible with the styrene phase of the triblock copolymer. The ratio of molecular weight between the isoprene and styrene phases is important to ensure the separation of these two phases. This phase separation of these PSAs provides physical crosslinking that helps to reduce creep, therefore additional crosslinking is not needed. With styrenic PSAs, the addition of tackifying resins is always necessary to impart needed tack levels.

These viscoelastic materials need both the viscous component to rapidly wet the target surface to produce solid tacky contact and the elastic component to improve internal adhesive connection to resist separation during debonding. These viscoelastic properties can be produced in a multitude of diverse ways including through block copolymers, crosslinking, and microphase separations. Triblock copolymers achieve the

required viscoelastic properties through the application of a glassy A-block phase and a rubbery B-block. The glassy A and end block allow for phase separation to occur, which acts as physical crosslinking improving the resistance to creep and providing cohesive strength. The rubbery B-block improves the flowability of the material, significantly increasing the adhesion and tack of the material. The adhesion of the midblock can be further modulated using small molecular tackifiers, which further lowers the loss modulus allowing for better contact to be established in a shorter timeframe.

The majority of commercially available pressure sensitive adhesives fall into one of these chemical architectures and are therefore nondegradable in nature. The use of adhesives in packaging applications is numerous; for example, labeling of products, sealing of seams with tape, or adhering two dissimilar materials together. This applied adhesive can have a negative impact on the potential waste streams for these products. Recycling paperboard through the repulping process is a common fate for cardboard shipping boxes, but if these boxes are sealed using an adhesive that does not break down during repulping it can have a damaging impact on the process. Additionally, packaging products that are compostable have non-compostable adhesive routinely applied to them. This directly impacts the overall material from breaking down under composting conditions and will leave behind races of the non-compostable adhesive as a contaminant in the soil. Addressing the need for a biodegradable adhesive is very important in order to continue to push forward biodegradable alternatives to current packaging plastics.

Crosslinking can be used for certain polymer systems to improve their application as pressure sensitive adhesive. Crosslinking can increase the storage modulus of these materials, thus increasing their resistance to flow and creep. An increase in crosslinking

content will also lead to a reduction in the loss modulus of the adhesive; furthermore, the ability of the material to wet a substrate. Understanding the entanglement molecular weight and the molecular weight between crosslinking can help significantly with managing these two competing moduli. Both the storage and loss moduli need to be well controlled when producing a PSA. The Dahlquist criterion gives guidance for a maximum elastic modulus for any type of PSA to have the requisite material properties. To meet the Dahlquist criterion the elastic modulus must be below 0.3MPa at 1Hz. The value of 1Hz is important, as typical adhesion occurs in a time scale less than one second; therefore, a timescale component needs to be included.

Adhesion occurs between the adhesive and two surfaces that are being adhered to each other. Several interactions occur during the work of adhesion including the interactions within the bulk adhesive and the interaction of the adhesive at the adhesive to adhered interface. In certain situations, there is an additional interaction of adhesion at a location considered the adhered interphase. This adhered interphase occurs when there is a chemical change due to the interaction of the adhesive and the adhered. This can occur between a variety of adhesives and adhered surfaces; one example is the interdiffusion of a lignocellulosic adhered material with a natural rubber adhesive. This causes a change in the interface between the adhesive and the adhered which interacts uniquely with the adhesive and the adhered.

The work of adhesion is a complex phenomenon spanning chemical and physical interactions with the scale ranging from molecular to macroscopic in nature. There are several theories in the field of adhesion science that attempt to encompass the total work of adhesion that can occur and the impact each form of adhesion. Some of these theories

include the Johns theory, Pizzi theory, Fourche theory, and Gardner theory. While each theory varies on what force is attributed as the predominate force for adhesive work, all of the theories contain the same group of forces. These include mechanical adhesion, electrostatic adhesion, diffusion adhesion, adsorption adhesion, and covalent bonding.

Mechanical adhesion has been attributed to the predominate bonding mechanism, especially for porous substrates. The theory postulates that the work of adhesion occurs because of the flow and penetration of the adhesive in the porous and rough surface of substrates. This flow and penetration is then followed by hardening of the adhesive causing interlocking of the substrate and adhesive through this increase surface area interaction. Mechanical adhesion can be a major contributing factor for the strength of adhesives, but for certain surfaces it may be less of a factor.

Electronic theory of adhesion proposes that adhesion occurs because of the attraction from electrostatic charge effects between the adhesion and the substrate. The resistance to debonding is attributed to the formation of an electronic double layer that produces electrostatic forces at the interface between the adhesive and the substrate. This mechanism of bonding due to electrostatic interaction is typically applied to the bonding of metals and polymers. Additionally, during debonding of these materials an electrical discharge has been recorded, which is attributed to the electrostatic interactions. These types of electrostatic bonding interactions have only been observed with metallic substrates.

Diffusion theory applies to an adhesive and substrate that are chemically compatible, such as two polymers, and relies on the understanding of autoadhesion with homogeneous systems. Specifically in polymers, this relates to the interactions of the

macromolecular chains of the two distinct systems due to molecular mobility and mutual miscibility of the two polymer chains. During this type of bonding the two distinct materials, adhesive and substrate, become less defined and form an interphase where the work of adhesion is occurring. With this form of adhesion, there is no stress concentration point because there is no discontinuity between the physical properties of the polymers. The bond strength is therefore determined by solubility parameters between the adhesive and the substrate.

The adsorption or wetting theory is a highly accepted model for the work of adhesion. Based on this theory, bonding first occurs through the formation of interfacial forces between the adhesive and the substrate. This occurs through the production of continual contact between the adhesive surface and the substrate surface. The contact, called wetting, occurs when the adhesive has a lower surface energy than the critical surface energy of the substrate. This surface energy difference is the precise reason why surface treatment is important prior to adhesive application. Surface treatments increase the surface energy and polarity of the substrate. Ideal wetting occurs when the material can sufficiently flow into the rough surface of a substrate. This flow increases surface interactions between the adhesive and the substrate, increasing overall bonding strength. Additionally, improper wetting creates voids between the adhesive and substrate allowing for an interfacial defect to occur where debonding can propagate from. This intimate contact relies primarily on molecular interactions between the adhesive and substrate in the form of van der Waals interactions and Lewis acid-base interactions.

Surface energy difference between the adhesive and substrates is extremely important for removable PSAs. The surface energy difference between the face film of a

label and the adhesive must be more similar than the adhesive to the surface to which the label will be adhered. If this does not occur, the adhesive will fail adhesively between the adhesive and the face film leaving an adhesive residue when debonding occurs.

Chemical bond theory is based on the formation of hydrogen, covalent, and ionic bonds between the adhesive and the substrate. Covalent bonds, which are not as applicable in removable PSAs, provide much higher bonding forces than secondary forces such as van der Waals interactions. These covalent bonds can occur between the two surfaces tightly bonding them together. This is a typical form of bonding between highly crosslinked polymer networks. Covalent bonding requires a reactive handle in both the adhesive and the substrate in order for the bond to form. Alternatively, chemical bonding also encompasses secondary interactions including hydrogen bonding and polar interactions. These are only prevalent in materials that contain heteroatoms able to hydrogen bond or produce a polar component that induces the interactions.

The application of all adhesives relies on both understanding how and why adhesion is occurring, but also on how and why debonding or adhesive failure occurs. A typical adhesive joint is shown in Figure 1.7. If the adhesive bond is tested under uniaxial extension, there are three different failure modes that can occur. If the failure occurs between the adhesive and the substrate, then an adhesive failure has occurred. For a removable PSA this is the failure that must occur to ensure no adhesive residue remains upon debonding. The debonding occurs between the adhesive and the substrate that has the lowest adhesive bond strength. Another failure mode is cohesive failure within the adhesive which is apparent when residue remains on both substrates upon depending. This occurs when the internal cohesive forces are lower than the adhesive bonding forces

between the adhesive and the substrates. Finally, cohesive failure of the substrate can occur where the substrate breaks upon mechanical action. This occurs when the material strength of the substrates is lower than the adhesive and cohesive strength of the adhesive. Cohesive failure of face films can occur when making PSA coated labels when the face film as a low young modulus. It is important to understand what type of failure is occurring during debonding, and typically it is not a single form of debonding and is instead addressed as a percentage of cohesive or adhesive failure. Targeting 100% adhesive failure for a removable PSA is important, but for some applications a combination of adhesive and cohesive failure may result in a higher bonding strength. In this case the overall strength of the adhesive bond is more important than the failure mode.

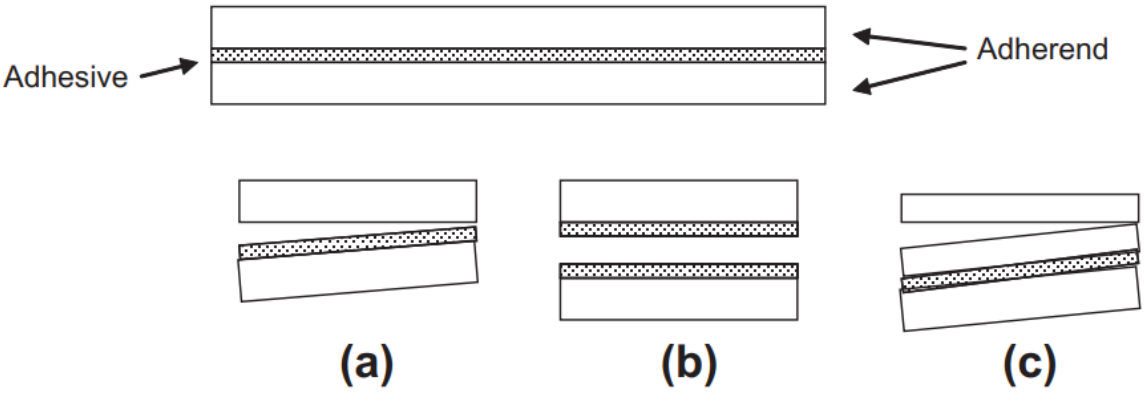

Figure 1.7 Adhesive failure modes: a) adhesive failure, b) cohesive failure of adhesive, c) cohesive failure of substrate.

Materials can be divided into two categories based on surface energy values low energy (<100 dynes/cm) and high energy (200-500 dynes/cm). High surface energy solids include glass, metals, and inorganic compounds. Low surface energy solids consist of

mainly organic compounds including polymeric materials, though polymers can be modified to have either low or high surface energy. High surface energy solids will spontaneously be wet through any contact with a low energy substance such as an oil or organic particulates. This is because the absorption of the material onto the high energy surface reduces the overall surface energy of the combined surface and contaminant. Therefore, a cleaned high energy surface will not remain clean for long as it will readily absorb contamination, such as water or organics. For this reason, surface treatments are traditionally applied immediately before the application of an adhesive or coating.

The surface energy of each component of a pressure sensitive adhesive label is important to understand to optimize adhesive vs cohesive failure. Measuring the surface energy can be readily completed using the contact angle measurement of different liquids of known surface tensions and converting this value into surface energy.

Measuring the adhesion of pressure sensitive adhesives is important to help determine the application of the product. There are several different test methods designed to assess different facets of adhesives and their potential failure modes. The most common for PSAs is the loop tack test. In this test the instant tack-ability of the adhesive is measured through pressing a looped sample into a glass or metal slide briefly before immediately pulling it in extension. The force required to remove the adhered sample is considered the loops tack value. This is directly related to the instant tack of an adhesive.

Objectives

Applying synthetic methodologies towards the production of functional materials is the main concern of the work described in this dissertation. Chapter Two details the

work done towards applying a high throughput fluorescence-based assay for the measurement of enzymatic degradation of polyester polyurethanes. Using the developed enzymatic degradation assay, the synthesis of a highly degradable polyester was first developed using conventional polycondensation methods. Furthermore, using this highly degradable polyester as a prepolymer, polyester polyurethanes were synthesized by polyaddition. The enzymatic degradation assay was validated for these polyester polyurethanes and then applied to determine the impact that three biobased crosslinkers – glycerol, sorbitan monooleate, and a mannan octyl urethane – had on enzymatic degradation. Additionally, the amount of crosslinker and the isocyanate indexing of the polyaddition reaction was varied to determine their impact on enzymatic degradation. Moreover, applying the assay as a guiding tool, a crosslinked polyester polyurethane was produced at scale and measured for mechanical and chemical properties. Additionally, the compostability under industrial composting conditions were determined using respirometry analysis. Finally, Chapter Three addresses the need for a home compostable pressure sensitive adhesive. A target polymer was modified synthetically to meet the material demands of a home compostable adhesive through the balance of adhesive and cohesive forces. Additionally, the adhesive was modified using stabilizers, tackifiers, antioxidants, and viscosity modifiers to meet the demands of coating, label conversion and application.

References

(1) Geyer, R.; Jambeck, J. R.; Law, K. L. Production, use, and fate of all plastics ever made. *Science Advances* **2017**, *3* (7), e1700782. DOI: doi:10.1126/sciadv.1700782.

(2) Schneiderman, D. K.; Hillmyer, M. A. 50th Anniversary Perspective: There Is a Great Future in Sustainable Polymers. *Macromolecules* **2017**, *50* (10), 3733-3749. DOI: 10.1021/acs.macromol.7b00293.

(3) Auras, R.; Harte, B.; Selke, S. An overview of polylactides as packaging materials. *Macromolecular Bioscience* **2004**, *4* (9), 835-864. DOI: 10.1002/mabi.200400043.

(4) Haque, F. M.; Ishibashi, J. S. A.; Lidston, C. A. L.; Shao, H.; Bates, F. S.; Chang, A. B.; Coates, G. W.; Cramer, C. J.; Dauenhauer, P. J.; Dichtel, W. R.; et al. Defining the Macromolecules of Tomorrow through Synergistic Sustainable Polymer Research. *Chemical Reviews* **2022**, *122* (6), 6322-6373. DOI: 10.1021/acs.chemrev.1c00173.

(5) Kaur, G.; Uisan, K.; Ong, K. L.; Lin, C. S. K. Recent Trends in Green and Sustainable Chemistry & Waste Valorisation: Rethinking Plastics in a circular economy. *Current Opinion in Green and Sustainable Chemistry* **2018**, *9*, 30-39. DOI: 10.1016/j.cogsc.2017.11.003.

(6) Jambeck, J. R.; Geyer, R.; Wilcox, C.; Siegler, T. R.; Perryman, M.; Andrady, A.; Narayan, R.; Law, K. L. Plastic waste inputs from land into the ocean. *Science* **2015**, *347* (6223), 768-771. DOI: 10.1126/science.1260352.

(7) Narayan, R. Biobased & Biodegradable Plastics: Rationale, Drivers, and Technology Exemplars. In *Degradable Polymers and Materials: Principles and Practice*, Khemani, K., Scholz, C. Eds.; ACS Symposium Series, Vol. 1114; 2012; pp 13-31.

(8) Narayan, R. Biodegradable and Biobased Plastics: An Overview. In *Soil Degradable Bioplastics for a Sustainable Modern Agriculture*, Malinconico, M. Ed.; Green Chemistry and Sustainable Technology, 2017; pp 23-34.

(9) Flury, M.; Narayan, R. Biodegradable plastic as an integral part of the solution to plastic waste pollution of the environment. *Current Opinion in Green and Sustainable Chemistry* **2021**, *30*. DOI: 10.1016/j.cogsc.2021.100490.

(10) Narayan, R. Carbon footprint of bioplastics using biocarbon content analysis and life-cycle assessment. *Mrs Bulletin* **2011**, *36* (9), 716-721. DOI: 10.1557/mrs.2011.210.

(11) Kulkarni, A.; Narayan, R. Morphology, Mechanical Properties, and Biodegradability of Modified Thermoplastic Starch/PETG Blends with In Situ Generated Graft Copolymers. *Sustainability* **2023**, *15* (3). DOI: 10.3390/su15032227.

(12) Stagner, J.; Narayan, R. Preparation and Properties of Biodegradable Foams. *Journal of Polymers and the Environment* **2011**, *19* (3), 598-606. DOI: 10.1007/s10924-011-0309-1.

(13) Mulchandani, N.; Narayan, R. Redesigning Carbon-Carbon Backbone Polymers for Biodegradability-Compostability at the End-of-Life Stage. *Molecules* **2023**, *28* (9). DOI: 10.3390/molecules28093832.

(14) Narayan, R. Using reactive extrusion to manufacture greener products - from laboratory fundamentals to commercial scale. *Abstracts of Papers of the American Chemical Society* **2017**, *253*.

(15) Foundation, E. M. The New Plastics Economy: Rethinking the Future of Plastics. 2016.

(16) Thiounn, T.; Smith, R. C. Advances and approaches for chemical recycling of plastic waste. *Journal of Polymer Science* **2020**, *58* (10), 1347-1364. DOI: 10.1002/pol.20190261.

(17) Kosloski-Oh, S. C.; Wood, Z. A.; Manjarrez, Y.; de los Rios, J. P.; Fieser, M. E. Catalytic methods for chemical recycling or upcycling of commercial polymers. *Materials Horizons* **2021**, *8* (4), 1084-1129. DOI: 10.1039/d0mh01286f.

(18) Coates, G. W.; Getzler, Y. Chemical recycling to monomer for an ideal, circular polymer economy. *Nature Reviews Materials* **2020**, *5* (7), 501-516. DOI: 10.1038/s41578-020-0190-4.

(19) Zhang, J.; Chevali, V. S.; Wang, H.; Wang, C. H. Current status of carbon fibre and carbon fibre composites recycling. *Composites Part B-Engineering* **2020**, *193*. DOI: 10.1016/j.compositesb.2020.108053.

(20) Oliveux, G.; Dandy, L. O.; Leeke, G. A. Current status of recycling of fibre reinforced polymers: Review of technologies, reuse and resulting properties. *Progress in Materials Science* **2015**, *72*, 61-99. DOI: 10.1016/j.pmatsci.2015.01.004.

(21) Schyns, Z. O. G.; Shaver, M. P. Mechanical Recycling of Packaging Plastics: A Review. *Macromolecular Rapid Communications* **2021**, *42* (3). DOI: 10.1002/marc.202000415.

(22) Ignatyev, I. A.; Thielemans, W.; Vander Beke, B. Recycling of Polymers: A Review. *Chemsuschem* **2014**, *7* (6), 1579-1593. DOI: 10.1002/cssc.201300898.

(23) Foundation, E. M. *The New Plastics Economy: Rethinking the Future of Plastics.* 2016. (accessed.

(24) Lim, B. K. H.; San Thian, E. Biodegradation of polymers in managing plastic waste-A review. *Science of the Total Environment* **2022**, *813*. DOI: 10.1016/j.scitotenv.2021.151880.

(25) Zhang, F.; Zhao, Y. T.; Wang, D. D.; Yan, M. Q.; Zhang, J.; Zhang, P. Y.; Ding, T. G.; Chen, L.; Chen, C. Current technologies for plastic waste treatment: A review. *Journal of Cleaner Production* **2021**, *282*. DOI: 10.1016/j.jclepro.2020.124523.

(26) Dris, R.; Gasperi, J.; Mirande, C.; Mandin, C.; Guerrouache, M.; Langlois, V.; Tassin, B. A first overview of textile fibers, including microplastics, in indoor and outdoor environments. *Environmental Pollution* **2017**, *221*, 453-458. DOI: 10.1016/j.envpol.2016.12.013.

(27) Murakami, S.; Oguchi, M.; Tasaki, T.; Daigo, I.; Hashimoto, S. Lifespan of Commodities, Part I. *Journal of Industrial Ecology* **2010**, *14* (4), 598-612. DOI: 10.1111/j.1530-9290.2010.00250.x.

(28) Kuczenski, B.; Geyer, R. Material flow analysis of polyethylene terephthalate in the US, 1996-2007. *Resources Conservation and Recycling* **2010**, *54* (12), 1161-1169. DOI: 10.1016/j.resconrec.2010.03.013.

(29) Linzner, R.; Salhofer, S. Municipal solid waste recycling and the significance of informal sector in urban China. *Waste Management & Research* **2014**, *32* (9), 896-907. DOI: 10.1177/0734242x14543555.

(30) Barnes, D. K. A.; Galgani, F.; Thompson, R. C.; Barlaz, M. Accumulation and fragmentation of plastic debris in global environments. *Philosophical Transactions of the*

Royal Society B-Biological Sciences **2009**, *364* (1526), 1985-1998. DOI: 10.1098/rstb.2008.0205.

(31) Geyer, R.; Kuczenski, B.; Zink, T.; Henderson, A. Common Misconceptions about Recycling. *Journal of Industrial Ecology* **2016**, *20* (5), 1010-1017. DOI: 10.1111/jiec.12355.

(32) Cooper, D. R.; Skelton, A. C. H.; Moynihan, M. C.; Allwood, J. M. Component level strategies for exploiting the lifespan of steel in products. *Resources Conservation and Recycling* **2014**, *84*, 24-34. DOI: 10.1016/j.resconrec.2013.11.014.

(33) Rochman, C. M.; Browne, M. A.; Underwood, A. J.; van Franeker, J. A.; Hompson, R. C. T.; Amaral-Zettler, L. A. The ecological impacts of marine debris: unraveling the demonstrated evidence from what is perceived. *Ecology* **2016**, *97* (2), 302-312. DOI: 10.1890/14-2070.1.

(34) Zalasiewicz, J.; Waters, C. N.; do Sul, J. A. I.; Corcoran, P. L.; Barnosky, A. D.; Cearreta, A.; Edgeworth, M.; Galuszka, A.; Jeandel, C.; Leinfelder, R.; et al. The geological cycle of plastics and their use as a stratigraphic indicator of the Anthropocene. *Anthropocene* **2016**, *13*, 4-17. DOI: 10.1016/j.ancene.2016.01.002.

(35) Mutha, N. H.; Patel, M.; Premnath, V. Plastics materials flow analysis for India. *Resources Conservation and Recycling* **2006**, *47* (3), 222-244. DOI: 10.1016/j.resconrec.2005.09.003.

(36) Davis, J.; Geyer, R.; Ley, J.; He, J.; Clift, R.; Kwan, A.; Sansom, A.; Jackson, T. Time-dependent material flow analysis of iron and steel in the UK Part 2. Scrap generation and recycling. *Resources Conservation and Recycling* **2007**, *51* (1), 118-140. DOI: 10.1016/j.resconrec.2006.08.007.

(37) Hoornweg, D.; Bhada-Tata, P.; Kennedy, C. Waste production must peak this century. *Nature* **2013**, *502* (7473), 615-617. DOI: 10.1038/502615a.

(38) Lucherelli, M. A.; Duval, A.; Averous, L. Biobased vitrimers: Towards sustainable and adaptable performing polymer materials. *Progress in Polymer Science* **2022**, *127*. DOI: 10.1016/j.progpolymsci.2022.101515.

(39) Belboom, S.; Leonard, A. Does biobased polymer achieve better environmental impacts than fossil polymer? Comparison of fossil HDPE and biobased HDPE produced from sugar beet and wheat. *Biomass & Bioenergy* **2016**, *85*, 159-167. DOI: 10.1016/j.biombioe.2015.12.014.

(40) Piorkowska, E. Overview of Biobased Polymers. In *Thermal Properties of Bio-Based Polymers*, DiLorenzo, M. L., Androsch, R. Eds.; Advances in Polymer Science, Vol. 283; 2019; pp 1-35.

(41) Nakajima, H.; Dijkstra, P.; Loos, K. The Recent Developments in Biobased Polymers toward General and Engineering Applications: Polymers that Are Upgraded from Biodegradable Polymers, Analogous to Petroleum-Derived Polymers, and Newly Developed. *Polymers* **2017**, *9* (10). DOI: 10.3390/polym9100523.

(42) Fache, M.; Boutevin, B.; Caillol, S. Vanillin, a key-intermediate of biobased polymers. *European Polymer Journal* **2015**, *68*, 488-502. DOI: 10.1016/j.eurpolymj.2015.03.050.

(43) Narancic, T.; Verstichel, S.; Chaganti, S. R.; Morales-Gamez, L.; Kenny, S. T.; De Wilde, B.; Padamati, R. B.; O'Connor, K. E. Biodegradable Plastic Blends Create New Possibilities for End-of-Life Management of Plastics but They Are Not a Panacea for

Plastic Pollution. *Environmental Science & Technology* **2018**, *52* (18), 10441-10452. DOI: 10.1021/acs.est.8b02963.

(44) Law, K. L.; Narayan, R. Reducing environmental plastic pollution by designing polymer materials for managed end-of-life. *Nature Reviews Materials* **2022**, *7* (2), 104-116. DOI: 10.1038/s41578-021-00382-0.

(45) Brooks, A. L.; Wang, S. L.; Jambeck, J. R. The Chinese import ban and its impact on global plastic waste trade. *Science Advances* **2018**, *4* (6). DOI: 10.1126/sciadv.aat0131.

(46) Taniguchi, I.; Yoshida, S.; Hiraga, K.; Miyamoto, K.; Kimura, Y.; Oda, K. Biodegradation of PET: Current Status and Application Aspects. *ACS Catalysis* **2019**, *9* (5), 4089-4105. DOI: 10.1021/acscatal.8b05171.

(47) Okada, M. Chemical syntheses of biodegradable polymers. *Progress in Polymer Science* **2002**, *27* (1), 87-133. DOI: 10.1016/s0079-6700(01)00039-9.

(48) Zhang, F.; Zhao, Y.; Wang, D.; Yan, M.; Zhang, J.; Zhang, P.; Ding, T.; Chen, L.; Chen, C. Current technologies for plastic waste treatment: A review. *Journal of Cleaner Production* **2021**, *282*, 124523. DOI: https://doi.org/10.1016/j.jclepro.2020.124523.

(49) Li, S. Q.; Zhang, Y. S.; Ma, X. Z.; Qiu, S. H.; Chen, J.; Lu, G. M.; Jia, Z.; Zhu, J.; Yang, Q.; Wei, Y. Antimicrobial Lignin-Based Polyurethane/Ag Composite Foams for Improving Wound Healing. *Biomacromolecules* **2022**, *23* (4), 1622-1632. DOI: 10.1021/acs.biomac.1c01465.

(50) Wendels, S.; Averous, L. Biobased polyurethanes for biomedical applications. *Bioactive Materials* **2021**, *6* (4), 1083-1106. DOI: 10.1016/j.bioactmat.2020.10.002.

(51) Tang, X. J.; Chen, Z. H.; Liu, J. Y.; Chen, Z. Y.; Xie, W. M.; Evrendilek, F.; Buyukada, M. Dynamic pyrolysis behaviors, products, and mechanisms of waste rubber and polyurethane bicycle tires. *Journal of Hazardous Materials* **2021**, *402*. DOI: 10.1016/j.jhazmat.2020.123516.

(52) Yin, R.; Yang, S. Y.; Li, Q. M.; Zhang, S. D.; Liu, H.; Han, J.; Liu, C. T.; Shen, C. Y. Flexible conductive Ag nanowire/cellulose nanofibril hybrid nanopaper for strain and temperature sensing applications. *Science Bulletin* **2020**, *65* (11), 899-908. DOI: 10.1016/j.scib.2020.02.020.

(53) Mohanan, N.; Montazer, Z.; Sharma, P. K.; Levin, D. B. Microbial and Enzymatic Degradation of Synthetic Plastics. *Frontiers in Microbiology* **2020**, *11*. DOI: 10.3389/fmicb.2020.580709.

(54) Jiang, C. Y.; Zhang, L. Z.; Yang, Q.; Huang, S. X.; Shi, H. P.; Long, Q.; Qian, B.; Liu, Z. H.; Guan, Q. B.; Liu, M. J.; et al. Self-healing polyurethane-elastomer with mechanical tunability for multiple biomedical applications in vivo. *Nature Communications* **2021**, *12* (1). DOI: 10.1038/s41467-021-24680-x.

(55) Zhao, X. P.; Hu, H.; Wang, X.; Yu, X. L.; Zhou, W. Y.; Peng, S. X. Super tough poly(lactic acid) blends: a comprehensive review. *Rsc Advances* **2020**, *10* (22), 13316-13368. DOI: 10.1039/d0ra01801e.

(56) Guo, B. L.; Ma, P. X. Synthetic biodegradable functional polymers for tissue engineering: a brief review. *Science China-Chemistry* **2014**, *57* (4), 490-500. DOI: 10.1007/s11426-014-5086-y.

(57) Alam, M.; Akra, D.; Sharmin, E.; Zafar, F.; Ahmad, S. Vegetable oil based eco-friendly coating materials: A review article. *Arabian Journal of Chemistry* **2014**, *7* (4), 469-479. DOI: 10.1016/j.arabjc.2013.12.023.

(58) Xie, F. W.; Zhang, T. L.; Bryant, P.; Kurusingal, V.; Colwell, J. M.; Laycock, B. Degradation and stabilization of polyurethane elastomers. *Progress in Polymer Science* **2019**, *90*, 211-268. DOI: 10.1016/j.progpolymsci.2018.12.003.

(59) Aguirresarobe, R. H.; Nevejans, S.; Reck, B.; Irusta, L.; Sardon, H.; Asua, J. M.; Ballard, N. Healable and self-healing polyurethanes using dynamic chemistry. *Progress in Polymer Science* **2021**, *114*. DOI: 10.1016/j.progpolymsci.2021.101362.

(60) Cornille, A.; Auvergne, R.; Figovsky, O.; Boutevin, B.; Caillol, S. A perspective approach to sustainable routes for non-isocyanate polyurethanes. *European Polymer Journal* **2017**, *87*, 535-552. DOI: 10.1016/j.eurpolymj.2016.11.027.

(61) Zhao, H.; Gao, W. C.; Li, Q.; Khan, M. R.; Hu, G. H.; Liu, Y.; Wu, W.; Huang, C. X.; Li, R. K. Y. Recent advances in superhydrophobic polyurethane: preparations and applications. *Advances in Colloid and Interface Science* **2022**, *303*. DOI: 10.1016/j.cis.2022.102644.

(62) Cheng, B. X.; Gao, W. C.; Ren, X. M.; Ouyang, X. Y.; Zhao, Y.; Zhao, H.; Wu, W.; Huang, C. X.; Liu, Y.; Liu, X. Y.; et al. A review of microphase separation of polyurethane: Characterization and applications. *Polymer Testing* **2022**, *107*. DOI: 10.1016/j.polymertesting.2022.107489.

(63) Magnin, A.; Pollet, E.; Phalip, V.; Avérous, L. Evaluation of biological degradation of polyurethanes. *Biotechnology Advances* **2019**, 107457. DOI: https://doi.org/10.1016/j.biotechadv.2019.107457.

(64) Cregut, M.; Bedas, M.; Durand, M. J.; Thouand, G. New insights into polyurethane biodegradation and realistic prospects for the development of a sustainable waste recycling process. *Biotechnology Advances* **2013**, *31* (8), 1634-1647. DOI: https://doi.org/10.1016/j.biotechadv.2013.08.011.

(65) Ghatge, S.; Yang, Y.; Ahn, J. H.; Hur, H. G. Biodegradation of polyethylene: a brief review. *Applied Biological Chemistry* **2020**, *63* (1). DOI: 10.1186/s13765-020-00511-3.

(66) Lwanga, E. H.; Thapa, B.; Yang, X. M.; Gertsen, H.; Salanki, T.; Geissen, V.; Garbeva, P. Decay of low-density polyethylene by bacteria extracted from earthworm's guts: A potential for soil restoration. *Science of the Total Environment* **2018**, *624*, 753-757. DOI: 10.1016/j.scitotenv.2017.12.144.

(67) Priyan, V. V.; Shahnaz, T.; Suganya, E.; Sivaprakasam, S.; Narayanasamy, S. Ecotoxicological assessment of micropollutant Diclofenac biosorption on magnetic sawdust: Phyto, Microbial and Fish toxicity studies. *Journal of Hazardous Materials* **2021**, *403*. DOI: 10.1016/j.jhazmat.2020.123532.

(68) Beyer, J.; Trannum, H. C.; Bakke, T.; Hodson, P. V.; Collier, T. K. Environmental effects of the Deepwater Horizon oil spill: A review. *Marine Pollution Bulletin* **2016**, *110* (1), 28-51. DOI: 10.1016/j.marpolbul.2016.06.027.

(69) Lammel, T.; Boisseaux, P.; Fernandez-Cruz, M. L.; Navas, J. M. Internalization and cytotoxicity of graphene oxide and carboxyl graphene nanoplatelets in the human hepatocellular carcinoma cell line Hep G2. *Particle and Fibre Toxicology* **2013**, *10*. DOI: 10.1186/1743-8977-10-27.

(70) McCormick, A. R.; Hoellein, T. J.; London, M. G.; Hittie, J.; Scott, J. W.; Kelly, J. J. Microplastic in surface waters of urban rivers: concentration, sources, and associated bacterial assemblages. *Ecosphere* **2016**, *7* (11). DOI: 10.1002/ecs2.1556.

(71) McCormick, A.; Hoellein, T. J.; Mason, S. A.; Schluep, J.; Kelly, J. J. Microplastic is an Abundant and Distinct Microbial Habitat in an Urban River. *Environmental Science & Technology* **2014**, *48* (20), 11863-11871. DOI: 10.1021/es503610r.

(72) Houtz, E. F.; Higgins, C. P.; Field, J. A.; Sedlak, D. L. Persistence of Perfluoroalkyl Acid Precursors in AFFF-Impacted Groundwater and Soil. *Environmental Science & Technology* **2013**, *47* (15), 8187-8195. DOI: 10.1021/es4018877.

(73) Vikrant, K.; Giri, B. S.; Raza, N.; Roy, K.; Kim, K. H.; Rai, B. N.; Singh, R. S. Recent advancements in bioremediation of dye: Current status and challenges. *Bioresource Technology* **2018**, *253*, 355-367. DOI: 10.1016/j.biortech.2018.01.029.

(74) LeFevre, G. H.; Paus, K. H.; Natarajan, P.; Gulliver, J. S.; Novak, P. J.; Hozalski, R. M. Review of Dissolved Pollutants in Urban Storm Water and Their Removal and Fate in Bioretention Cells. *Journal of Environmental Engineering* **2015**, *141* (1). DOI: 10.1061/(asce)ee.1943-7870.0000876.

(75) Lu, D. N.; Sha, S.; Luo, J. Y.; Huang, Z. R.; Jackie, X. Z. Treatment train approaches for the remediation of per- and polyfluoroalkyl substances (PFAS): A critical review. *Journal of Hazardous Materials* **2020**, *386*. DOI: 10.1016/j.jhazmat.2019.121963.

(76) (ACC), A. C. C. *Resin Review: The Annual Statistical Report of the North Ameican Platics Industry*; ACC, 2009.

(77) Geyer, R.; Jambeck, J. R.; Law, K. L. Production, use, and fate of all plastics ever made. *Science Advances* **2017**, *3* (7). DOI: 10.1126/sciadv.1700782.

(78) Liu, E. K.; He, W. Q.; Yan, C. R. 'White revolution' to 'white pollution'-agricultural plastic film mulch in China. *Environmental Research Letters* **2014**, *9* (9). DOI: 10.1088/1748-9326/9/9/091001.

(79) Ragauskas, A. J.; Williams, C. K.; Davison, B. H.; Britovsek, G.; Cairney, J.; Eckert, C. A.; Frederick, W. J.; Hallett, J. P.; Leak, D. J.; Liotta, C. L.; et al. The path forward for biofuels and biomaterials. *Science* **2006**, *311* (5760), 484-489. DOI: 10.1126/science.1114736.

(80) O'Keefe, B. J.; Hillmyer, M. A.; Tolman, W. B. Polymerization of lactide and related cyclic esters by discrete metal complexes. *Journal of the Chemical Society-Dalton Transactions* **2001**, (15), 2215-2224. DOI: 10.1039/b104197p.

(81) Bourissou, D.; Moebs-Sanchez, S.; Martin-Vaca, B. Recent advances in the controlled preparation of poly(alpha-hydroxy acids): Metal-free catalysts and new monomers. *Comptes Rendus Chimie* **2007**, *10* (9), 775-794. DOI: 10.1016/j.crci.2007.05.004.

(82) Hormnirun, P.; Marshall, E. L.; Gibson, V. C.; White, A. J. P.; Williams, D. J. Remarkable stereocontrol in the polymerization of racemic lactide using aluminum initiators supported by tetradentate aminophenoxide ligands. *Journal of the American Chemical Society* **2004**, *126* (9), 2688-2689. DOI: 10.1021/ja038757o.

(83) Anderson, K. S.; Lim, S. H.; Hillmyer, M. A. Toughening of polylactide by melt blending with linear low-density polyethylene. *Journal of Applied Polymer Science* **2003**, *89* (14), 3757-3768. DOI: 10.1002/app.12462.

(84) Chae, Y.; An, Y. J. Current research trends on plastic pollution and ecological impacts on the soil ecosystem: A review. *Environmental Pollution* **2018**, *240*, 387-395. DOI: 10.1016/j.envpol.2018.05.008.

(85) Xanthos, D.; Walker, T. R. International policies to reduce plastic marine pollution from single-use plastics (plastic bags and microbeads): A review. *Marine Pollution Bulletin* **2017**, *118* (1-2), 17-26. DOI: 10.1016/j.marpolbul.2017.02.048.

(86) To, M. H.; Uisan, K.; Ok, Y. S.; Pleissner, D.; Lin, C. S. K. Recent trends in green and sustainable chemistry: rethinking textile waste in a circular economy. *Current Opinion in Green and Sustainable Chemistry* **2019**, *20*, 1-10. DOI: 10.1016/j.cogsc.2019.06.002.

(87) Zumstein, M. T.; Narayan, R.; Kohler, H.-P. E.; McNeill, K.; Sander, M. Dos and Do Nots When Assessing the Biodegradation of Plastics. *Environmental Science & Technology* **2019**, *53* (17), 9967-9969. DOI: 10.1021/acs.est.9b04513.

(88) Zumstein, M. T.; Kohler, H.-P. E.; McNeill, K.; Sander, M. High-Throughput Analysis of Enzymatic Hydrolysis of Biodegradable Polyesters by Monitoring Cohydrolysis of a Polyester-Embedded Fluorogenic Probe. *Environmental Science & Technology* **2017**, *51* (8), 4358-4367. DOI: 10.1021/acs.est.6b06060.

(89) Mistry, A. N.; Kachenchart, B.; Pinyakong, O.; Assavalapsakul, W.; Jitpraphai, S. M.; Somwangthanaroj, A.; Luepromchai, E. Bioaugmentation with a defined bacterial consortium: A key to degrade high molecular weight polylactic acid during traditional composting. *Bioresource Technology* **2023**, *367*. DOI: 10.1016/j.biortech.2022.128237.

(90) Gathman, T.; Schoephoerster, J.; Vasdev, R.; Liffland, S.; Batiste, D.; Amer Soc Mech, E. EVALUATION OF SUSTAINABLE P4MCL/PLLA BLOCK COPOLYMERS

AS PVC REPLACEMENT IN MEDICAL PLASTICS. In *Design of Medical Devices Conference (DMD) held as part of the Institute-for-Engineering-in-Medicine's Innovation Week*, Minneapolis, MN, Apr 11-14, 2022; 2022.

(91) Kalita, N. K.; Hakkarainen, M. Integrating biodegradable polyesters in a circular economy. *Current Opinion in Green and Sustainable Chemistry* **2023**, *40*. DOI: 10.1016/j.cogsc.2022.100751.

(92) Jia, Z. W.; Li, Y. J.; Wu, J. C. Sequence-Controlled Alternating Copolyesters Synthesis via Selective Ring-Opening Polymerization. *Macromolecular Chemistry and Physics* **2021**, *222* (24). DOI: 10.1002/macp.202100323.

(93) Batiste, D. C.; De Hoe, G. X.; Nelson, T. F.; Sodnikar, K.; McNeill, K.; Sander, M.; Hillmyer, M. A. Site-Specific Mineralization of a Polyester Hydrolysis Product in Natural Soil. *Acs Sustainable Chemistry & Engineering* **2022**, *10* (4), 1373-1378. DOI: 10.1021/acssuschemeng.1c07948.

(94) Fournier, L.; Mirabal, D. M. R.; Hillmyer, M. A. Toward Sustainable Elastomers from the Grafting-Through Polymerization of Lactone-Containing Polyester Macromonomers. *Macromolecules* **2022**, *55* (3), 1003-1014. DOI: 10.1021/acs.macromol.1c02349.

CHAPTER 2

INVESTIGATION INTO THE ENZYMATIC DEGRADABILITY OF GLYCOLIC URETHANES VIA A FLUORESENCE ASSAY[1]

[1]Ethan Stinchcomb, Jason Locklin, Austin Wright, Kush Patel, Lawrence Ferguson, Nataraja Sekhar Yadavalli, Breeanna Urbanowicz, Daniel Charles Josey, Evan M. White. To be submitted to ACS Sustainable Chemistry and Engineering.

Abstract

The continual rise of plastic production globally has placed a heightened focus on the end-of-life destination for these durable products. Replacing current nondegradable commodity plastics with degradable alternatives, specifically those that are compostable, can help alleviate the disposal burden that these products present. Through the application of a high-throughput fluorescence-based enzymatic degradation screening method, we have produced a methodology for directing the synthesis of crosslinked polyurethanes to target degradability in an industrial composting setting. The base polymer composition poly(butylene glutarate-co-butylene succinate) (PBGS), was chosen for its high level of enzymatic degradation, which was determined using a fluorescence-based assay. The impact of diisocyanate indexing using hexamethylene diisocyanate (HDI) and content of three different crosslinking agents – glycerol, sorbitan monooleate, and a mannose derivative – on enzymatic degradation was then determined. Directed by the enzymatic degradation assay and mechanical properties, a final polyester polyurethane formulation with each cross-linker was determined. These materials were then subjected to respirometry studies under industrial composting conditions to further corroborate similarities in degradation profiles between the assay and respirometry for the polymer/crosslinker pairs.

Introduction

Globally, the production of plastic has been dramatically increasing since its invention, with a 20x increase in production occurring between 1964 (15MT produced) to 2014 (311MT produced).[1, 15] The growth over this period of time has substantially outpaced that of any other industrially produced material.[76] With this increase in plastic production, the final fate for these materials has become a major concern.[45, 77, 78] The majority of plastics produced, as of a 2015 study, are disposed of via landfill (40%), leaching into the natural environment (32%), incineration (12%), and recycling (9%). With a finite amount of landfill space available and considering the impact that plastic pollution has on the natural environment, alternatives must be found for this waste.

One strategy to address the plastic waste problem is to produce degradable plastics to replace their non-degradable counterparts[3, 47, 79-83]. In particular, industrial and home composting has shown promise as a waste stream for plastics due to its nutrient rich, biodiverse environment that can facilitate biotic and abiotic degradation.[5, 43, 84-86] Currently, compostable plastics account for only a small percent of the overall commodity plastic market with the majority being aliphatic polyesters, such as polybutylene succinate (PBS), polyhydroxyalkanoate (PHA), and polylactic acid (PLA). The chemical and physical properties of the current compostable plastics limit their uses; therefore, additional work is needed to produce more chemically diverse polymers through the inclusion of different polymer architectures to improve their physiochemical properties.

A major hurdle during the development of new compostable materials is being able to accurately and easily measure their biodegradation.[87, 88] The optimal method for

biodegradation testing is through respirometry analysis.[89-94] Using this technique, the CO_2 evolved during the carbon mineralization of a sample due to biological degradation in a bio-rich media filled reactor. This technique requires highly specialized equipment and a large time investment – between 90-180 days – to understand the true biodegradation rate of a test material. Therefore, respirometry is not a suitable test for early product development where polymer architecture, additives and formulation are constantly in flux. In order to better facilitate the development of these compostable plastics, rapid screening techniques are needed to assess biotic and abiotic degradation.

An important factor when addressing the problem of plastic waste [26, 31, 32] is the application for the manufactured plastic materials. The strength, resistance, barrier properties, and cost to produce make plastic a great material for many applications, but its long lifespan should dissuade its use in short-term applications. Unfortunately, this has not be the case, since it is heavily used for single-use items, such as in packaging materials. A comprehensive review focusing on the usage lifetime for plastics based on their functions determined that packaging materials have an average lifespan from production to waste of less than one year.[6, 27-29, 35-37] This short life span is in dramatic opposition to other sectors, such as building and construction (35 year average) or transportation (15 year average). The packaging sector spans approximately 42% of the total non-fiberous plastic produced each year, and it accounts for approximately 54% of plastic waste. Therefore, it is clear that targeting the reduction in production of or finding alternative disposal mechanisms for plastics that are bound for packaging materials is key to reducing overall plastic waste.

In this work, we are applying a method for measuring the enzymatic degradation of polyester polyurethanes using a high-throughput fluorescence-based assay. Using this methodology, we are targeting the production of novel compostable polyurethane plastics with compostability at the end of life. Additionally, the assay could be used to screen a large library of enzymes against singular polymer architectures to target possible soil additives to improve the rate of degradation of these polymer materials.

Experimental

Synthesis of Lauroyl chloride

Thionyl chloride (3.569g, 0.0300mols) was added to a three neck round bottom flask under a nitrogen blanket lauric acid (4.002g, 0.0233mols). The reaction was then refluxed for 4hr at 50^{o}C. Then, the excess thionyl chloride was removed under reduced pressure distillation with an inline liquid nitrogen cold trap yield a colorless liquid of lauroyl chloride.

Synthesis of Fluorescein Dilaurate

A round bottom flask was charged with cat. pyridine, fluorescein free acid (3.323g, 0.01mols), and dichloromethane under nitrogen atmosphere. Lauroyl chloride was added dropwise to the stirring liquid, and the reaction was allowed to react at 70^{o}C overnight. The resulting crude mixture was washed with 2M HCl, brine, and dried with $NaSO^{4}$ prior to removing solvent on a rotary evaporator. The crude solid was brought up in ethyl acetate and purified via silica gel column chromatography with hexane: ethyl acetate (70:30) mobile phase.

Polyester Synthesis

The same methodology was used to synthesize each polyester homopolymer with different diacids being used. The method for poly(butylene succinate) is described here as an example: To a three neck round bottom flask equipped with an overhead stirrer, short path distillation apparatus, heating probe, and mantle 1,4 butanediol (37.24mL, 0.374mols) and succinic acid (49.76g, 0.354 mols) were added. The reaction was heated to 180^{o}C for 4 hours under a nitrogen stream. The distillate was removed, and a vacuum was slowly pulled on the reaction vessel until a maximum value was reached, ideally ~<500mTorr. The reaction was held at 180^{o}C overnight. The round bottom was then back filled with nitrogen and zirconium n-butoxide catalyst (0.438mg, 0.001mols) was added. The vacuum was reapplied slowly to a maximum vacuum pressure, and the temperature was increased to 210^{o}C and allowed to react for an additional 4 hours. The resulting polymer was used without further purification.

Polyurethane Synthesis

Polyurethane synthesis was completed using a cylindrical reaction tube into which the hydroxy end capped prepolyester, crosslinker, hexamethylene diisocyanate, and bismuth 2-ethylhexanoate were added in accordance with desired crosslinker content and isocyanate indexing. The reaction was stirred for one minute at 250 rpms using a blade stirrer attached to an overhead mixer. The reaction was then deposited into the well of a nonstick silicon release form and placed into a vacuum oven at 60°C overnight.

Microplate Fluorescence Assay

Films were solvent cast into flat bottomed black polypropylene 96-well plates from a chloroform solution containing 0.5% (w/w) polymer and 0.005% (w/w)

fluorescein dilaurate. Solvent casting was completed through the addition of 30uL of chloroform solution into each individual well and allowing the solvent to evaporate overnight in a vacuum oven.

To each well, 180 uL of a pH 7.2 PBS buffer solution (100mM) was added and allowed to equilibrate for one hour. During this time, fluorescence was monitored every minute in a temperature controlled microplate reader (Varioskan lux, Thermo Fisher Scientific). Prior to each reading, the plate was shaken for 10 seconds. Enzyme stock solution was then added to the wells, and fluorescence was continually measured every ten minutes for eight hours. Using a fluorescein calibration curve run on the same plate, the amount of fluorescein released from each film was determined.

Differential Scanning Calorimetry (DSC)

DSC experiments were conducted on a DSC 250 (TA Instruments) under a nitrogen atmosphere. Samples weighing 8-12 mg were heated at a rate of 5 °C/min from 25 to 200 °C to remove thermal hysteresis. They were then cooled to -70 °C at 5 °C/min and then heated to 200 °C at 5 °C/min. The thermal transitions, including glass transition temperature and melting temperature of the samples, were determined using the second heating curve.

Mass Loss Experiments

A solvent cast film of poly(butylene glutarate) (0.5% w/w) and FDL (0.005% w/w) was produced in a flat bottom Pyrex dish and allowed to dry fully in a vacuum oven overnight. Each sample was cut from the film, measuring approximately 2.5cm x 2.5cm square, and was weighed before being placed in a flat bottom reaction dish with lid. To these reaction dishes 10mL of PBS buffer was added and shaken at 35°C for 30 minutes.

Then to each reaction vessel an enzyme stock solution of the lipase from *Rhizopus Oryzae* was added. At the time intervals 15 minutes, 30 minutes, 1 hour, 2 hours, 3 hours, 4 hours, 6 hours, and 8 hours, the solid films were removed from the reaction vessel, placed on a flat dish, and dried in a vacuum oven overnight. The films were then weighed, and mass loss values were determined. Additionally, from each sample, fluorescence values were determined using an aliquot of the reaction media. The amount of fluorescein released was determined using a fluorescein standard curve run on the same microplate.

pH Stat Titration Experiments

A solvent cast film of poly(butylene glutarate) and FDL was produced in a flat bottom Pyrex dish and allowed to dry fully in a vacuum oven overnight. Each sample was cut from the film, measuring approximately 2.5cm x 2.5cm square, and was weighed before being placed in a flat bottom reaction dish with lid. To these reaction dishes 20mL of KCl solution was added. Using an auto titrator Titrando (Metrohm) the pH was set at 6 and then maintained using the automated pH stat titration function using a KOH solution (10 mM). The reaction system was allowed to equilibrate for one hour prior to the addition of the enzyme stock solution of 70mg/mL *Rhizopus Oryzae lipase.* The number of ester bonds hydrolyzed in the test sample was directly measured by the amount of KOH added to maintain the constant pH. Throughout the measurement, 0.1mL aliquots were removed for fluorescence measurements. The aliquots were analyzed using a black polypropylene 96-well plate using a fluorescence plate reader (Varioskan lux, Thermo Fisher Scientific).

Scanning Electron Microscopy

Surface morphology changes from enzymatic degradation were investigated using a FEI Teneo field emission-SEM at an accelerating voltage of 5kV with a spot size of 7. Polyurethane films were produced through curing on a carver press at 60°C overnight. The films were placed in flat-bottomed reaction vessels. To the vessels PBS buffer and enzyme solution of *Rhizopus Oryzae* were added and maintained at 35°C for eight hours. The films were removed from the solution, washed with a syringe of deionized water, and dried overnight under high vacuum. Using a LEICA EM ACE200 sputter coater, the films were sputter coated with a gold/palladium coating.

Tensile Testing

The tensile properties of produced polyurethane films were measured using a tensile tester (Shimadzu, AGS-X series). Dog-bone shaped test samples were produced using a die-cutter (Qualitest, ASTM-D1708-96-MET). All samples were tested in triplicate at room temperature using a crosshead speed of 10 mm/min.

Composting Biodegradation Test

Two sets of compost inoculum were collected from an industrial-scale compost facility located at the University of Georgia, Athens, GA. These two compost sets were about 4−5 months old and derived from composting the organic fraction of green waste, forest residue, food waste, and livestock manure. The temperature in the composting pile (50 cm depth) while collecting was 49 °C for the first set and 51 °C for the second set. Both sets of compost were sieved using a 4.75 mm screen (Sieve No. 4) to discard any large items such as stone, wood, and glass. The properties of fine and homogeneous compost such as pH, volatiles, and total solids were measured by pH probe and

thermogravimetric analysis. Carbon and nitrogen contents of the two compost sets and samples were measured. Approximately 250 g of fine and homogeneous compost inoculum was introduced into 18 reactors. In each experimental set, samples were run in three replicates composed of 5 g of two test materials, 5 g of cellulose (positive reference), and blank (control), which is compost inoculum only. Synthesized polyurethane films were cut into a size of 25 mm × 25 mm. Cellulose was used as received, in powder form. The compost inoculum in all reactors was stirred weekly to prevent clumping and provide an even distribution of moisture. Water was added into the reactors as necessary to maintain a constant moisture level and prevent drying of the compost inoculum. The actual carbon dioxide (CO2) emission from each sample was measured and calculated by subtracting the average CO2 production from the blank. The composting biodegradability was calculated from the ratio of actual CO2 emission to the theoretical amount of the evolved CO2 in each test period according to the testing method from ASTM standard D5338-15.43

Results and Discussion

The fluorescence assay consists of a non-fluorescent probe, fluorescein dilaurate, that is intercalated into the polymer matrix. This intercalation can occur in multiple ways, for example solvent casting or extrusion blending, depending on the target polymeric substrate of interest. Then when the polymer is degraded enzymatically, hydrolytically, or chemically the non-fluorescent probe can be released and subsequently be hydrolyzed into its fluorescent form, fluorescein (Figure 2.1). This fluorescence can then be measured using a fluorometer. This allows for the direct correlation of the amount of fluorescence produced with the amount of polymeric material that is degraded.

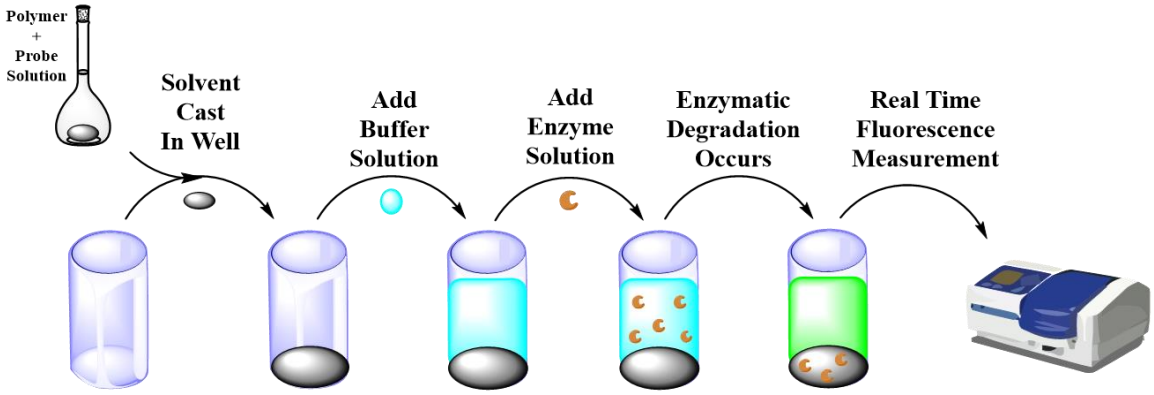

Figure 2.1 Fluorescence assay method showing the solvent casting of polymer : FDL solution into 96-well plate, addition of buffer solution, addition of enzyme solution, and measurement of fluorescence in real time using a fluorescence plate reader.

Polyesters were chosen as the base polymer for the production of polyurethanes because of the breadth of work that has shown aliphatic polyesters as being highly degradable materials. It has been well described that for polyurethane degradation to occur the soft segment has to be degradable so that the material has a good starting point to breakdown from long chains to oligomers. Therefore, a highly degradable polyester is needed for the soft segment of these polyurethanes for them to be potentially industrially compostable at the end of life.

The fluorescence assay needed to be validated against other techniques to confirm that the amount of fluorescence released is directly related to the amount of polymer degradation. To achieve this, we focused on mass loss experiments and pH stat titration experiments. Mass loss experiments are a staple of polymeric degradation lab work, where a film of the polymer can be made, weighed, degraded, and weighed again to view the amount of mass that is lost during the degradation of the polymer.

The mass loss experiments were conducted side by side with the fluorescence assay using poly(butylene glutarate) as the polymer to be studied. Ten samples were produced to measure at intervals over the eight-hour experiment. Prior to enzyme addition, no mass loss occurred, which is in line with the lack of fluorescence observed from the plate samples. After enzymes were added, mass loss was observed as well as fluorescence release. Using a standard curve and the known amount of FDL added to each sample, the mass loss to fluorescence released was tracked (Figure 2.2). The addition of the enzyme is directly responsible for mass loss of the polymeric films and fluorescence released. The data for mass loss and fluorescence released shows a strong correlation, lending support to the postulation that fluorescence released values can be directly related to the amount of polymer degradation.

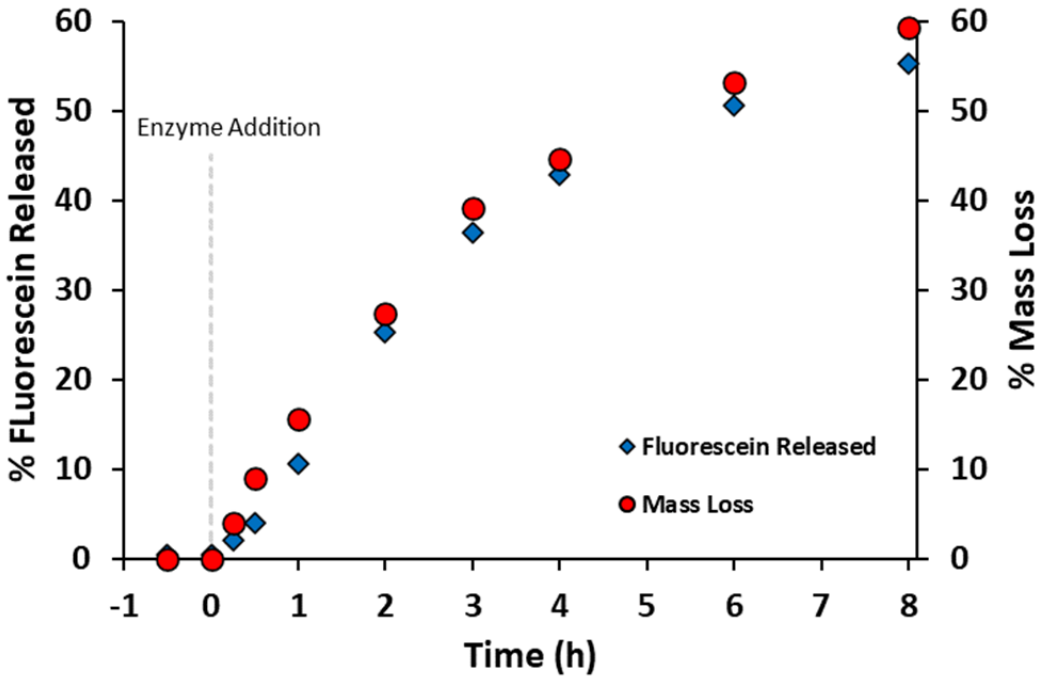

Figure 2.2 Percent mass loss of poly(butylene glutarate) films compared to fluorescein released values.

To further validate the fluorescence assay, a pH stat titration method was employed where the amount of ester bonds hydrolyzed was monitored in real time through the application of an auto titrator. This methodology works because as the ester bond is hydrolyzed free carboxylic acid groups are liberated, which decreases the solution pH, and the auto titrator detects this change in pH and automatically dispenses a strong base to maintain the pH at a constant value. The amount of base dispensed is directly proportional to the number of ester bonds hydrolyzed.

The pH stat titration method was completed on solvent cast films of poly(butylene glutarate) and FDL. The samples were allowed to equilibrate to the 35°C temperature and held at pH 6 for 30 minutes. During this time, no ester bond hydrolysis was observed, owing to no base being added by the auto titrator (Figure 2.3). After the addition of the enzyme stock solution was added, ester hydrolysis was immediately apparent through the addition of base by the auto titrator. Additionally, samples were aliquoted and measured on the fluorescence plate reader, and no fluorescence was detected until enzyme addition. After 75 minutes running, the amount of ester bonds being hydrolyzed began to plateau, indicating that the polymer is no longer being enzymatically degraded. It is hypothesized that the enzyme has become fully inactivated due to the changes in the pH in this unbuffered system. It is well known that enzyme stability and activity are heavily influenced by environmental factors. At this 75-minute time point, the fluorescence values also began to plateau showing that fluorescence released is directly related to the activity of the enzyme on the polymeric material.

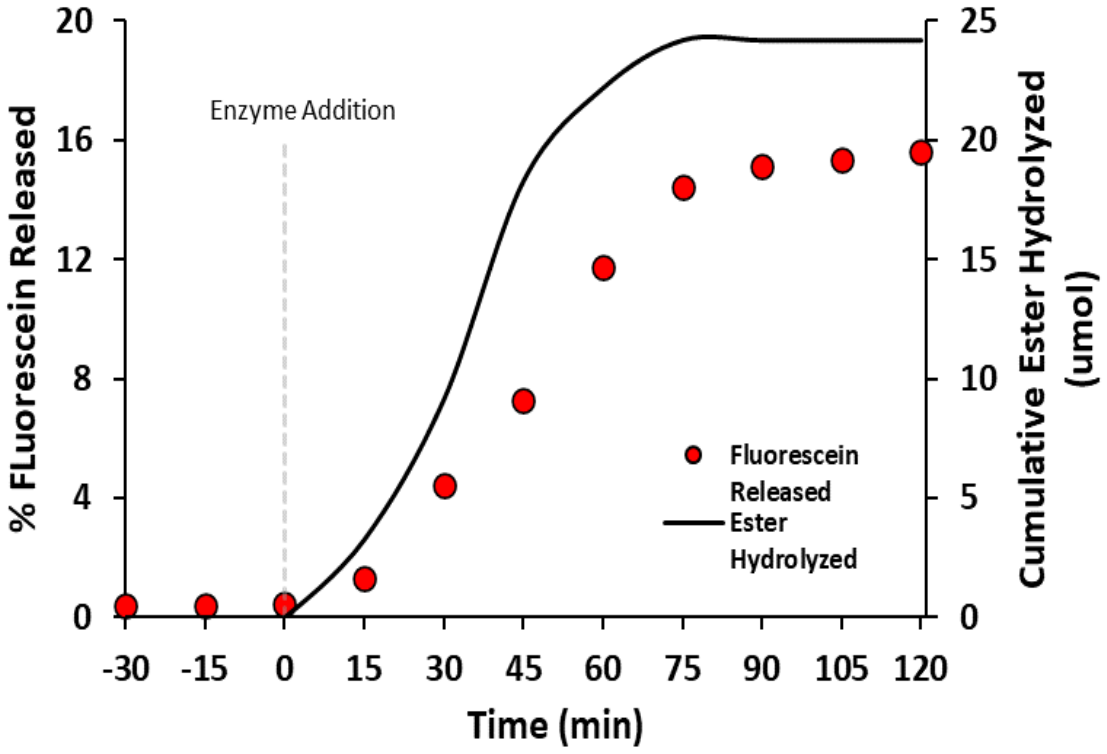

Figure 2.3 Cumulative ester bond hydrolyzed of poly(butylene glutarate) films determined by pH stat titration compared to amount of fluorescein released.

With the method now well understood from an analytical perspective and from a validation perspective, it can be applied to measure the degradation of the synthesized aliphatic polyesters. Five polyesters were screened for their susceptibility to enzymatic degradation with the hypothesis that the polyester that was most susceptible to enzymatic degradation would help produce a highly degradable polyurethane. The monomers chosen for the synthesis of the polyesters are all potentially biobased and only differ on the number of carbons along their linear chain. The synthesis of the polyesters followed a typical polycondensation methodology, resulting in high yielding and high molecular weight products (Table 2.1).

Table 2.1 Molecular weight values determined for each polyester derived from the dicarboxylic used.

Dicarboxylic Acid	Carbon Atoms in Chain	Number Average Molecular Weight (Mn)	Weight Average Molecular Weight (Mw)
Succinic Acid	4	31,105	114,266
Glutaric Acid	5	51,105	107,648
Adipic Acid	6	26,039	84,337
Azelaic Acid	9	39,034	81,490
Sebacic Acid	10	28,488	14,266

The produced aliphatic polyesters were then subjected to the fluorescent assay using the lipase of *Rhizopus Oryzae* enzyme. The testing window for these measurements was set to 8 hours – based upon previous optimization. A solution of each polymer and FDL was created using chloroform, and then solvent cast into individual wells of a 96-well plate. The samples were allowed to equilibrate at 35°C inside the plate reader and were measured for background fluorescence for one hour prior to enzyme addition. Once the enzyme solution was added at time 0, fluorescence was detected by the fluorometer, indicating the enzymatic degradation of the sample. The total amount of fluorescein released during the degradation of the polymers was determined using a standard curve and can be used as a way to directly compare each sample to determine which is more susceptible to enzymatic degradation (Figure 2.4). Poly(butylene glutarate) showed the greatest enzymatic degradation of any of the tested polyesters.

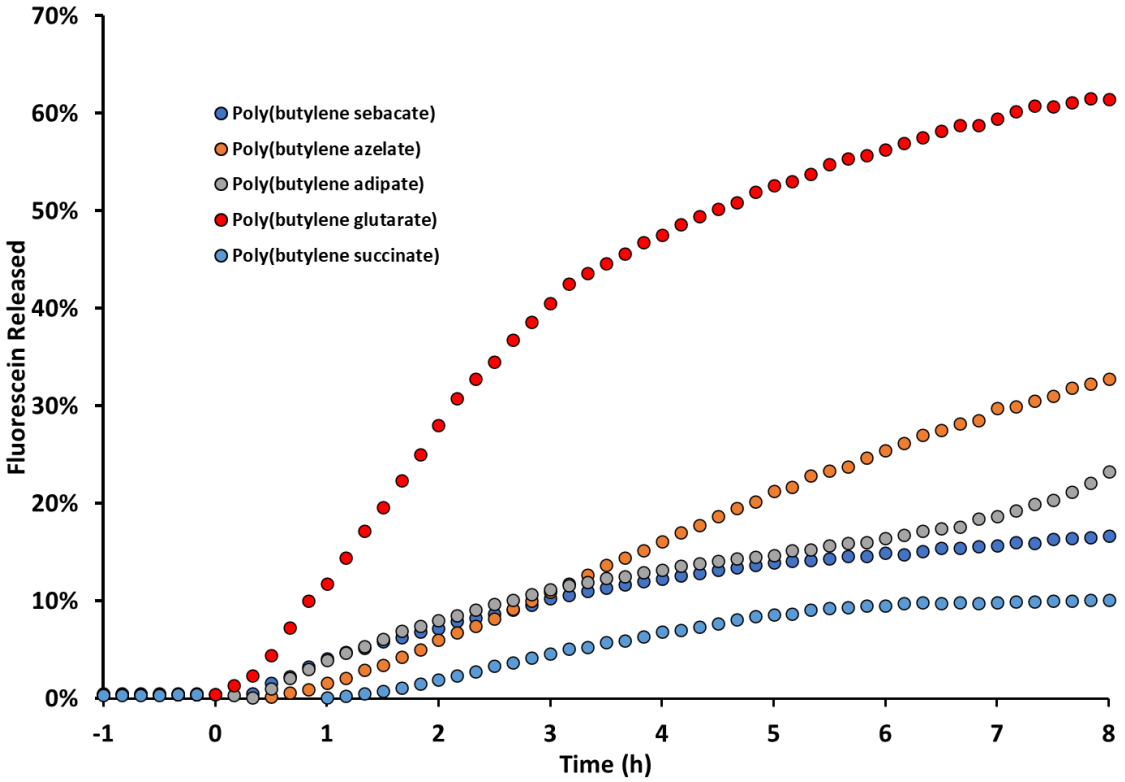

Figure 2.4 Enzymatic degradation of synthesized aliphatic polyesters by lipase from *Rhizopus Oryzae* determined using microplate assay.

Having determined a highly enzymatically degradable polymer in poly(butylene glutarate), copolymerizing glutaric acid and other diacids was explored to determine if a more degradable polymer could be produced with different physical and chemical properties. To accomplish this, succinic acid was chosen as the diacid with which glutaric acid would be copolymerized. The synthesis of these copolymers was successfully completed and produced high molecular weight polymers that were analyzed. One trend that was noted during analysis was that as glutaric acid content was increased from 0% glutaric acid, poly(butylene succinate) homopolymer, to 100% glutaric acid content, poly(butylene glutarate) homopolymer the melting temperature decreased(Figure 2.5).

This trend was disrupted at a glutaric acid content of 75%, with this material being amorphous at room temperature.

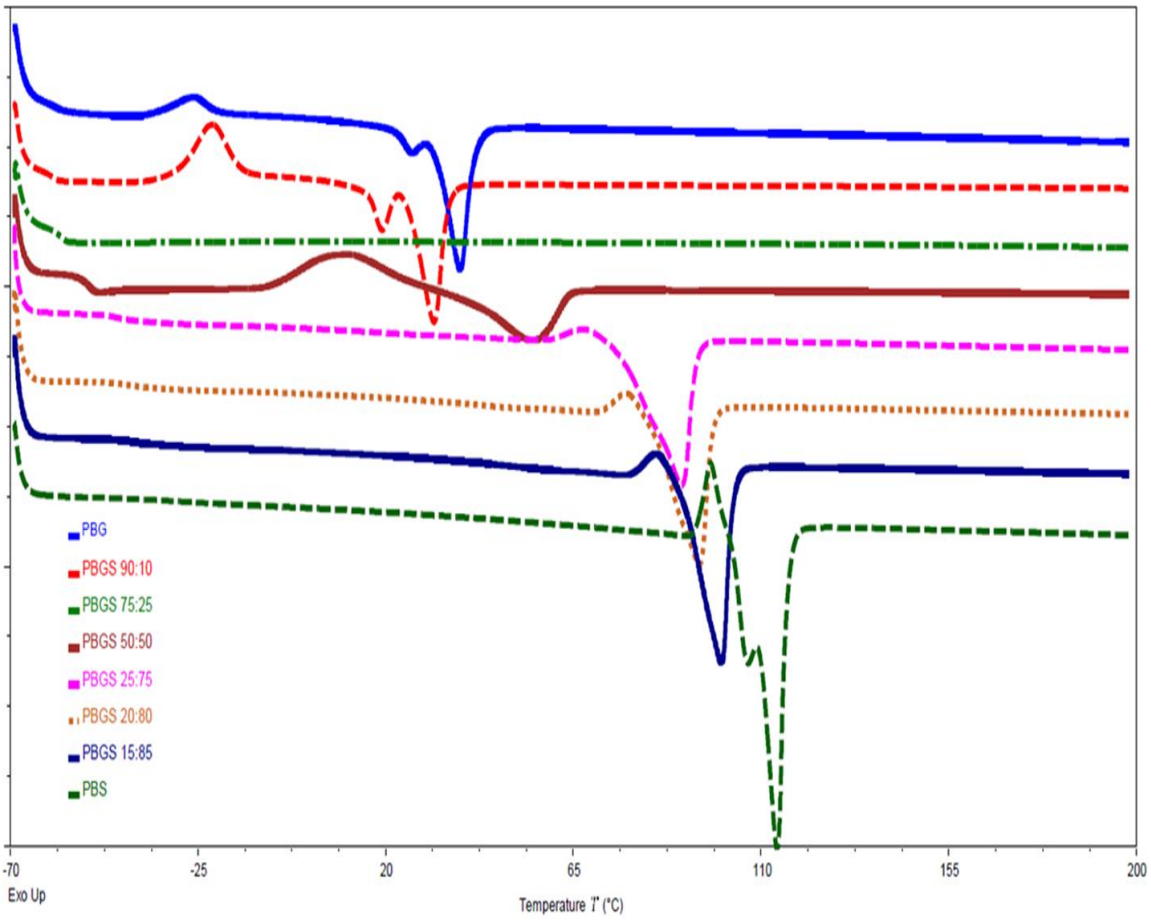

Figure 2.5 Differential scanning calorimetry curves for copolymers of poly(butylene glutarate-co-butylene succinate) showing second heating curve.

These synthesized copolymers were then measured for enzymatic degradability via the fluorescence assay. Of interest, the degradation amount increased with decreasing melting temperature (Figure). This screening elucidated the highly degradable copolymer, poly(butylene glutarate-co-butylene succinate) (PBGS) with a diacid ratio of 75:25. This copolymer ratio was chosen as the base polyester for polyurethane synthesis

due to its high enzymatic degradability and because of its amorphous nature at room temperature.

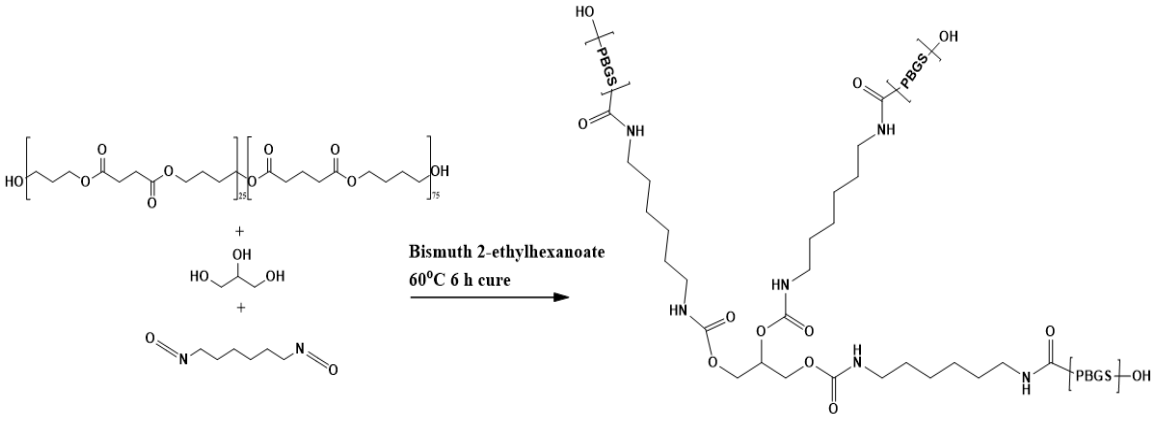

Scheme 2.1 Polyaddition reaction of hydroxy end capped polyester with hexamethylene diisocyanate and glycerol crosslinker.

The polyurethane synthesis followed a typical polyaddition mechanism with the application of a diisocyanate, hydroxy terminated monomers, and a bismuth catalyst (Scheme 2.1). The base polyester PBGS was produced as a low molecular weight, hydroxy end capped prepolymer. This prepolymer was a viscous liquid at room temperature. The three important variables that were investigated for their impact on enzymatic degradability were: type of crosslinker, amount of crosslinker, and isocyanate indexing. The isocyanate indexing is simply the ratio of isocyanate function groups to hydroxy functional groups within the polyaddition reaction. This value is important because it directly relates to the amount of urethane bonds that can potentially form. Additionally, over indexed samples can produce side reactions, producing urea, amides, biurets, and allophanates. This indexing can be calculated empirically and then applied to the monomer contents of the polymerization (Equation 2.1)

$$Index = \frac{n_{eq_{iso}}\, x\, m_{iso}}{(n_{eq_{crosslinker}}\, x\, m_{crosslinker}) + (n_{eq_{polyester}}\, x\, m_{polyester})}$$

Equation 2.1 Isocyanate indexing value determined from the equivalent weight of the hydroxy and isocyanate groups.

The crosslinkers studied were glycerol, sorbitan monooleate, and a mannan octyl urethane. The polyurethane reactions were successfully completed using a small open top reaction vessel that allowed for high sheering mixing via an overhead stirrer. The reaction could then be dispensed into a silicon release pan and cured in an oven at 60°C overnight.

Applying the fluorescence assay to the polyurethanes produced was challenging as the materials became less soluble as crosslinker content increased. To address this issue, FDL was mixed into the polyester prepolymer prior to the polyurethane production. This methodology was tested to ensure that the polyurethane production did not indirectly cleave the ester linkages in the FDL molecule and that the FDL was still able to intercalate into the polymer matrix and was held in the matrix until acted upon by the enzyme. Because of this change in the methodology and to ensure that the fluorescence assay continued to produce reliable data, validation using mass loss and pH stat titration was completed again on the crosslinked polyester polyurethanes.

Mass loss experimentation was completed using the exact same method as previously described. The polyurethane chosen for testing was a 15% sorbitan monooleate, 1.5 isocyanate indexed polyurethane. Rather than solvent casting the films when the polyurethane was being produced, it was placed in the middle of two pieces of silicon release paper and cured under pressure on a carver press at 60°C. The mass loss

experiment showed that the addition of the FDL into the prepolymer did not change the ability of the assay to measure enzymatic degradation (Figure 2.6).

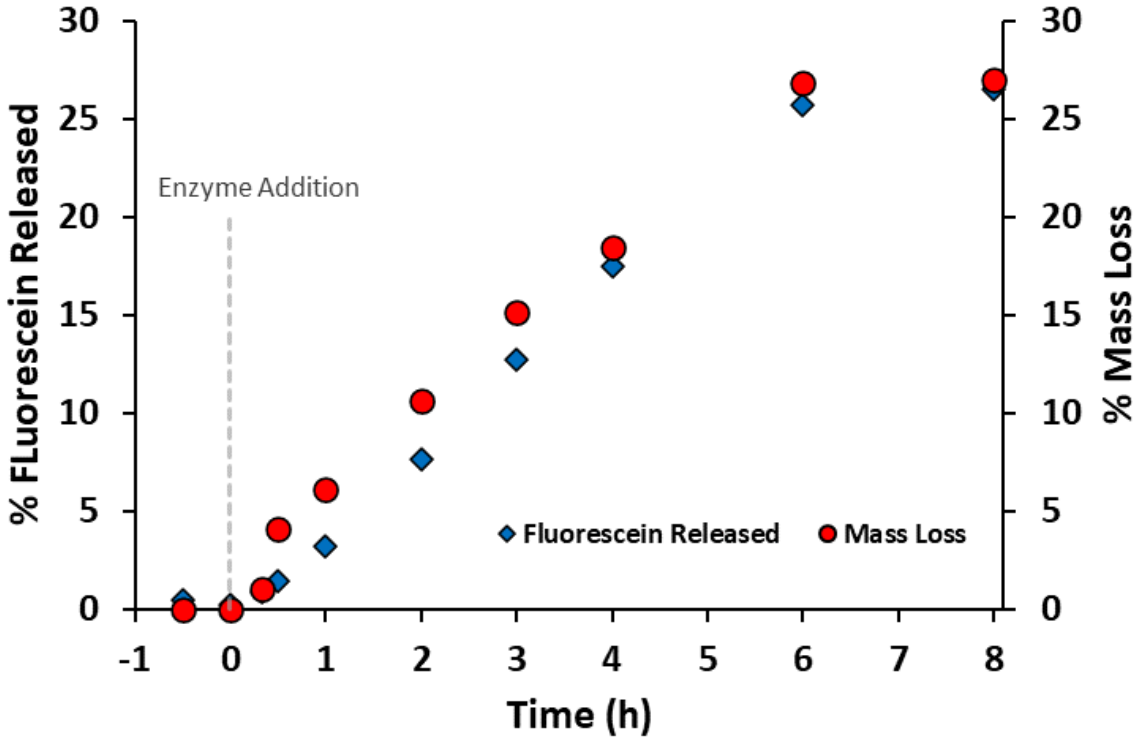

Figure 2.6 Percent mass loss of 15% sorbitan monooleate crosslinked, 1.5 isocyanate indexed polyurethane films compared to fluorescein released values.

The pH start titration validation experiments were also conducted on the 15% crosslinked, 1.5 isocyanate indexed polyurethane films. The films were produced in the same manner as outlined previously. The pH stat titration method yielded similar results as with the base polyester validation screening (Figure 2.7). The hydrolysis of ester bonds and release of fluorescent probe ceased at the 75-minute time point.

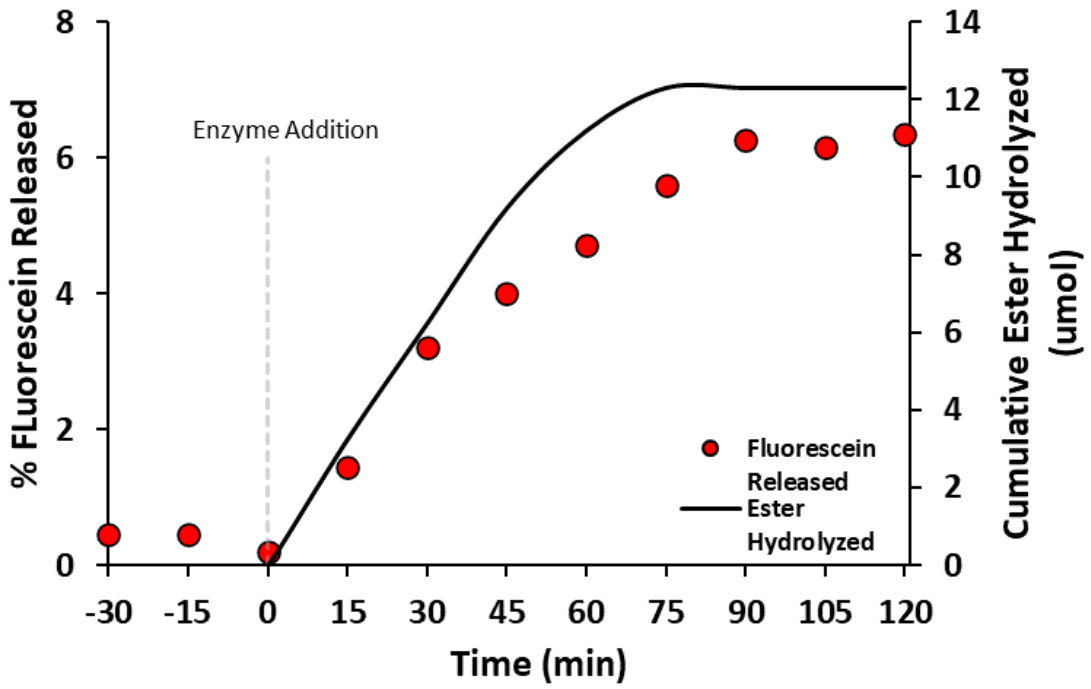

Figure 2.7 Cumulative ester bond hydrolyzed of 15% sorbitan monooleate crosslinked polyurethane films compared to fluorescein released values determined by pH stat titration.

With the new process for adding in the FDL probe validated for efficiency, the library of polyurethanes could be produced varying crosslinker type, crosslinker content, and isocyanate indexing. The physical properties of the materials varied wildly with respect to their appearance. The low isocyanate indexed samples all were paste-like and did not produce a solid material.

The fluorescence assay was run on all the polyurethane samples produced using the standard conditions detailed above (Figure 2.8). The differences the crosslinkers have on the enzymatic degradation of the produced polyurethanes is stark. The glycerol crosslinker has a major impact, showing the least enzymatic degradation of the three crosslinker. The two sugar based crosslinkers, sorbitan monooleate and mannan, were enzymatically degraded to a higher degree. When considering the amount of crosslinker

content, the trend shows that as the crosslinker content increases the enzymatic degradation decreases. This supports the idea that increased crosslinking content decreases chain mobility, which is needed for the enzymes to chain interaction. Finally, isocyanate indexing did not have any significant impact on the enzymatic degradation of the polyurethanes.

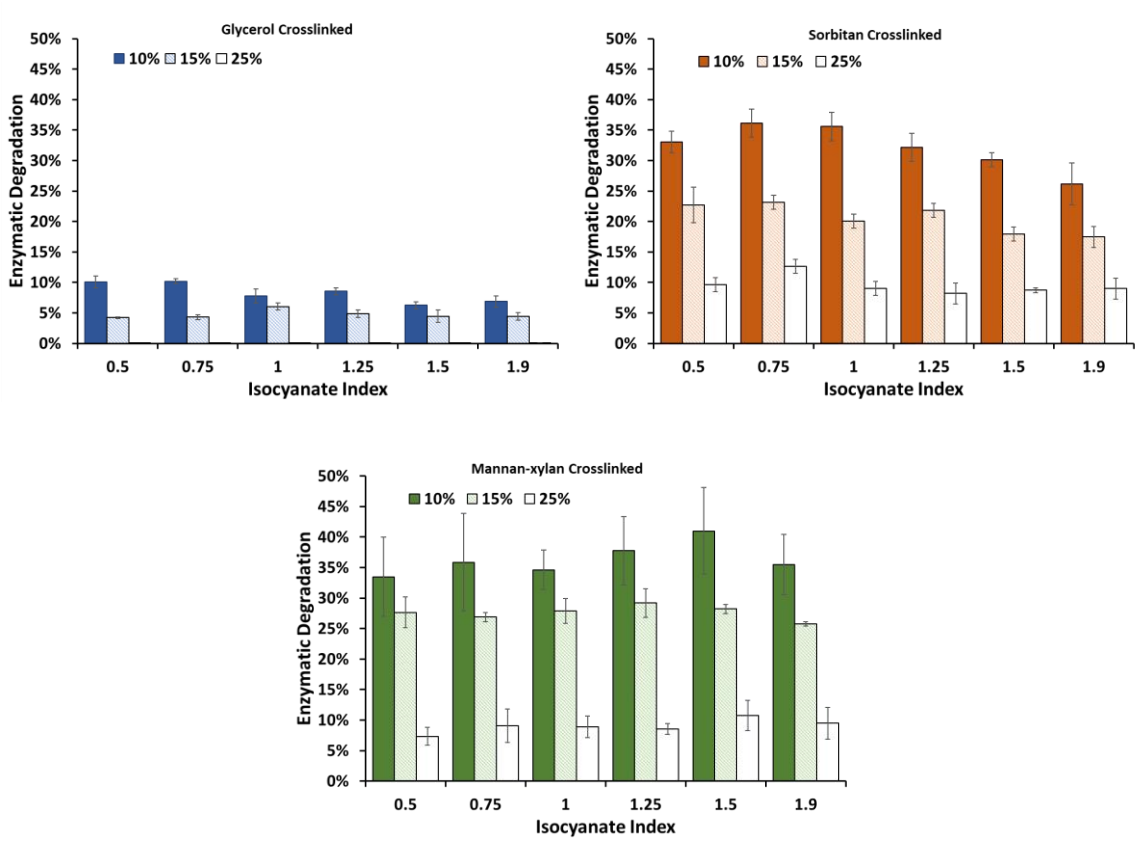

Figure 2.8 Enzymatic degradation of crosslinked polyurethanes comparing crosslinker type, crosslinker content, and isocyanate index.

Considering the library of polyurethanes measured for enzymatic degradation, the physical properties of each sample, and the end goal of producing a functional compostable material, the samples consisting of 15% crosslinker and an isocyanate indexing 1.5 were moved forward for additional mechanical and physical testing. The

impact of the crosslinking and urethane bonds to the enzymatic degradation of the base polyester are apparent (Figure 2.9).

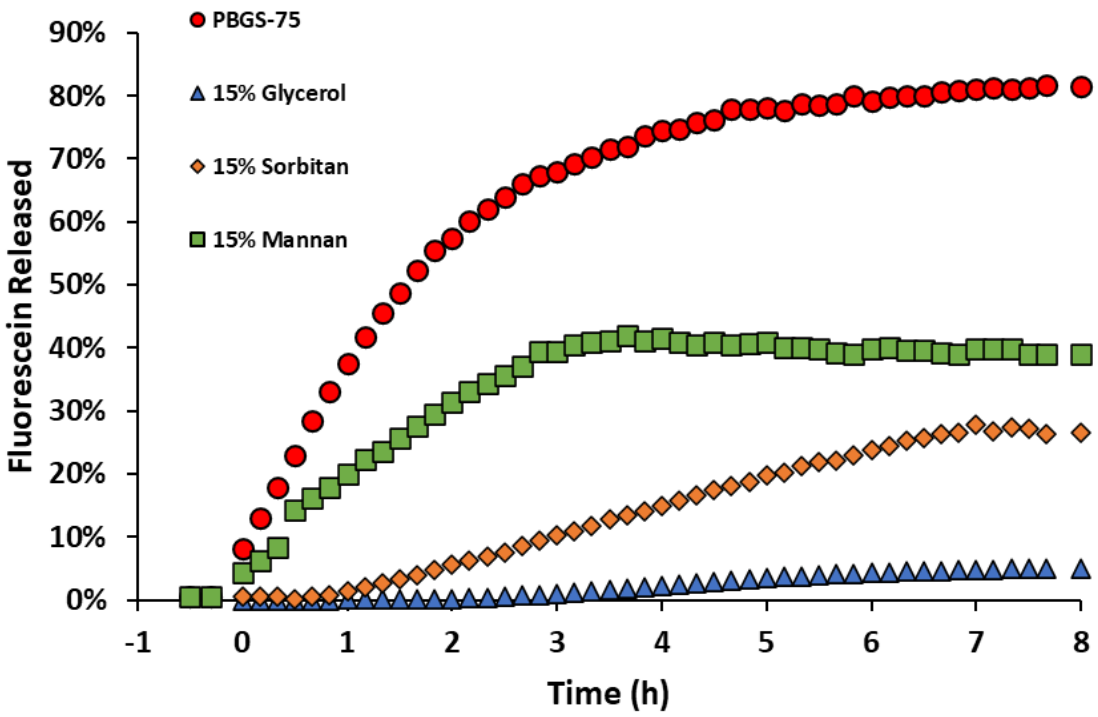

Figure 2.9 Enzymatic degradation determined via fluorescence assay of 15% crosslinker content polyurethanes and base polyester.

Scanning electron microscopy was used to view the surface degradation that should occur when the enzyme is degrading the polymer. This surface-initiated degradation is important for the fluorescence assay to function in the correct manner. The polyurethane films with 15% crosslinker were produced using a carver press, as described above. Each film was cut and placed in a flat bottom reaction vessel, PBS buffer was added, and then enzyme stock solution was added. Before and after enzymatic degradation images were taken and compared (Figure 2.10). The enzymatic degradation of the sorbitan monooleate and mannan crosslinked polyurethanes is apparent in the

before and after picture. The increase in surface roughness and the appearance of surface cracking is caused by the enzymatic breakdown of the polymers. The glycerol samples did not show any changes after the addition of the enzyme showing the low level of enzymatic degradation that is occurring.

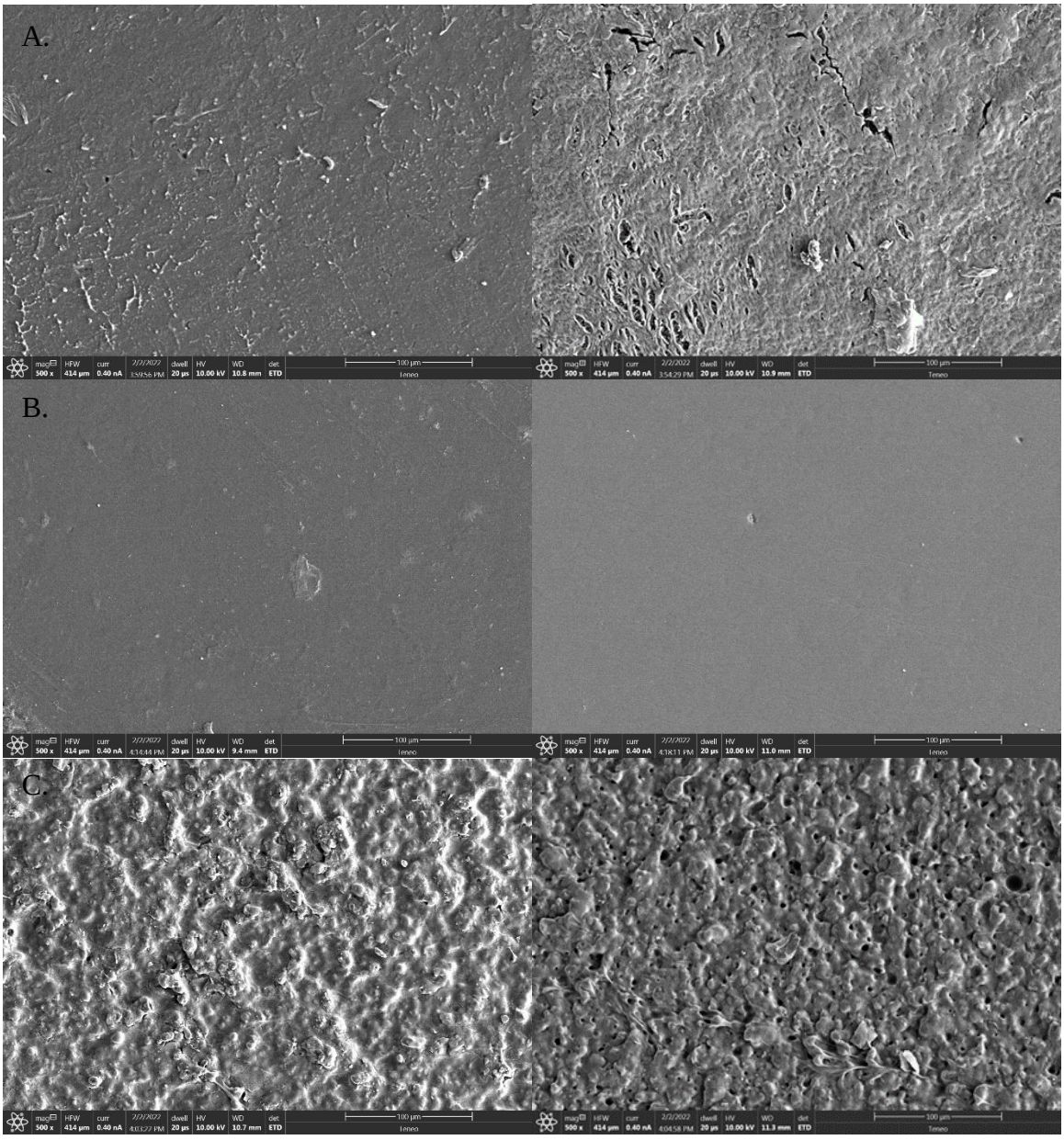

Figure 2.10 Scanning electron microscopy images of before (left) and after (right) enzymatic degradation of polyurethanes crosslinked with sorbitan monooleate (A), glycerol(B), and mannan-octyl urethane(C).

With the level of enzymatic degradability of the produced polyurethanes well understood, samples and films were made using each crosslinker for additional physical and chemical testing. The films produced using the carver press with an overnight cure

were functional materials that were optically transparent (Figure 2.11). This property is of great interest for packaging applications where the product needs to be in clear repose.

Figure 2.11 Photography of crosslinked polyurethane films using glycerol (A), sorbitan monooleate (B), and mannan-octyl urethane (C) crosslinkers.

The water vapor transmission rate (WVTR) of each produced film was measured to assess the potential for packaging applications. The 15% glycerol crosslinked polyurethanes showed the lowest water vapor transmission rate at 879.9 g/m^2 per 24 hours (Table 2.2). The sugar sorbitan monooleate and mannan both had much higher WVTR values consisting with fully transpirable materials. The level lower WVTR value for the glycerol sample is interesting as it may point to a difference in hydrophobicity that could have impacted the ability of the enzymes to interact with the surface of the polymers and therefore degrade the polymer. This potential should be investigated more using different techniques for measuring the surface chemistry of the produced polyurethane films and the interaction of the enzymes with the surfaces of the polymers based upon the differences in surface chemistry.

Table 2.2 Water vapor transmission values determined for produced 15% crosslinked polyurethane films.

	Water Vapor Transmission Rate (g/m^2 *24h)	**Water Permeability Coefficient ($g*cm/cm^2*s*Pa$)**
15% Glycerol	879.9	7.16E-13
15% Sorbitan	2662.1	2.17E-12
15% Mannan-Xylan	2223.9	1.81E-12

Tensile data was then collected for the three crosslinked polyurethane films. The three materials were very different in their tensile properties (Figure 2.12). The glycerol crosslinked polyurethane had a much high stress at break, but a lower strain at break with a Young's modulus of 27.88±2.99 MPa. The sorbitan monooleate crosslinked polyurethane film had a much higher strain at break with a lower stress at break and a Young's modulus of 11.58±0.99 MPa. The mannan-octyl urethane polyurethane film had the lowest elongation and stress at break with a Young's modulus of 5.69±1.47 MPa.

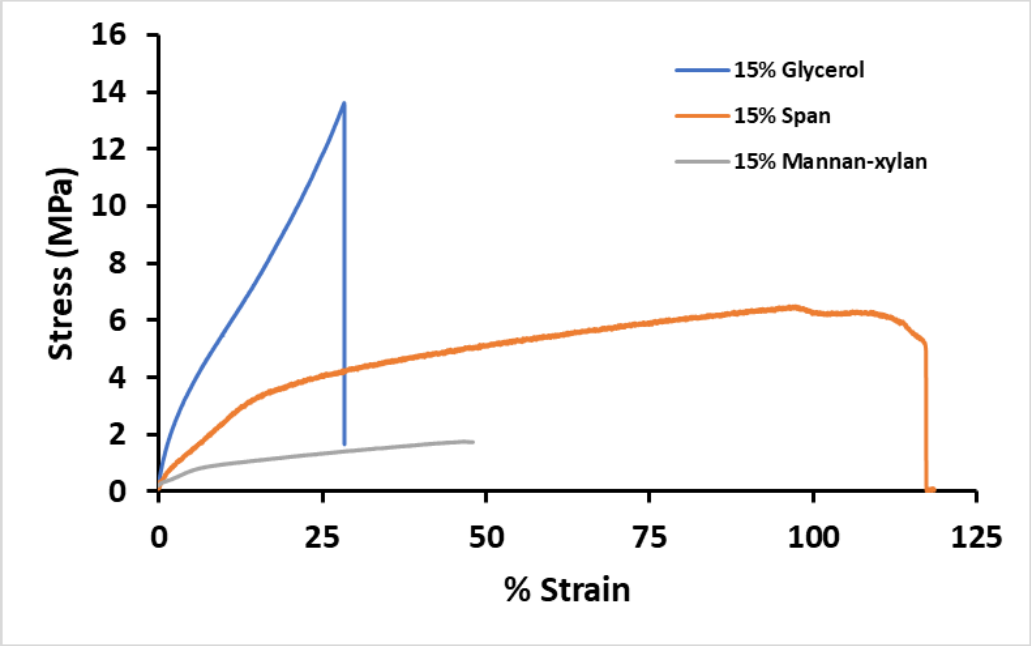

Figure 2.12 Tensile values for 15% crosslinked polyurethane films.

Having completed the enzymatic degradation testing and mechanical testing of the films, the films were submitted for respirometry testing. Respirometry testing was conducted to assess if the enzymatic assay is a useful tool in early material development as a guide towards compostability. Respirometry was completed following ASTM D5338 modified conditions. These conditions include a temperature maintained at 58±2°C and a mass balance of 6 grams compost to cellulose outline in ASTM D6400.

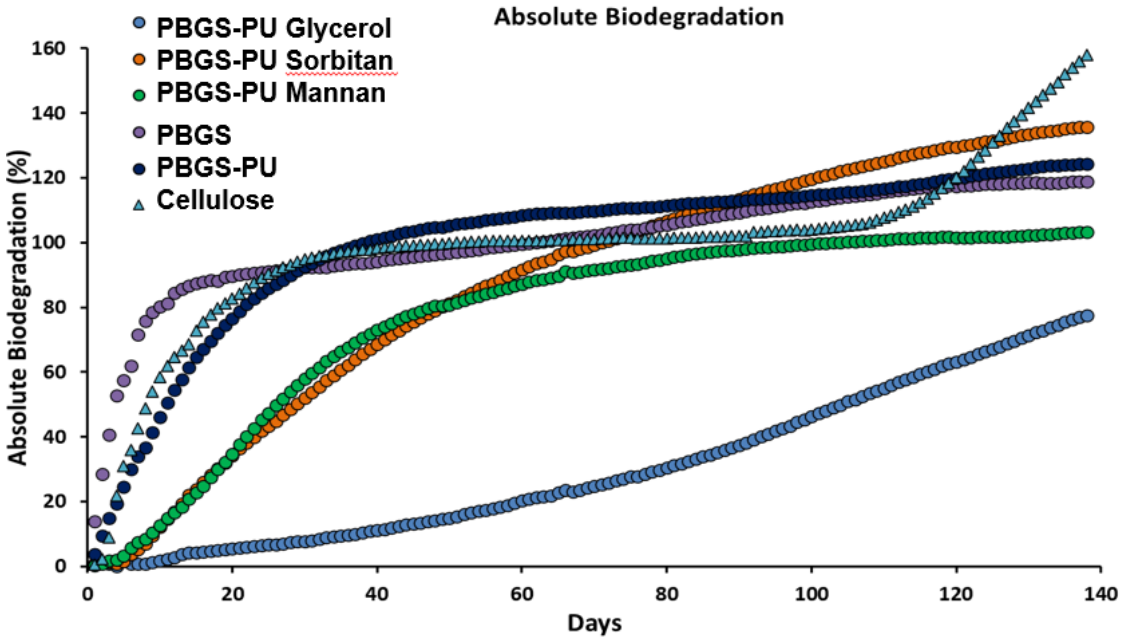

Figure 2.13 Absolute biodegradation of base polyester, linear polyurethane, and crosslinked polyurethanes using 15% crosslinker and an isocyanate index of 1.5 determined using respirometry analysis.

The standard set for an industrially compostable product is having 90% of its absolute carbon content mineralized to CO_2 within 180 days (Figure 2.13). Alternatively, the standard also allows for the material to meet the standard of 90% carbon mineralization when compared to a cellulose control (Figure 2.14). As expected, the polyester prepolymer used for the synthesis of the polyester polyurethanes was highly compostable and passed the standard by day 20. The linear polyester polyurethane that was produced from the hexamethylene diisocyanate and the polyester prepolymer met the standard at day 32. This confirms that the inclusion of urethane bonds has a negative impact on the compostability of these materials. The 15% sorbitan monooleate crosslinked sample was the first to meet the industrially compostable standard at 59 days.

Shortly after the sorbitan monooleate sample met the standard, the 15% crosslinked mannan octyl urethane sample met the standard at day 66. The respirometry analysis was not continued through the 180 mark and was instead halted at day 140. At day 140 the 15% glycerol crosslinked polyurethane had not met the requirement to be labeled as industrially compostable with a final absolute biodegradation value of 77.5%.

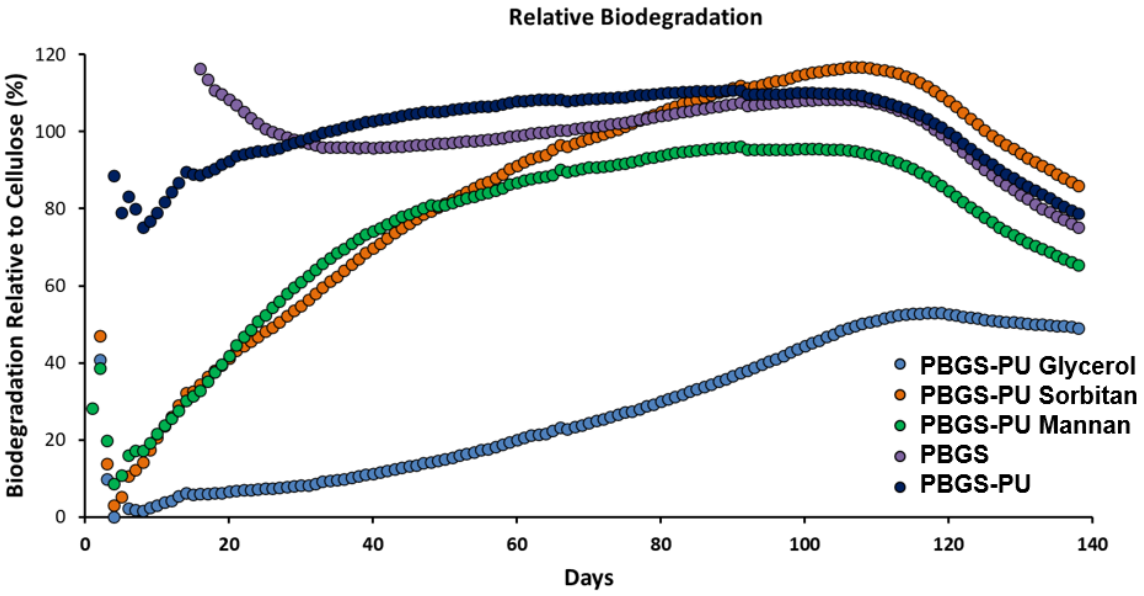

Figure 2.14 Relative biodegradation of base polyester, linear polyurethane, and crosslinked polyurethanes using 15% crosslinker and an isocyanate index of 1.5 determined using respirometry analysis.

Conclusion

A fluorescence-based enzymatic degradation assay was successfully produced and applied to measure the enzymatic degradation of crosslinked polyurethanes. The assay was used as a guiding tool for the synthesis of a highly enzymatically degradable prepolymer poly(butylene glutarate-co-butylene succinate). This prepolymer was then applied to the production of crosslinked polyester polyurethanes with an emphasis on the

impact of crosslinker type, crosslinker content, and isocyanate indexing on the enzymatic degradation of these materials. Samples were then studied under industrial composting conditions using respirometry analysis, and it was determined that the assay for these materials was a useful guiding tool towards compostability.

References

(1) Foundation, E. M. The New Plastics Economy: Rethinking the Future of Plastics. 2016.

(2) Geyer, R.; Jambeck, J. R.; Law, K. L. Production, use, and fate of all plastics ever made. *Science Advances* **2017**, *3* (7), e1700782. DOI: doi:10.1126/sciadv.1700782.

(3) (ACC), A. C. C. *Resin Review: The Annual Statistical Report of the North Ameican Platics Industry*; ACC, 2009.

(4) Brooks, A. L.; Wang, S. L.; Jambeck, J. R. The Chinese import ban and its impact on global plastic waste trade. *Science Advances* **2018**, *4* (6). DOI: 10.1126/sciadv.aat0131.

(5) Geyer, R.; Jambeck, J. R.; Law, K. L. Production, use, and fate of all plastics ever made. *Science Advances* **2017**, *3* (7). DOI: 10.1126/sciadv.1700782.

(6) Liu, E. K.; He, W. Q.; Yan, C. R. 'White revolution' to 'white pollution'-agricultural plastic film mulch in China. *Environmental Research Letters* **2014**, *9* (9). DOI: 10.1088/1748-9326/9/9/091001.

(7) Okada, M. Chemical syntheses of biodegradable polymers. *Progress in Polymer Science* **2002**, *27* (1), 87-133. DOI: 10.1016/s0079-6700(01)00039-9.

(8) Auras, R.; Harte, B.; Selke, S. An overview of polylactides as packaging materials. *Macromolecular Bioscience* **2004**, *4* (9), 835-864. DOI: 10.1002/mabi.200400043.

(9) Ragauskas, A. J.; Williams, C. K.; Davison, B. H.; Britovsek, G.; Cairney, J.; Eckert, C. A.; Frederick, W. J.; Hallett, J. P.; Leak, D. J.; Liotta, C. L.; et al. The path forward for biofuels and biomaterials. *Science* **2006**, *311* (5760), 484-489. DOI: 10.1126/science.1114736.

(10) O'Keefe, B. J.; Hillmyer, M. A.; Tolman, W. B. Polymerization of lactide and related cyclic esters by discrete metal complexes. *Journal of the Chemical Society-Dalton Transactions* **2001**, (15), 2215-2224. DOI: 10.1039/b104197p.

(11) Bourissou, D.; Moebs-Sanchez, S.; Martin-Vaca, B. Recent advances in the controlled preparation of poly(alpha-hydroxy acids): Metal-free catalysts and new monomers. *Comptes Rendus Chimie* **2007**, *10* (9), 775-794. DOI: 10.1016/j.crci.2007.05.004.

(12) Hormnirun, P.; Marshall, E. L.; Gibson, V. C.; White, A. J. P.; Williams, D. J. Remarkable stereocontrol in the polymerization of racemic lactide using aluminum initiators supported by tetradentate aminophenoxide ligands. *Journal of the American Chemical Society* **2004**, *126* (9), 2688-2689. DOI: 10.1021/ja038757o.

(13) Anderson, K. S.; Lim, S. H.; Hillmyer, M. A. Toughening of polylactide by melt blending with linear low-density polyethylene. *Journal of Applied Polymer Science* **2003**, *89* (14), 3757-3768. DOI: 10.1002/app.12462.

(14) Narancic, T.; Verstichel, S.; Chaganti, S. R.; Morales-Gamez, L.; Kenny, S. T.; De Wilde, B.; Padamati, R. B.; O'Connor, K. E. Biodegradable Plastic Blends Create New Possibilities for End-of-Life Management of Plastics but They Are Not a Panacea for Plastic Pollution. *Environmental Science & Technology* **2018**, *52* (18), 10441-10452. DOI: 10.1021/acs.est.8b02963.

(15) Chae, Y.; An, Y. J. Current research trends on plastic pollution and ecological impacts on the soil ecosystem: A review. *Environmental Pollution* **2018**, *240*, 387-395. DOI: 10.1016/j.envpol.2018.05.008.

(16) Xanthos, D.; Walker, T. R. International policies to reduce plastic marine pollution from single-use plastics (plastic bags and microbeads): A review. *Marine Pollution Bulletin* **2017**, *118* (1-2), 17-26. DOI: 10.1016/j.marpolbul.2017.02.048.

(17) Kaur, G.; Uisan, K.; Ong, K. L.; Lin, C. S. K. Recent Trends in Green and Sustainable Chemistry & Waste Valorisation: Rethinking Plastics in a circular economy. *Current Opinion in Green and Sustainable Chemistry* **2018**, *9*, 30-39. DOI: 10.1016/j.cogsc.2017.11.003.

(18) To, M. H.; Uisan, K.; Ok, Y. S.; Pleissner, D.; Lin, C. S. K. Recent trends in green and sustainable chemistry: rethinking textile waste in a circular economy. *Current Opinion in Green and Sustainable Chemistry* **2019**, *20*, 1-10. DOI: 10.1016/j.cogsc.2019.06.002.

(19) Zumstein, M. T.; Narayan, R.; Kohler, H.-P. E.; McNeill, K.; Sander, M. Dos and Do Nots When Assessing the Biodegradation of Plastics. *Environmental Science & Technology* **2019**, *53* (17), 9967-9969. DOI: 10.1021/acs.est.9b04513.

(20) Zumstein, M. T.; Kohler, H.-P. E.; McNeill, K.; Sander, M. High-Throughput Analysis of Enzymatic Hydrolysis of Biodegradable Polyesters by Monitoring Cohydrolysis of a Polyester-Embedded Fluorogenic Probe. *Environmental Science & Technology* **2017**, *51* (8), 4358-4367. DOI: 10.1021/acs.est.6b06060.

(21) Mistry, A. N.; Kachenchart, B.; Pinyakong, O.; Assavalapsakul, W.; Jitpraphai, S. M.; Somwangthanaroj, A.; Luepromchai, E. Bioaugmentation with a defined bacterial consortium: A key to degrade high molecular weight polylactic acid during traditional composting. *Bioresource Technology* **2023**, *367*. DOI: 10.1016/j.biortech.2022.128237.

(22) Gathman, T.; Schoephoerster, J.; Vasdev, R.; Liffland, S.; Batiste, D.; Amer Soc Mech, E. EVALUATION OF SUSTAINABLE P4MCL/PLLA BLOCK COPOLYMERS AS PVC REPLACEMENT IN MEDICAL PLASTICS. In *Design of Medical Devices Conference (DMD) held as part of the Institute-for-Engineering-in-Medicine's Innovation Week*, Minneapolis, MN, Apr 11-14, 2022; 2022.

(23) Kalita, N. K.; Hakkarainen, M. Integrating biodegradable polyesters in a circular economy. *Current Opinion in Green and Sustainable Chemistry* **2023**, *40*. DOI: 10.1016/j.cogsc.2022.100751.

(24) Jia, Z. W.; Li, Y. J.; Wu, J. C. Sequence-Controlled Alternating Copolyesters Synthesis via Selective Ring-Opening Polymerization. *Macromolecular Chemistry and Physics* **2021**, *222* (24). DOI: 10.1002/macp.202100323.

(25) Batiste, D. C.; De Hoe, G. X.; Nelson, T. F.; Sodnikar, K.; McNeill, K.; Sander, M.; Hillmyer, M. A. Site-Specific Mineralization of a Polyester Hydrolysis Product in Natural Soil. *Acs Sustainable Chemistry & Engineering* **2022**, *10* (4), 1373-1378. DOI: 10.1021/acssuschemeng.1c07948.

(26) Fournier, L.; Mirabal, D. M. R.; Hillmyer, M. A. Toward Sustainable Elastomers from the Grafting-Through Polymerization of Lactone-Containing Polyester Macromonomers. *Macromolecules* **2022**, *55* (3), 1003-1014. DOI: 10.1021/acs.macromol.1c02349.

(27) Geyer, R.; Kuczenski, B.; Zink, T.; Henderson, A. Common Misconceptions about Recycling. *Journal of Industrial Ecology* **2016**, *20* (5), 1010-1017. DOI: 10.1111/jiec.12355.

(28) Cooper, D. R.; Skelton, A. C. H.; Moynihan, M. C.; Allwood, J. M. Component level strategies for exploiting the lifespan of steel in products. *Resources Conservation and Recycling* **2014**, *84*, 24-34. DOI: 10.1016/j.resconrec.2013.11.014.

(29) Dris, R.; Gasperi, J.; Mirande, C.; Mandin, C.; Guerrouache, M.; Langlois, V.; Tassin, B. A first overview of textile fibers, including microplastics, in indoor and outdoor environments. *Environmental Pollution* **2017**, *221*, 453-458. DOI: 10.1016/j.envpol.2016.12.013.

(30) Murakami, S.; Oguchi, M.; Tasaki, T.; Daigo, I.; Hashimoto, S. Lifespan of Commodities, Part I. *Journal of Industrial Ecology* **2010**, *14* (4), 598-612. DOI: 10.1111/j.1530-9290.2010.00250.x.

(31) Kuczenski, B.; Geyer, R. Material flow analysis of polyethylene terephthalate in the US, 1996-2007. *Resources Conservation and Recycling* **2010**, *54* (12), 1161-1169. DOI: 10.1016/j.resconrec.2010.03.013.

(32) Linzner, R.; Salhofer, S. Municipal solid waste recycling and the significance of informal sector in urban China. *Waste Management & Research* **2014**, *32* (9), 896-907. DOI: 10.1177/0734242x14543555.

(33) Jambeck, J. R.; Geyer, R.; Wilcox, C.; Siegler, T. R.; Perryman, M.; Andrady, A.; Narayan, R.; Law, K. L. Plastic waste inputs from land into the ocean. *Science* **2015**, *347* (6223), 768-771. DOI: 10.1126/science.1260352.

(34) Mutha, N. H.; Patel, M.; Premnath, V. Plastics materials flow analysis for India. *Resources Conservation and Recycling* **2006**, *47* (3), 222-244. DOI: 10.1016/j.resconrec.2005.09.003.

(35) Davis, J.; Geyer, R.; Ley, J.; He, J.; Clift, R.; Kwan, A.; Sansom, A.; Jackson, T. Time-dependent material flow analysis of iron and steel in the UK Part 2. Scrap generation and recycling. *Resources Conservation and Recycling* **2007**, *51* (1), 118-140. DOI: 10.1016/j.resconrec.2006.08.007.

(36) Hoornweg, D.; Bhada-Tata, P.; Kennedy, C. Waste production must peak this century. *Nature* **2013**, *502* (7473), 615-617. DOI: 10.1038/502615a.

CHAPTER 3

SYNTHESIS AND FORMULATION OF A HOME COMPOSTABLE PRESSURE SENSITIVE ADHESIVE FOR PRODUCE LABELS[2]

[2]Ethan Stinchcomb, Jason Locklin

To be submitted to ACS Sustainable Chemistry and Engineering.

Abstract

Home compostable materials as an alternative waste stream for polymeric materials can be highly effective depending upon the material application. Packing and labeling that directly contacts food is a prime example of an application where home composting the product after use would be highly advantageous. In this work, a home compostable pressure sensitive adhesive for direct food contact produce labeling was produced. Following different synthetic techniques to modify adhesive, viscoelastic, and thermal properties the polymer produced was tailored to the application. Home compostability of the produce material was determined via respirometry analysis confirming its highly degradable nature. The polymer was then scaled to a pilot reactor size producing 200kgs of material and addressing the scalability of the material production. The produced material was then applied in an industrial hot melt coating trail where rolls of adhesive coated material were produced. These rolls were converted into produce labels using a commercial printing and dye cutting press. The labels were then applied using an automated labeling machine and scored based upon their adhesive properties.

Introduction

Pressure sensitive adhesives (PSAs) are used in a wide variety of applications such as tapes, labels, stamps, and sticky notes due to their tunable adhesion that is applied under minimal force.[1-5] The global market for PSAs is approximately 10 billion USD per year with a growth rate of ~10% annually. The majority of current commercial PSAs are nondegradable and produced from petroleum feedstocks.[3, 5-7] PSAs are composed of two main components, a polymeric backbone that comprises the bulk of the material and small molecule tackifiers that promote adhesion and instant tack. These polymeric structures are primarily acrylic, triblock styrenics, or natural rubber that rely on physical and chemical crosslinking to modulate the chemical and mechanical properties of the adhesive.[8-13]

The production of plastic materials has skyrocketed over the past fifty years, outpacing the production of any other manufactured material.[14-19] This ever-increasing production of plastic has led to an emphasis on the end-of-life fate for the materials. One avenue for addressing this issue is to replace current nondegradable commodity plastics with compostable alternatives. This movement has been most prevalent in the packaging sector, especially targeting single use plastic items such as bags, clamshells, utensils, and straws. The majority of these products are composed of thermoplastic materials which have been the main focus for these compostable products. Adhesives that hold these packages together including cold seal adhesives, laminate adhesives, and pressure sensitive adhesives have not found the same level of interest. The commercial adhesives

that are available are difficult to work with, have lower performance than their nondegradable counterparts, and are only degradable under industrial composting conditions.[20-23] For the PSA market, the availability of commercial compostable options is even slimmer, with no home compostable options available on the market.

Making a polymer, especially a polymer with high crystallinity, home compostable is very difficult when compared to targeting industrially compostable. The classic example is polylactic acid which is a highly crystalline thermoplastic that is industrially compostable.[24-28] This material will degrade under the higher temperature found in industrial compost because it allows for the breakdown of the crystalline lattice of the polymer. At the lower temperatures found in home compost this cannot occur and therefore will never fully degrade. If a product is home compostable, it is more than likely going to be industrially compostable as well.

Home compost degradable materials are a growing market of products that are finding niche applications.[27-31] Similar to industrial compostable materials, home compostable products have focused on the packaging sector. One potentially lucrative market for home compostable products is takeout food containers. With food takeout containers there is significant organic contamination from food that was placed in the container. This contamination would be potentially damaging to recycling streams, but for home composting it would have no negative impact on the compost. Another large swath of products that could become home compostable are shipping boxes, envelopes, and mailers. One major hurdle to overcome for these products is the amount of adhesive that is used during their construction. For a cardboard shipping box all sides are typically sealed using a tape that is coated with a PSA. For recycling some manufacturers have

produced a water-soluble adhesive that is conducive to the repulping process, but this also causes issues with adhesive failure in moist environments. As an alternative to recycling, these packages could be shredded and placed into a home compost bin. Another interesting application that home compostable materials could fill is labels and wrapping of produce. Unfortunately, there is currently no home compostable PSA that can meet these needs.

Produce labeling is an industry standard that helps to differentiate each fruit or vegetable through its price look up (PLU) code.[32, 33] These codes help to differentiate between different grades of the same type of fruit, such as apples that may be small, medium, or large and also from different varieties of apples such as gala, honey crisp, or cosmic crisp. These PLU codes were implemented in 1990 by the International Federation of Produce Standards to help grocers stock and sell more produce. These labels progressed to also including a universal product code (UPC) to allow for scanning of produce at grocery store checkout.[34, 35] With the increase in forced self-checkout and the reduction in employee staffed checkout lanes the labeling of these items has become even more important. Due to this increase in self-checkout, stores have started to require a larger amount of produce be labeled to ensure customers are paying the correct amount for each item. Aside from this practical need for produce labeling, the labels also help to differentiate the growers and producers of these products. For instance, this allows a consumer to know what brand of banana they are buying rather it be from Dole, Chiquita, or Del Monte. These producers are very interested in maintaining this type of brand recognition for their products through labeling.

Produce labeling comes with several strict requirements to meet the application needs and also to meet regulatory and safety requirements. The adhesive used in these labels will have direct contact with a multitude of produce surfaces that may or not be consumed by the end users, therefore the adhesive has to fully debond without leaving any residue. This is complicated by the different surfaces that will need to be adhered to. For instance, an apple will have a rather smooth surface while a banana will have a highly porous surface, and a kiwi will have a hair rough surface. Additionally, some produce items are coated during packing to improve freshness, clean any debris, and apply bactericide. Regulatory requirements for food contact approval are another hurdle that will need to be addressed before commercialization can be completed.

Internal cohesive strength of an adhesive dictates its failure mode as either cohesive failure or adhesive failure. During adhesive failure, the interfacial tension between the adhesive and the surface it is adhered to is lower than the internal tension between the adhesives molecular chains allowing complete debonding of the adhered and adhesive to occur. Having lower cohesive forces compared to adhesive forces causes cohesive failure causing the adhesive to fracture internally causing debonding between the adhesive and adhered to partially or not occur. This causes adhesive to remain on the surface after debonding occurs, which can be a major failure depending on application of the adhesive.

Improving the cohesive strength of the chosen aliphatic polyester will be challenging as increasing the cohesive strength of the polymer network will also decrease the inherent tack of the polymer due to changes in the flow state of the polymer. Adding crosslinking or branching points within the polymer will dramatically improve the

cohesive strength of our polymer but will also impact its compostability, physical and chemical properties. Two approaches will be explored for crosslinking our aliphatic polyester.

In this work a food contact safe pressure sensitive adhesive will be produced from a series of polymers. The produced adhesives will be characterized for their physical and material properties and compared to current commercial PSAs. The synthesis of the adhesive will be optimized and scaled to a pilot scale reactor. The produced material will then be applied in an industrial hot melt coating trial to produce rolls of coated films. Finally, the rolls will be converted into produce labels and tested on produce using labeling machines.

Experimental

Nuclear Magnetic Resonance

NMR spectroscopy data was obtained at the University of Georgia Complex Carbohydrate Research Center using a combination of 500 MHz Varian DD with 5mm CH probe, Varian DD 600 MHz with 5mm HCN cold probe and sample carousel, Bruker NEO 800 MHz with 1.7mm TCI HCN cryoprobe and sample jet, and Bruker NEO 900 MHz with 5 mm TXO CNH cryoprobe. Samples were prepared using appropriate deuterated solvent. All NMR data was analyzed using Nova software (Mestrelab Research).

Different Scanning Calorimeter (DSC)

DSC experiments were completed using a TA Instruments DSC 250. Samples weighing 8-12 mg were loaded into sealed aluminum pans. Thermal hysteresis was removed through an initial heating to 120 °C. A cooling ramp was then completed to -50°C at 10°C/min. The sample was then heated at 10°C/min to 40°C.

Isothermal experiments were run in a similar fashion. Thermal history was removed through heating to 120 °C, samples were cooled to -50°C and held isothermally for 1 hour. The samples were then heated to 40°C at 10°C/min.

Hot Melt Blade Coating

Samples were produced using a hot melt blade coater and laminator (HLCL-1000,ChemInstruments). The instrument was set up with a siliconized backing paper running through the blade coater. The heater was set to the desired temperature 300-400°F and allowed to equilibrate for 20 minutes. Sample was placed in the heated trough of the blade coater and allowed to equilibrate for 10 minutes, unless otherwise stated. The thickness of the coating was adjusted using the thickness gauges attached to the blade coater. Thickness was varied across the samples as described. Using the mechanized rolling from the attached laminator the siliconized paper was pulled through the blade coater at a speed of 60ft/min, unless otherwise stated, metering the sample into a controlled thickness. The adhesive coated silicon was then laminated to a face film of choice at a pressure of 70psi.

Loop Tack Testing

A 1 inch wide strip of adhesive coated film was cut to a length of 12 inches. Using a loop tack testing rig from Stable Micro Systems, the test sample was made into a teardrop shape and mounted into the upper grip of the texture analyzer (TA XT plus-100,

Stable Micro Systems). A freshly isopropanol cleaned glass slide was affixed to the base of the rig. The looped sample was slowly lowered at 5mm/sec onto the glass slide creating a 1 inch x 1 inch contact space between the adhesive and the glass slide. The sample was held in this position for 10 seconds and then the sample was pulled in extension at 5mm/sec. The loop tack force was recorded as the peak force measurement. Each sample was tested in triplicate and averaged across the sample set.

90° Peel Test

A 1 inch wide x 12 inch long sample of adhesive coated sample was cut. The strip was adhered to a freshly isopropanol cleaned glass panel that was secured into a 90° testing rig from Stable Micro Systems. One end of the sample was clamped into the upper grip of the texture analyzer (TA XT Plus-100, Stable Micro Systems). The sample was pulled at a constant rate of 5mm/sec for 100mm. Peel data was determined as an average value over the pull area. Each sample was tested in triplicate and averaged across the sample set.

Drop Shape Analysis

Drop shape analysis of target films and substrates was completed using a Kruss DSA100. Surface energy calculations were completed through the application of the sessile drop method. Using water, diiodomethane, and ethylene glycol samples were measured through the application of liquid drops to the surface of a sample. Each drop was measured for its contact angle to the surface. The drops were taken for each liquid sample and averaged. Using the

Infrared Spectroscopy

Infrared spectroscopy was completed using a Nicolet 6700 (Thermo Electron Corporation). Residue upon debonding was measured for the base adhesive and blended samples. Sample adhesive was pressed into the sample stage under moderate pressure and then allowed to sit for a set time frame, typically 1 minute. The sample was then removed as a solid chunk from the sample stage. Any residue after debonding was measured using percent transmission values after 64 scans in the range of 4000-650 cm^{-1} with a spectral resolution of 4 cm^{-1} using OMNIC software.

Extrusion Blending

Extrusion blending was completed on a Thermo Fisher HAAKE Minilab II conical twin screw extruder. Seven gram samples of adhesive and additive were fed into the extruder at 60°C and allowed to cycle for 5 minutes prior to being extruded from the instrument. High temperature extrusion was used for additives that possessed a higher melting point.

Brookfield Viscometer

Sample viscosity was measured using a Brookfield Viscometer with an attached Thermosel heating chamber. Measurements were taken using a SC4-27 spindle and a testing speed of 1 rpm. Temperature ranges varied across testing from 300-400 °F. Samples weighing 10g were placed in a cylindrical sample holder from Brookfield Scientific and placed into the Thermosel heating chamber and allowed to equilibrate for 5 minutes. Viscosity measurements were taken every 10 seconds over the testing timeframe and plotted.

Results and discussion

To address the need for a home compostable pressure sensitive adhesive, a polymer was targeted as the base polymer architecture. This polymer was chosen based on previous work where it was determined that the material was highly degradable under composting conditions, it possessed a low glass transition temperature, and was amorphous at room temperature. Because the material was amorphous at room temperature the material was able to freely flow upon contact giving it a high level of instant tack.

The main issue with the material was that it had very little cohesive strength. For a pressure sensitive adhesive that is considered removable the cohesive strength must be higher than the adhesive strength. This would allow for the material to debond from the surface without leaving any residue behind. Crosslinking will increase the entanglements of the polymer chains increasing the cohesion of the adhesive.

The synthesis of the polymeric pressure sensitive adhesive began through the screening of different crosslinkers that could be applied during polymerization or post polymerization. Adding crosslinking or branching points within the polymer will dramatically improve the cohesive strength of our polymer but will also impact its compostability, physical and chemical properties.

Screening of crosslinker content began at 1% and was increased from there to determine the concentration that was needed to maintain the natural tack of the polymer but also to increase the cohesive strength enough to ensure clean debonding. After a library of these polymers were produced, they were qualitatively characterized based on several factors including tack, cohesion, and flowability (Table 3.1). After examining these produced materials, it became apparent that a crosslinker content above 3% would

not be viable as the base polymer for an adhesive. Therefore, additional work was done to produce samples below 3% crosslinker content.

Table 3.1 Characteristics of synthesized crosslinked adhesives.

% Crosslinker 1	Tack	Flow	Residue	Cohesion	Solubility
5%	None	None	N/A	Gel	Gel
3%	None	None	N/A	Gel	Gel
1.5%	None	None	None	High	Low Acetone, chloroform
1%	None to skin, tacky to metal and glass	Low	None	High	Soluble
0.75%	Tacky	Moderate	Residue	Low	Soluble

The flow state of these materials was further investigated using parallel plate rheology experiments. The samples were measured at room temperature across a range of frequency values to investigate the loss and storage moduli. These values can be compared to the Dahlquist Criteria, which is a good rule of thumb for a pressure sensitive adhesive. The Dalquist Criteria states that a material with a storage modulus below 0.3 MPa at 1 Hz will have the stiffness and flexibility that is required for a pressure sensitive adhesive. The 1% crosslinked polymer sample met the Dalquist Criteria (Figure 3.1).

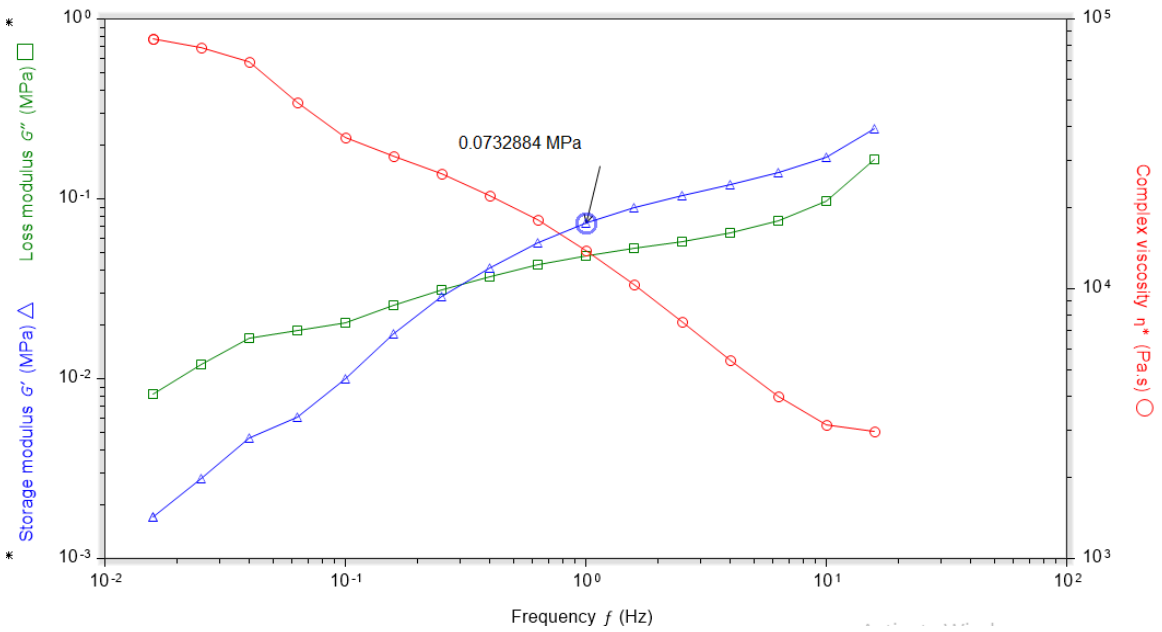

Figure 3.1 Oscillatory frequency sweep of crosslinked adhesive with the storage modulus at 1 Hz shown.

To improve the adhesive strength of these crosslinked polymers, tackifying resins were added (Table 3.2). Tackifying resins are predominately from pine resins such as rosin, phenolics, and terpenes. Each of these resins will be modified to modify their solubility, stability, and application properties through various chemical modifications such as esterification or amidation. One issue with most tackifying resins is their degradability under composting conditions. Terpenes, while biobased, are not degradable under composting conditions and therefore would negatively impact the compostability of the final product. Additionally, because of the final application being food contact, the tackifying resin must have food contact approvals. The relevant code of federal regulations (CFR) for food contact approval for produce is CFR 175.125. Any commercially available tackifier should hold this designation. Addition tackifying resins are available that act as a small molecule plasticizer. These tackifying resins would not

hold this CFR designation, but the generally recognized as safe (GRAS) list was used as a guide.

Table 3.2 List of commercial tackifying resins that meet food contact standards, and small molecule tackifiers with their status on the generally recognized as safe (GRAS) list.

Commercial		Small Molecule	
Type	Name	Name	GRAS
Rosin Acid	Snowtack 765A	Tall Oil	x
Rosin Ester	Snowtack SE780G	Oleic Acid	x
Rosin Ester	Sylvalite 2010	Lineolic Acid	x
Polyterpene	Sylvares TR A25L	Isoteraic Acid	x
Polyterpene	Sylvares 3125	Isosorbide	
Phenolic Terpene	Sylvares TP 300	Sucrose Benzoate	
Phenolic Terpene	Sylvares 1095	Sucrose Acetate Isobutyrate	

As expected, the increase of crosslinker content decreased the solubility of the resulting polymers produced. This decrease in solubility makes certain characterization methods such as gel permeation chromatography impossible. Additionally, initially these polymers were being cast into films using a solvent casting method (Figure 3.2). Using this method allowed for easy mixing of the polymer and the tackifiers through the creation of a mixed solution and then allowing the solvent to evaporate off. This method for mixing in additives and producing adhesive films was applied initially.

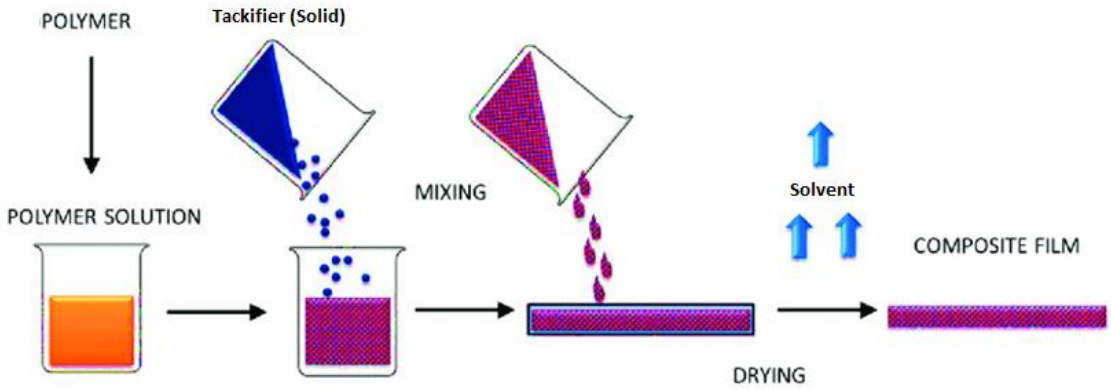

Figure 3.2 Solvent casting method used for blending additives into the polymer matrix. A solution with a known amount of crosslinked adhesive was produced and then tackifier were added into the solution. The solution was then cast onto a flat surface and allowed to dry.

To address the issue of solubility and mixing, extrusion blending using a twin screw extruder was applied to these polymeric materials. The additives could easily be added to the polymers of choice at a fixed weight percent. The extrusion was completed on vacuum oven dried polymer and additive of course at a temperature of 60°C and a 50-rpm mixing speed. Tack values for these blended samples were determined and were much lower than the needed value (Figure 3.3).

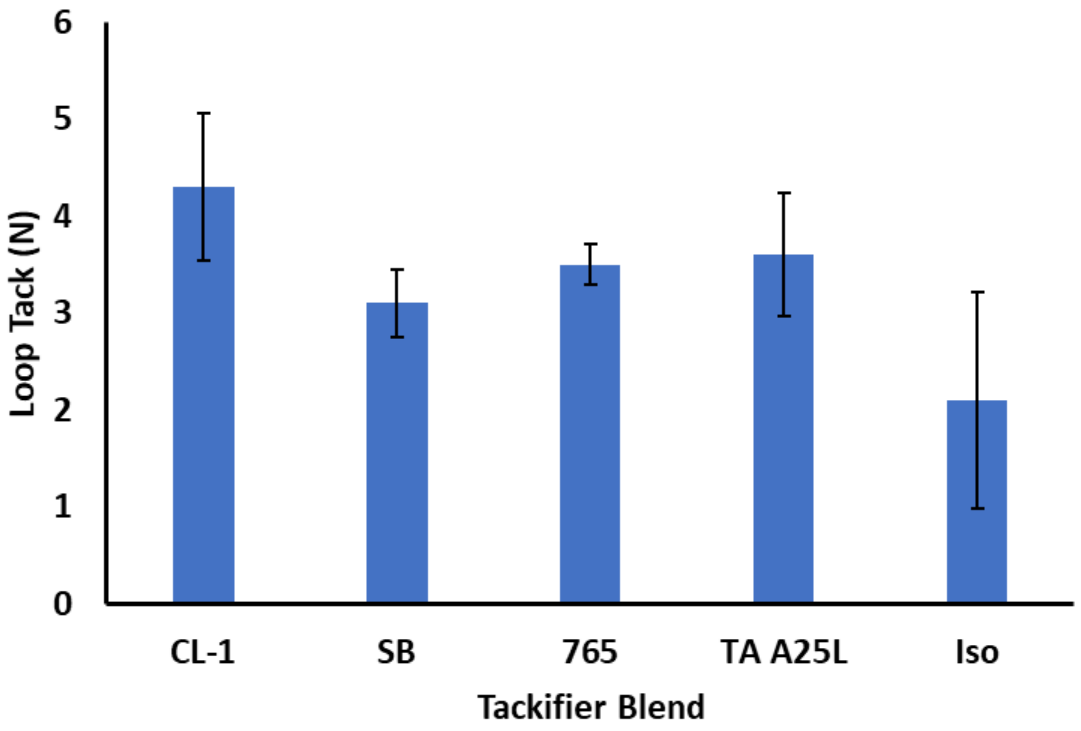

Figure 3.3 Loop tack measurements for tackifier blended crosslinked adhesive (CL-1).

The synthesis of the crosslinked # 2 polymer was also explored as a potential home compostable PSA. Previous work surrounding the application of this crosslinking agent showed its applicability towards industrial compostability. Its degradation rate and overall degradation level significantly outpaced the degradation of similar crosslinked polymers. With this understanding, crosslinking during polymerization using crosslinker #2 was explored and a library of these produced polymers was created through varying crosslinker content (Table 3.3).

Table 3.3 Characteristics of synthesized crosslinked adhesives.

% Crosslinker 2	Tack	Flow	Residue	Gel	Solubility
10%	None	None	N/A	Gel	Gel
5%	None	None	N/A	Gel	Gel
4%	High Tack	Very Low	None	High	Low: acetone, chloroform
3%	High Tack	Very Low	None	High	Low: acetone, chloroform
1%	High Tack	High	Residue	Low	Soluble

Increasing the crosslinking content posed several challenges that needed to be addressed through the synthetic process. The initial issue that was encountered was the dramatic shift to dark brown and black polymers being produced using the crosslinker. The thermal and chemical properties of the crosslinker were determined. Using thermal gravimetric analysis (TGA) it was determined that the thermal decomposition temperature of the crosslinker was much lower than the other monomers, with the crosslinker having a very broad decomposition temperature of ~152°C. This broad decomposition is directly related to the heterogeneous nature of the supplied crosslinker. This can be easily seen in the 2D NMR data with the region between 3.5-4.5ppm having multiple peaks correlated to multiple carbons indicating the presence of numerous species in the supplied crosslinker.

The increase in crosslinker content also leads to the formation of a gel fraction within the produced polymer. A gel fraction can be helpful for the application of pressure sensitive adhesives. The increased crosslinked portions can improve interfacial cohesion of the polymers, reducing ghosting and residue upon debonding. However, a gel fraction will also create problems with solubility through the presence of an insoluble fraction.

This can have a negative impact on the characterization of the polymer, but also it has a negative impact on the processability of the polymer for extrusion, coating, and lamination. Gelation can be measured using Soxhlet extraction to measure the solid content that is not soluble after several days of solvent extraction. Measuring the solids content of the produced polymers did not follow the typical trend, which is increasing crosslinker content leads to an increase in solids content. This was investigated through synthesizing multiple replicates of the same crosslinker content. It was determined through these replicates that the mixing during polymerization is key to the level of gelation. As the polymerization progresses the viscosity of the material continues to rise until it reaches a point where the force of mixing causes the material to be drawn up the stirring shaft. This phenomenon is coined as the Weissenberg effect. This effect occurs to viscoelastic materials when they are no longer following Newtonian fluid dynamics. As the polymerization proceeds the polymer will reach a critical viscoelastic state at which it will begin to rise up the stir shaft of the overhead stirrer. At this point two things can occur that will negatively impact polymerization causing additional gelation. The first is the heating probe will no longer be submerged into the polymer and therefore the heat will dramatically increase as the mantel attempts to maintain the temperature within the flask. This increased temperature will cause thermal degradation and allow for secondary crosslinking to occur through radical mechanisms. Additionally, the polymer will begin to ball around the stir shaft creating a region of still reacting polymer at the surface and an unreacted regime within the polymer ball. This will allow for increased localized polymerization to occur. The issue of erratic gelation issues was able to be controlled

through careful monitoring of the material during polymerization and to ensure proper mixing is continually occurring.

Other characterization completed on the crosslinked adhesive were differential scanning calorimetry (DSC), gel permeation chromatography (GPC), and nuclear magnetic resonance (NMR). DSC was completed to ensure the thermal transitions of the produced polymers were not significantly different from the linear polymer. The melting temperature of the adhesive during a normal 10°C/min heating ramp from -50°C was not present similar to the linear polymer, indicating an amorphous polymer at room temperature. The glass transition temperature was elevated slightly as the crosslinker content increased but was still an acceptable value for adhesive application. The GPC chromatograms showed a high molecular weight polymer with a nonuniform dispersity owing to the low amount of crosslinker. Running GPC on the different formulations was difficult due to the low solubility of the higher crosslinked polymers and the inclusion of solid within these samples.

For a pressure sensitive adhesive, the two most important adhesion values are the loop tack and the 90° peel values. These two measurements give a lot of information on the adhesive properties of PSAs. The loop tack testing allows the instant adhesion to a surface to be accurately quantified. This value is very important for the end use application of the adhesive on a produce label. A high instant tack value is needed to ensure that the produce label is firmly adhered to the produce as it travels through the packing process. The 90° peel value provides information on the overall force needed to debond the adhesive from a substrate. The 90° peel value will increase over time until a maximum value is reached, typically after 12-24 hours. Understanding the time that it

takes for the maximum value to be reached and the value that is reaches is important for targeting potential applications for adhesive. For produce labeling the 90° peel values need to be moderate to ensure that the label can be easily removed from some produce, but high enough to ensure debonding does not occur during shipping and handling. These two tests were completed using a loop tack peel testing rig and a 90° peel rig on a texture analyzer.

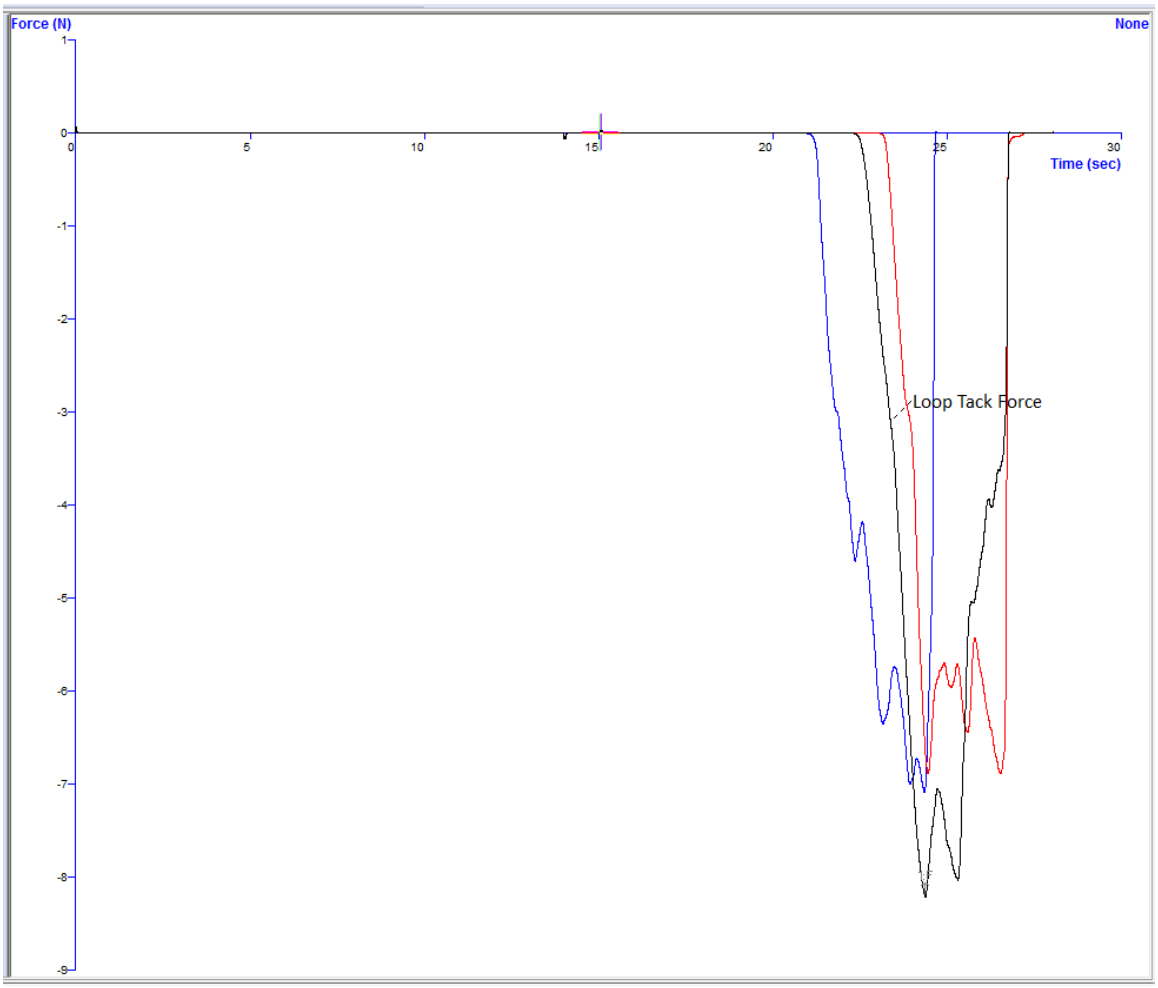

Figure 3.4 Loop tack data for crosslinked pressure sensitive adhesive determined using texture analyzer and loop tack rig.

Loop tack samples were produced from laminated samples using provided film and cut into 12” x 1” stripes. The loop tack value is determined by the maximum force

required to debond the sample from a glass slide which it is adhered to after brief contact (Figure 3.4). The value determined here gives a good understanding of the instant tack for the sample and allows for easy comparison between samples and formulations. Additionally, the failure mode for the debonding is also of interest. Cohesive failure, where the adhesive leaves a residue behind after debonding, would not be acceptable for the application in fruit labeling. Initial loop tack testing was focused on the impact of the adhesive thickness from the blade coating process on the adhesive performance. Increasing the adhesive thickness does not have an immediate impact on the loop tack values determined, but as the thickness rises to 80um and 100um the loop tack values are substantially higher (Figure 3.5). With increased adhesive thickness ghosting, or a slight adhesive residue was prevalent. To produce an adhesive that is commercially viable, the thickness must be as low as possible to lower the financial cost of the coated product.

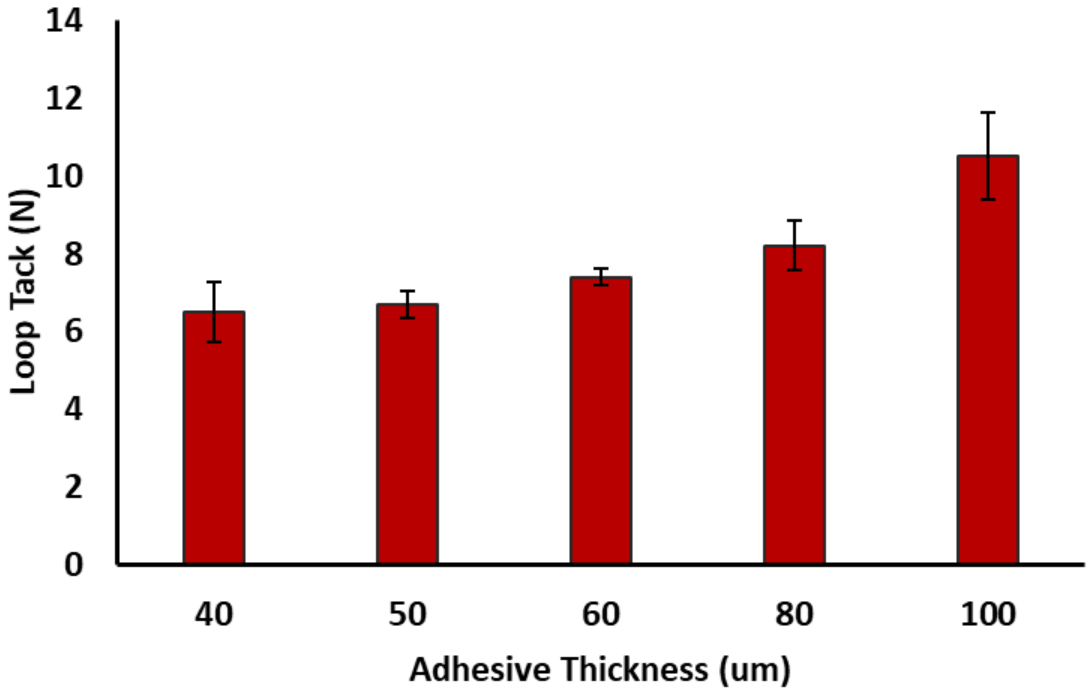

Figure 3.5 Loop tack data for crosslinked adhesive coated at various thicknesses using a hot melt blade coater.

The PSA that is being produced needs to be removable for its application in produce labeling. One facet of a removable PSA is that the peel force between the initial adhesion to a surface and the subsequent removal and adherence to a surface should not have a dramatic decrease in the peel force. To test this, three cycles of loop tack were completed using the same 12in x 1 in test sample (Figure 3.6). The 40um thick coated sample performed very poorly in the subsequent peeling values with a substantial decrease from the initial peel to the second peel. Upon observation of the adhesive film, it was apparent that the adhesive coating was significantly deformed during debond leaving behind pockets of reduced adhesive coverage. It is potentially this deformation that reduced the peel strength substantially during the subsequent loop tack testing. This can be attributed to the viscoelastic properties of the adhesive and its tendency to flow. The

100 um thick adhesive coated sample had a similar dramatic decrease in its subsequent loop tack values, but this was attributed to the cohesive failure that occurred on debonding.

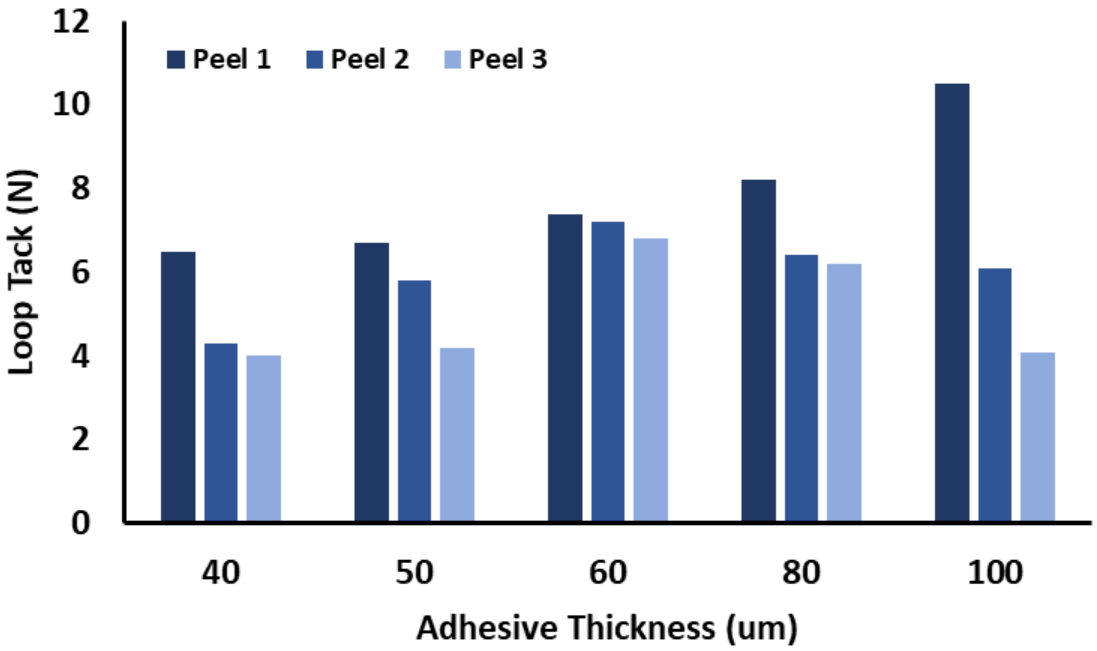

Figure 3.6 Three cycles of loop tack testing at different adhesive coating thickness.

The 90° peel values give additional information on how the adhesive will perform under a typical debonding force. For certain applications, a very high 90° peel value would be ideal, such as with packing tape. However, with the target application of produce labeling the 90° peel value should be moderate to allow for easy removal by the end user but also high enough to ensure that shipping and handling of the produce does not allow for debonding. The 90° test was completed using a peel rig accompanied by a texture analyzer. Samples were cut out coated film samples to produce 12in x 1in stripes. These stripes were then applied to a glass substrate under 10lbs of rolling pressure.

Similarly, the 90° peel values were determined for different adhesive coat thicknesses produced (Figure 3.7). The adhesive strength increases above 60um thickness with a maximum value determined for the 100um thick sample. Additionally, the 100um thick sample showed cohesive failure upon debonding.

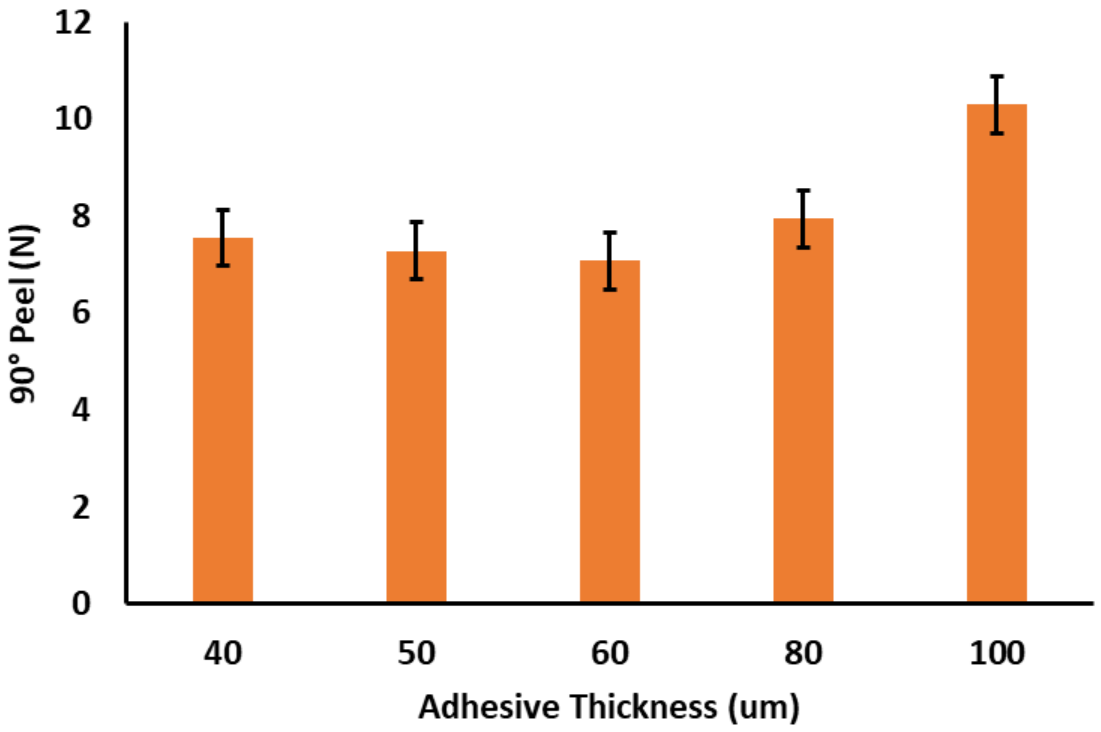

Figure 3.7 90° peel data for different adhesive coating thicknesses using 90° peel rig for texture analyzer.

The adhesive strength will slowly increase to a maximum peel strength over a certain time period. This increase in adhesive strength is important to understand and also the time period over which the adhesive strength is increasing. To do this, 90° peel was measured for samples at certain time intervals until the peel strength reaches a steady state. Additionally, the adhesive coating thickness is an important component and needs to be understood on how this impacts setting time and strength. The 90° peel values of

different coating thickness samples were measured over 24 hours (Figure 3.8). The high coat weight adhesives have a higher initial peel strength and increase to the maximum peel strength faster than lower coat weight samples. However, all samples reach approximately the same maximum peel strength over time. The higher coat thickness samples experienced more cohesive failure.

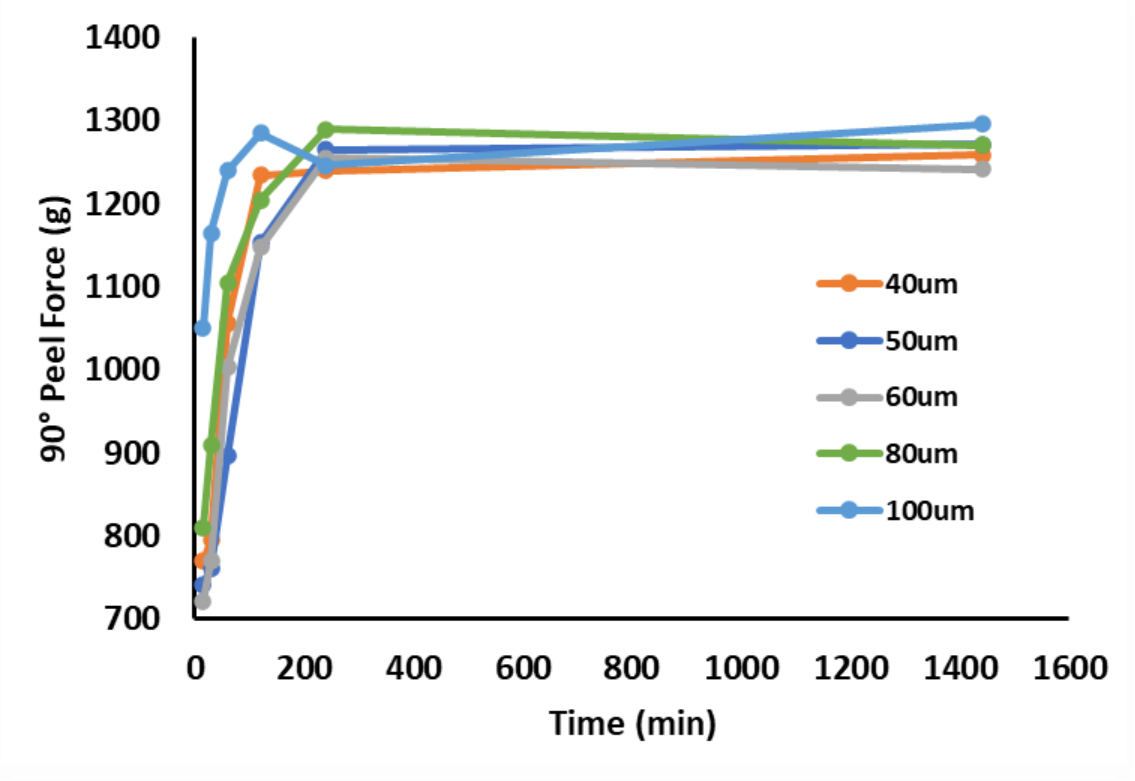

Figure 3.8 90° peel strength values for the adhesive coated at different thicknesses over a 24-hour time period.

Surface free energy is a major contributing factor for the adhesion of two surfaces together. Materials with similar surface energies are going to have greater attractive forces and therefore will have a higher force of adhesion. This phenomenon easily explains why a majority of tackifying resins had carboxylic acid or short chain ester functionalities. These functionalities give rise to an increase in the polar component of

the adhesives surface energy allowing lower energy base adhesives, such as acrylics, to successfully bond to high surface energy materials such as glass or metal. For removable PSAs, the surface energy of the face film and the adhesive are extremely important to ensure clean debonding from a surface without residue. The face film and the adhesive must have a closely aligned surface energy so that the adhesion strength between the face film and the adhesive is stronger than the adhesive strength between the adhesive and the substrate. To measure surface energy, contact angle measurements were completed.

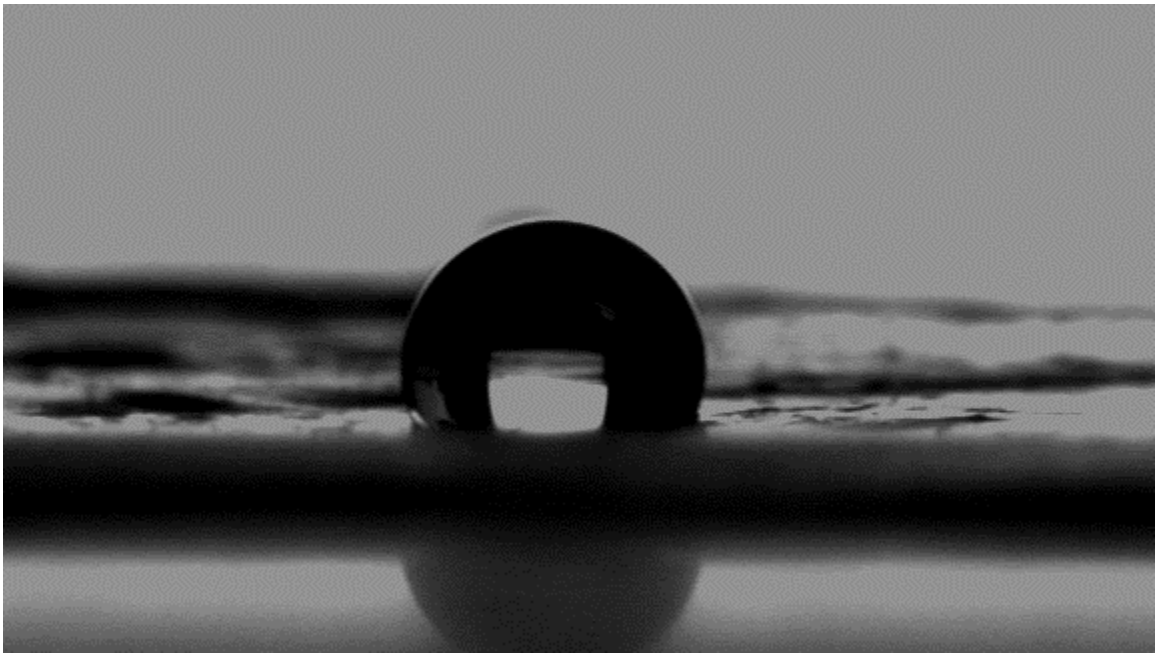

Figure 3.9 Water droplet on compostable face film imaged by drop shape analyzer.

Surface energy from contact angle is extrapolated by the interaction of at least three liquids with different surface tensions with a target surface (Figure 3.9). The three liquids used for contact angle measurements were water, diiodo methane, and ethylene glycol. Each liquid was deposited onto the test surface three times and measured for the contact angle via the sessile drop method using a drop shape analyzer. The contact angles are averaged and input into the equation for surface energy. Based on the surface tensions

of the liquids and their interfacial components the surface energy of the target surface can be calculated . The interfacial tension (IFT), also known as surface energy, is the sum of the polar and dispersive interfacial tensions. The surface energy of the provided face film was determined to be 36.49 dynes/cm (Figure 3.10).

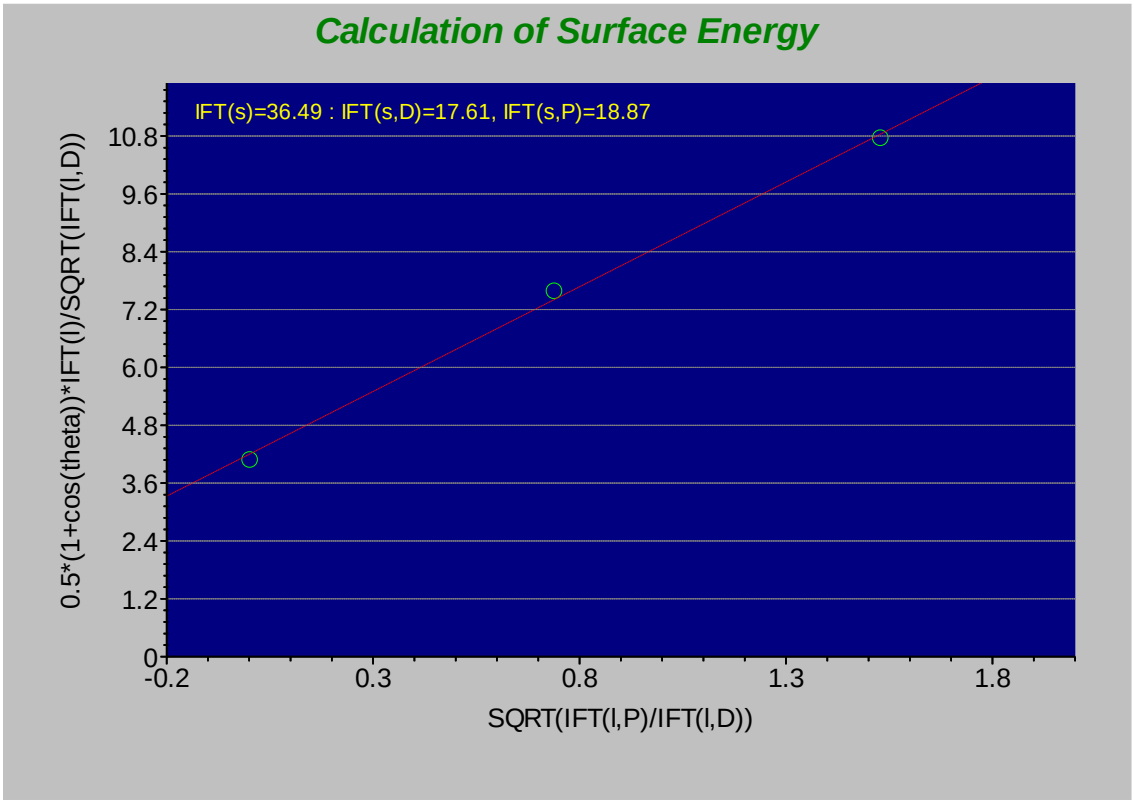

Figure 3.10 Surface energy calculation for compostable face film determined using sessile drop contact angle measurements.

The surface energies of the various films tested, and surfaces adhered to provide a better understanding of how and why adhesive or cohesive failure is occurring (Table 3.4). For example, when the adhesive is coated onto polyethylene film it undergoes adhesive failure from the face film when adhered to glass, metal, or paper products.

Table 3.4 Surface energy values of various surfaces determined using sessile drop contact angle measurements on a drop shape analyzer.

Substance	IFT mN/m	IFT(D)	IFT(P)
Polyethylene	13.12	7.42	5.70
S1 Face film	36.49	17.61	18.87
Glass	63.69	34.15	29.54
PBGS 4%	41.05	20.40	20.65

In collaboration with our partner, several iterations of a compostable face film were provided. Upon receipt of the finalized version of the face film, after the adhesive was coated to a nominal thickness cohesive failure was the predominate failure mode. This was in stark contrast with the data that was collected for other face films and adhesive combinations. The surface energy of the finalized face film was measured, and it was found to be much lower than previously provided films. Surface energy can be improved through several processes to clean the surface of contaminants and to free polar groups to increase the polar interfacial energy. On the industrial scale this is typically done through the application of corona treatments. In corona treatment high voltage electric arcs are used to produce ozone at the surface of the material which can then react through triplet state oxygen radical mechanisms to remove surface contamination. In the laboratory, a plasma cleaner can complete the same task using a tesla coil induced plasma state which produces the ozone needed for cleaning. This was completed on the film and measured before and after treatment (Figure 3.11).

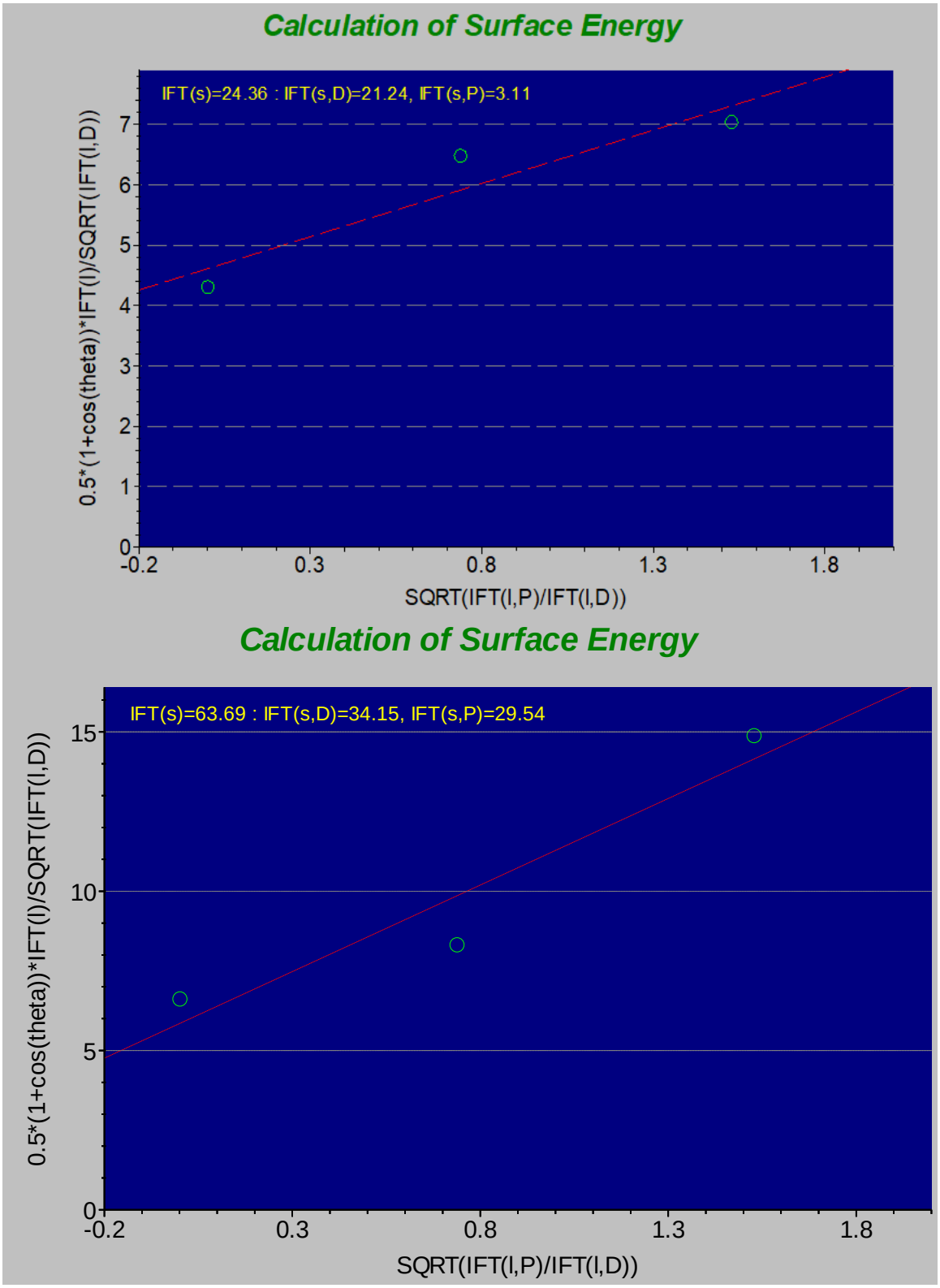

Figure 3.11 Surface energy calculations for finalized compostable face film as provided (A) and after surface cleaning with laboratory plasma cleaner (B).

This increase in surface is dramatic compared to the untreated face film value indicating significant surface contamination. Using a plasma cleaner gives a very uniform clean surface but the laboratory plasma cleaner used has a very small interna volume and could not be used to treat a roll of film for use on the hot melt coater. To address this issue, a home-made corona treater was created using a handheld tesla coil, articulating stand, and metal backing (Figure 3.12). The application of this home-made corona treater relies on the production of ozone around the electric current between the tesla coil and the grounding back plate.

Figure 3.12 Photography image of home-made coroner treatment device set up in line with hot melt blade coater allowing face film surface energy modification immediately prior to adhesive coating.

. Dyne pens were used to track the change in surface energy of the treated film to dial in the energy input, the distance between the coil and the ground, and the exposure time. Using the dyne pens, the surface was increased from a dyne value of 34 dyne/cm to 60 dyne/cm without burning or distorting the film with the high energy exposure from the

corona treater. The homemade coroner treater was attached to the hot melt blade coater and was used to treat the film during coating. The increased surface energy of the film eliminated residue upon debonding showing the importance of control surface energy for adhesive applications (Figure 3.13).

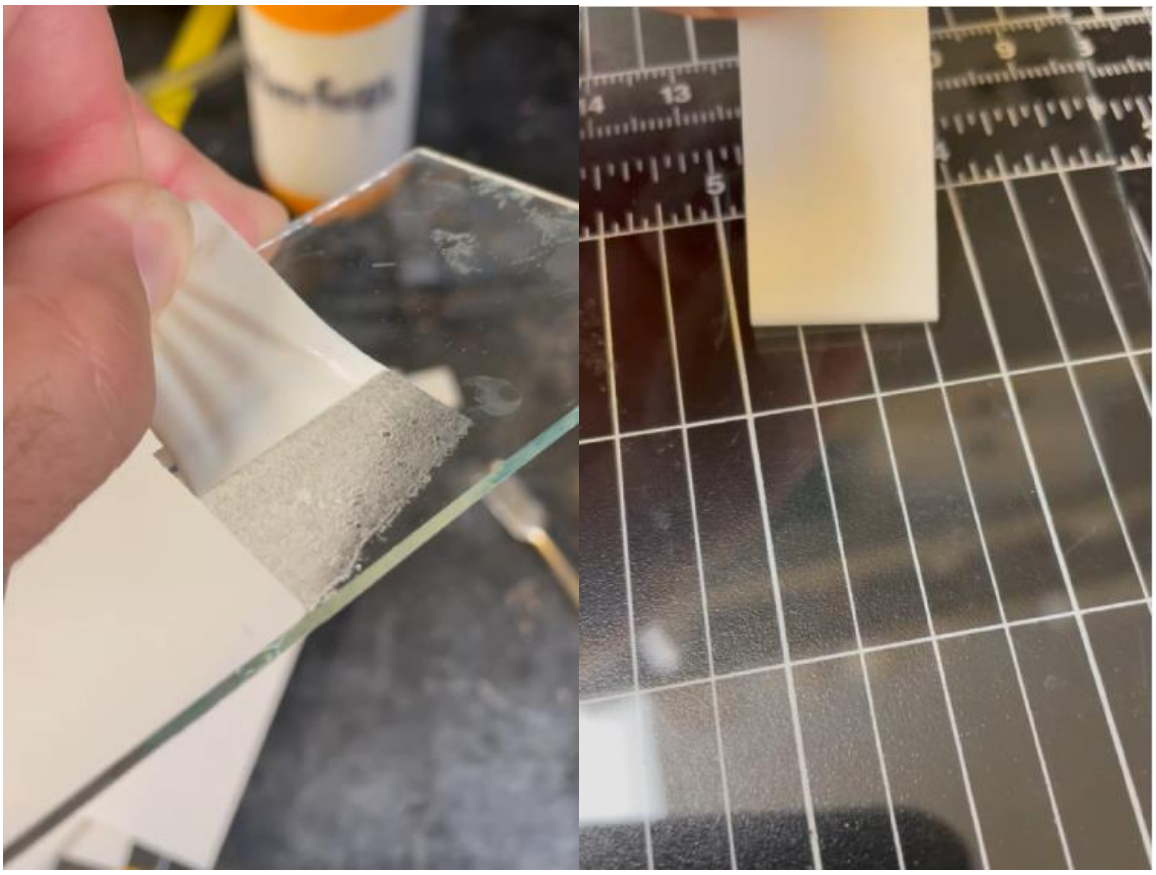

Figure 3.13 Photography images of adhesive coated film sample undergoing cohesive failure after debonding with low surface energy face film (A) and no adhesive residue after debonding with corona treated face film (B).

Stability testing was then completed on the adhesives produced to determine the long-term properties of the adhesive when it sits for an extended period of time without being adhered to a substrate. After conversion to labels the adhesive could be introduced into dramatically different temperature and humidity conditions prior to being applied to a substrate. The extremes and the average condition were tested over a 60 day period

using both loop tack and 90° peel values. Samples were placed in a heated stirring chamber with an set temperature of 38°C, into a refrigerator with a temperature of 3°C and placed in a container in the laboratory at its room temperature of 22°C. Samples of different thickness were measured to determine if coating thickness had any impact on its temperature stability overtime. Several tackifying resins that were blended into the polymer were also measured during this testing.

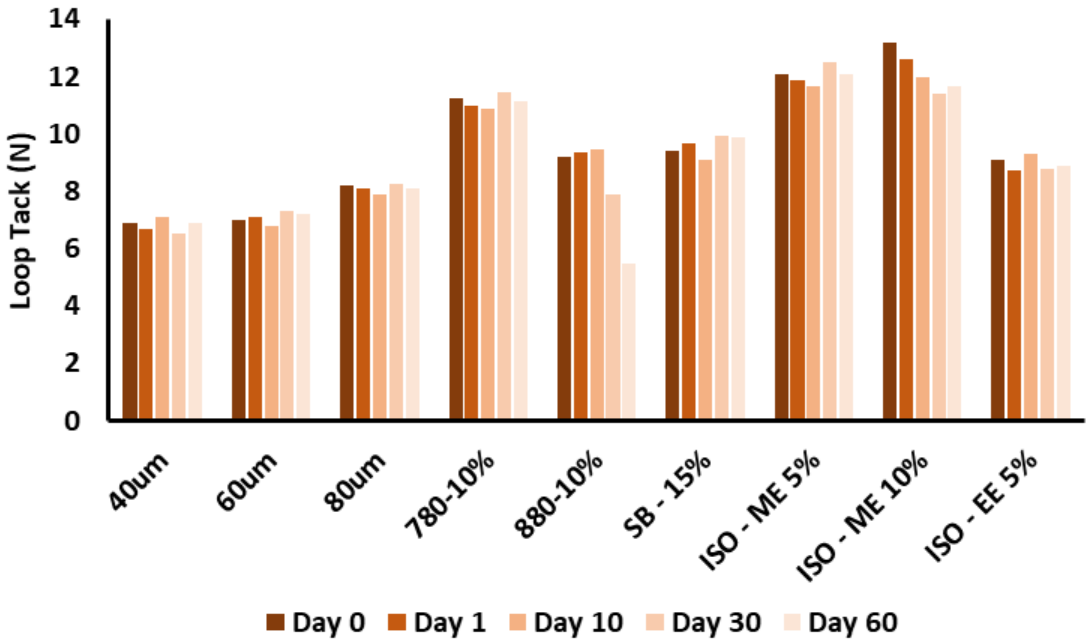

Figure 3.14 Stability loop tack data over 60 days at elevated temperature (38°C). Samples include: samples of various thickness and samples blended with tackifier including sucrose benzoate (SB), isosorbide methyl ester (ISE-ME), and isosorbide ethyl ester (ISO-EE).

Samples were cut into 1in x 12 in stripes and placed in the heated chamber set at 38°C. One sample was removed at each time interval of 1 day, 7 days, 14 days, 30 days, and 60 days and measured for loop tack and 90° peel values (Figure 3.14). Over the course of the stability test the values for loop tack testing were consistent across all

samples except the sample that contained 10% Snowtack 880 . For this sample, the adhesive value dropped significantly across the testing window indicating a change in the physical properties of the adhesive. Additionally, residue was observed after debonding for the 880 sample for each time period after the 14 day sample. To investigate this scanning electron microscopy (SEM) was employed to observe the surface of the adhesive film. An additional sample of 880 was placed into the heated chamber and on day 14 it was mounted to a SEM sample puck adhesive side up. The phase separation of the tackifying resin and the base adhesive polymer can be clearly seen in the SEM image obtained (Figure 3.15). This separation and residue clearly indicates a nonviable formulation for the application of produce labeling. Other samples were found to meet stability needs.

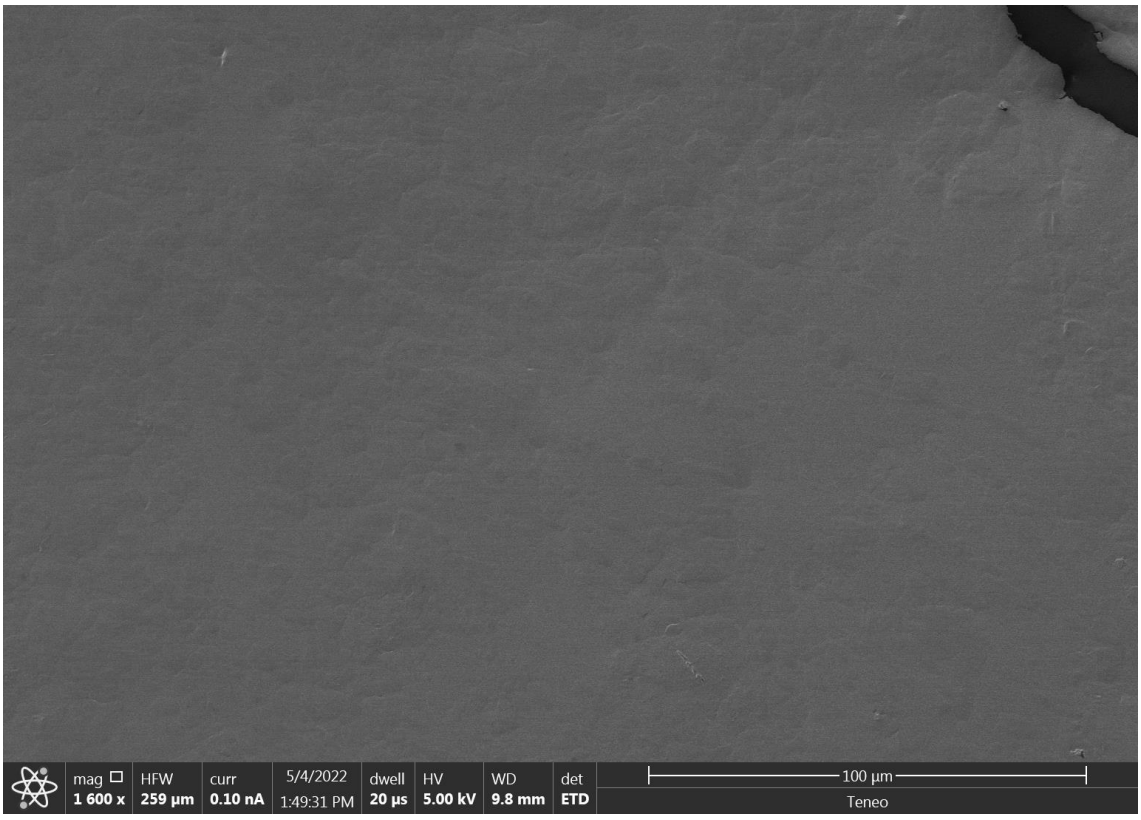

Figure 3.15 Scanning electron microscopy of adhesive blended with tackifying resin 880 after 30 days in a high temperature environment.

Samples were cut into 1in x 12 in stripes and placed in the laboratory refrigerator set at 3°C. One sample was removed at each time interval of 1 day, 7 days, 14 days, 30 days, and 60 days. These samples were measured for loop tack values and 90° peel values. All samples measured maintained look tack values (Figure 3.16) and 90° peel values consistently across the testing time frame. When removed from the fridge samples were much stiffer than at room temperature, but this was initially attributed to the stiffening of the face film at the lower temperature. All samples tested met stability needs at this lower temperature indicating that the labels could be stored at refrigeration temperatures and still perform upon application.

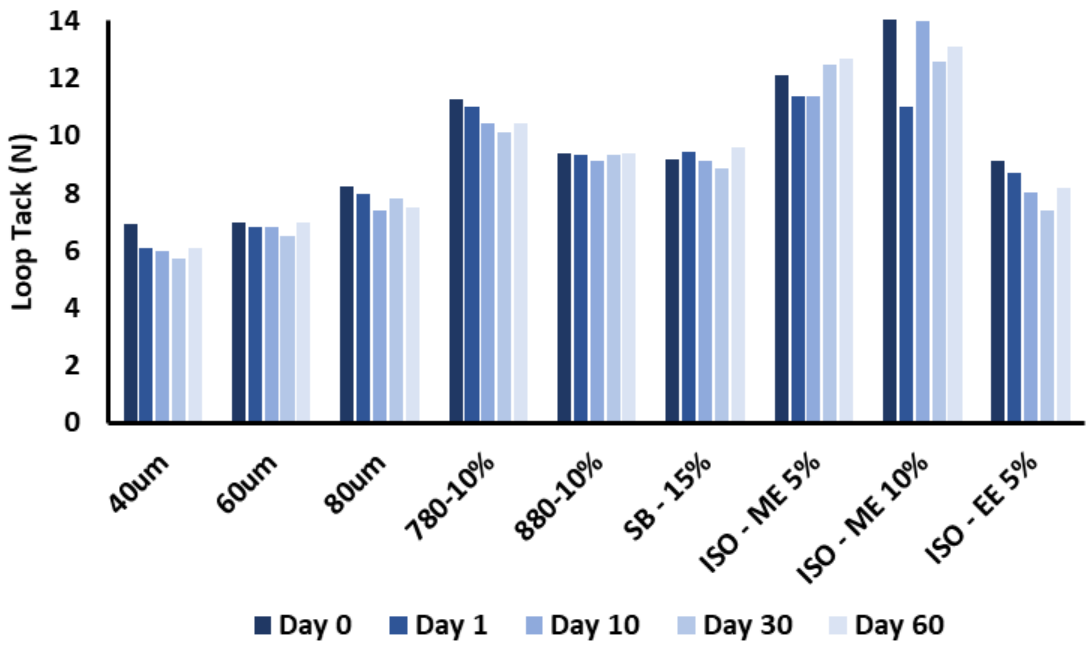

Figure 3.16 Stability loop tack data over 60 days at refrigeration temperature (3°C). Samples include: samples of various thickness and samples blended with tackifier including sucrose benzoate (SB), isosorbide methyl ester (ISE-ME), and isosorbide ethyl ester (ISO-EE).

Samples were cut into 1in x 12 in stripes and placed in an open to air container on the laboratory bench with an ambient temperature of 22°C. One sample was removed at each time interval of 1 day, 7 days, 14 days, 30 days, and 60 days. The sample compounded with the isosorbide methyl ester at 10% weight loading was the only sample that did not pass the stability testing. This sample had a statistically significant decrease in loop tack values determined across the testing time (Figure 3.17). Additionally, some adhesive creep was observed with these samples which began between the 7 day and 14-day tests. This adhesive creep could be due to the increased plasticization of the base adhesive polymer by the small molecule additive. This was not explored further. This sample was found to not meet the potential application demands and therefore was no longer of interest. All other samples met the stability testing requirements.

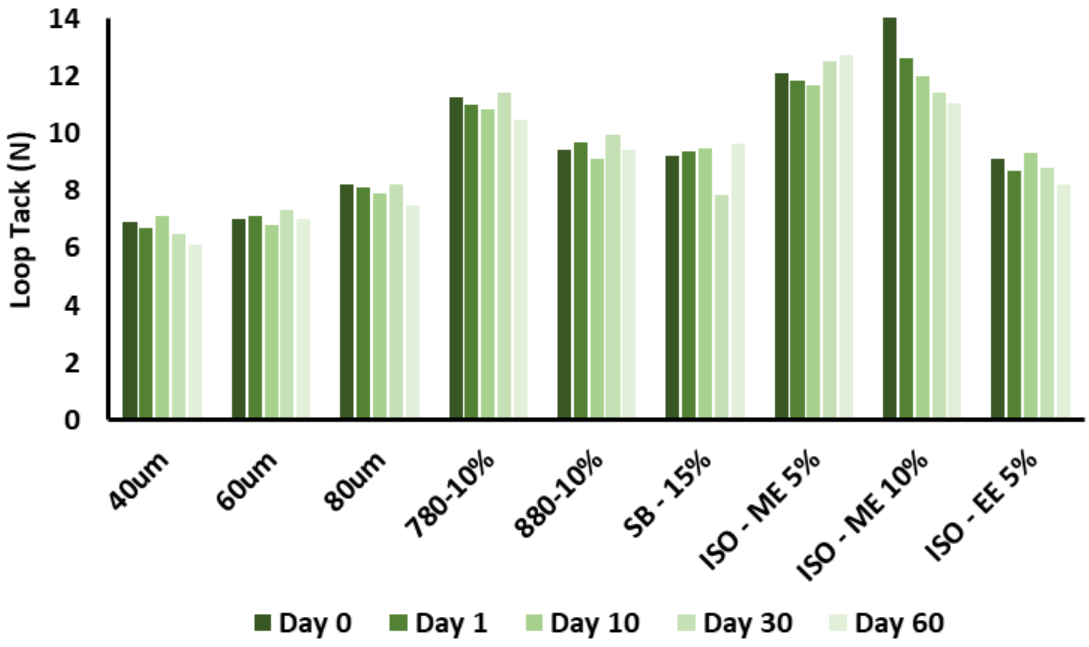

Figure 3.17 Stability loop tack data over 60 days at room temperature (22°C). Samples include: samples of various thickness and samples blended with tackifier including sucrose benzoate (SB), isosorbide methyl ester (ISE-ME), and isosorbide ethyl ester (ISO-EE).

The stability of the produced adhesive labels was also investigated when applied to a variety of substrates. The same temperature conditions were investigated as previously described. Produce is labeled and stored in a variety of conditions. Watermelons in the deep south can be picked and labeled extremely hot, 32°C – 37°C, and at high humidity, 85-95% relative humidity. A plethora of produce is picked at elevated temperatures and then labeled at lowered temperature ~3°C followed by storage in refrigerated containers during shipping and by the end consumer. Understanding how the adhesive will function at elevated and lowered temperatures while being adhered to a large variety of surfaces is important. These tests were done on gala apples, avocado, bananas, red bell peppers, Roma tomatoes, and sun gold kiwi. The adhesive samples included all of the samples tested as described above.

Adhesive samples were produced by cutting coated film into ½ inch squares and then applying them adhesive side down by hand to the selected produce items. These pieces of produce were then placed in the heated chamber at 38°C. Each produce item labeled was removed and inspected for delamination and on fruit stability at 1 day, 7 days, 14 days, 30 days, and 60 days. The banana, avocado, sun gold kiwi, and apple had full coverage of the applied samples over the 60-day period with no visible lifting and no issues with debonding. Additionally, when the samples were removed from the apple and avocado no residue was observed. All samples left significant residue on the banana and sun gold kiwi when debonded at high temperature, but this could be attributed to the high level of softening that occurred to the banana and sun gold kiwi items over the testing time. The red bell pepper and Roma tomato had slight lifting on the corners of the square

test samples after 7 days but did not progress continue to debond after day 7. This should be retested using a circular or oval test sample to mimic the true label geometry that is used to label produce. If squares labels were produced and the corners lifted than debonding would be a significant worry as the produce is shipped and placed on supermarket shelves. No residue was found on either produce item after debonding of the samples, but the samples removed from the Roma tomato had a significant red color to the adhesive after debonding.

Adhesive samples were produced by cutting coated film into ½ inch squares and then applying them adhesive side down by hand to the selected produce items. These pieces of produce were then placed in a laboratory refrigerator at a temperature of 3°C. Each produce item labeled was removed and inspected for delamination and on fruit stability at 1 day, 7 days, 14 days, 30 days, and 60 days. The avocado, banana, and apple had no debonding or label curling over the testing period. The banana had significant residue upon debonding at the 30 and 60 day testing period. This is likely due to the ripening of the banana and therefore softening of the outer banana peel. The Roma tomato and red bell pepper had multiple labels debond after 7 days in the refrigerator. Interestingly only these two pieces of produce had debonding issues in the lowered temperature and also lifting in the elevated temperature test. This debonding at lower temperature could be ascribed to the differences in the surfaces that are being bonded to. Alternatively, the adhesive could be crystalizing at the lower temperature which is causing debonding. Potentially the debonding could be caused by multiple factors, but debonding of these labels would not be acceptable for the commercial application.

Determining why the applied labels were debonding from the produce in the refrigerator was important to then fix the issue. Previous work had shown that the adhesive was amorphous at room temperature using a differential scanning calorimeter. However, if the crystallization phenomenon was occurring at a very slow rate, the melting transition would not occur on the thermographs. To test this theory, polarized optical microscopy (POM) was applied to probe crystal formation during low temperature application. Samples were made by applying a small amount of adhesive to a POM glass slide and covering with another glass slide. The slides were gently pressed together to allow for a thin polymer layer to form between the discs. These discs were then placed into the refrigerator, to be removed at time intervals to inspect for crystal formation. POM allows for the observation of crystals formed due to their birefringent nature when probed with polarized light.

Samples were removed from the fridge at four hours, eight hours, and twelve hours. Each sample was removed from the fridge and immediately placed into an insulated container that was filled with ice. When observed using POM no crystalline structures were observed for any of these samples. While observing the 24 hours sample it was determined that crystallization had occurred (Figure 3.18). Upon fixture onto the microscope slide and focusing the crystals rapidly melted. The total time the sample was out of the insulated container was less than 30 seconds prior to crystal melting.

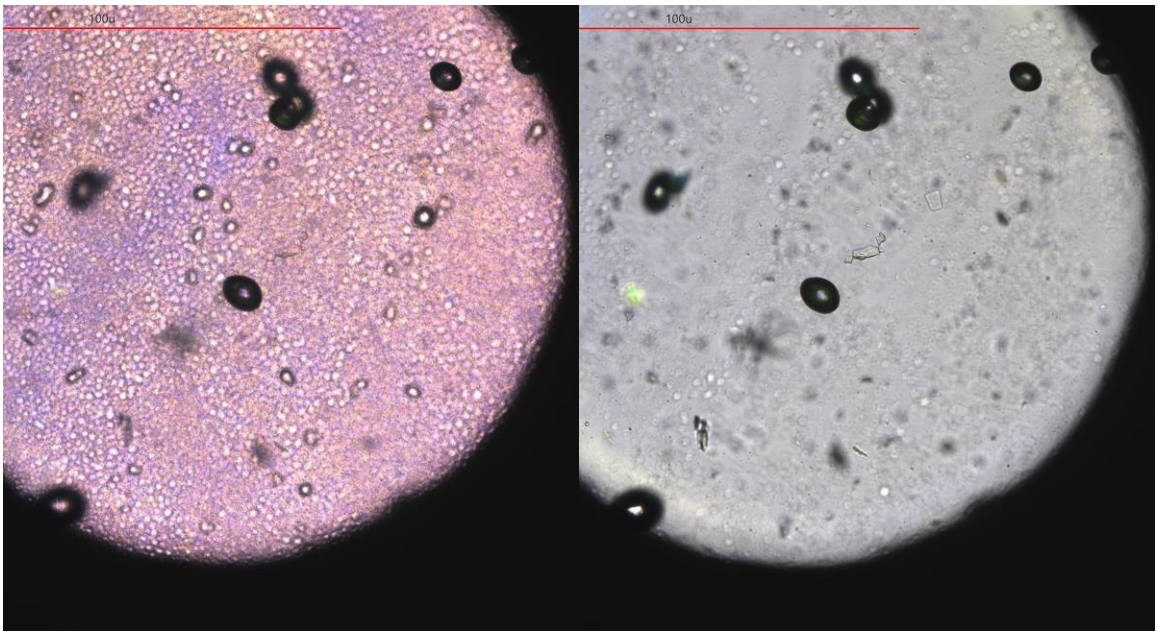

Figure 3.18 Polarized optical microscopy images of crosslinked adhesive after 24 hours in refrigerator. Left image shows crystallization that occurs at the lowered temperature. The right image shows the immediate melting of crystalline domains at room temperature.

Crystallization occurring at the temperature common to a refrigerator, around 4°C, would not be acceptable for the application of the adhesive as produce is routinely stored at the temperature. In order to reduce the melting temperature, and therefore ensure no crystallization, the polymer backbone would need to be altered synthetically. First, a method for screening the polymers produced was needed to determine the melting temperature of these slow crystallizing polymers.

To accomplish this, different methodologies were tested on differential scanning calorimetry (DSC) to find a method that would accurately determine the melting temperature. Following typical DSC methodology, a first heat ramp is used to remove any thermal hysteresis from the material. A cooling ramp is then completed to bring the polymer below 0°C, which was determined as the lowest temperature that the adhesive

would ever be subjected to. Next an isothermal step was completed where the temperature of the sample was held constant for an hour. The temperature of this isothermal step and the time period of it were both optimized over several experiments. The optimized temperature was set at -70°C for one hour. This forced the crystallization to occur for all tested samples. This can be seen by the newly determined melting transition seen after the isothermal step that is not seen in the normal temperature ramp (Figure 3.19).

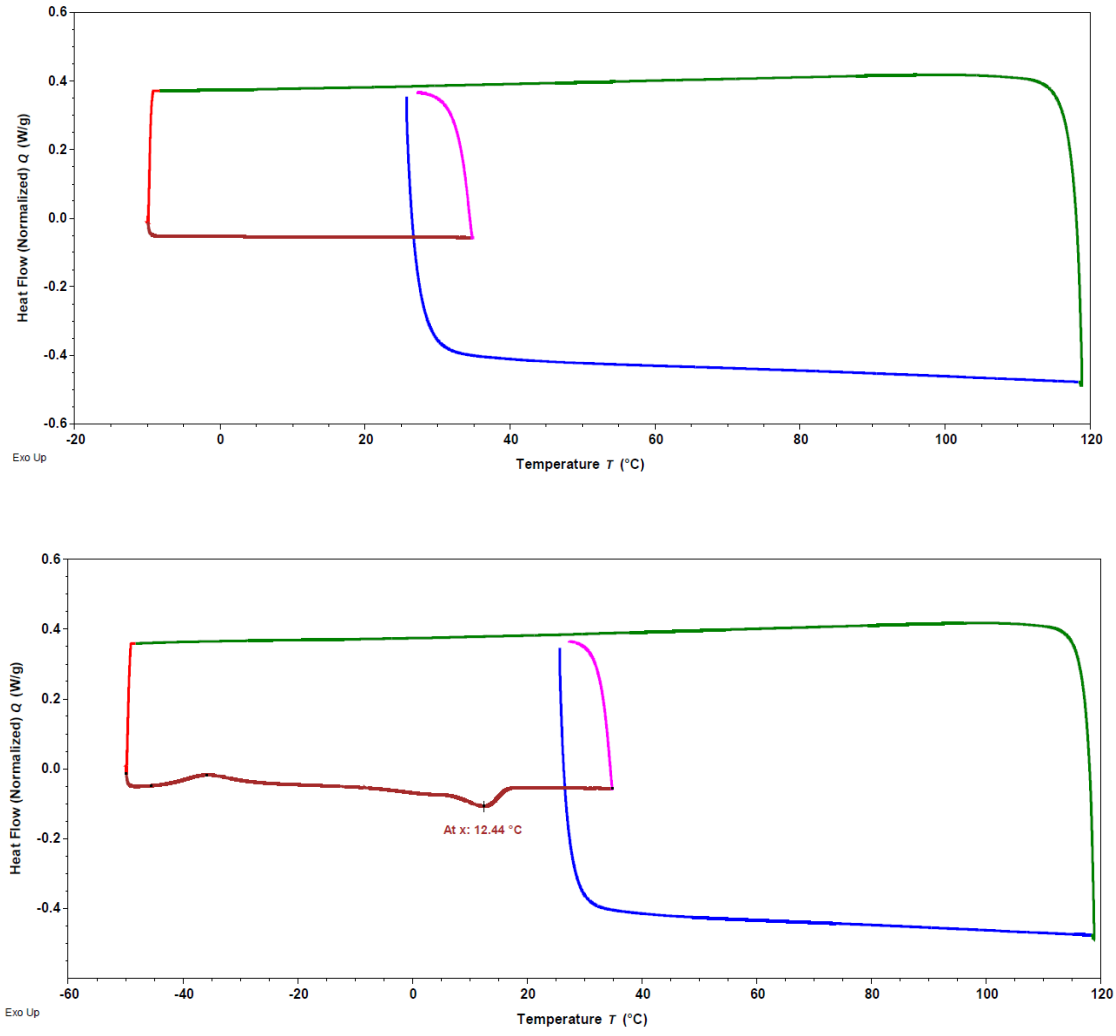

Figure 3.19 Differential scanning calorimetry using typical 10°C/min ramp (Top) and isothermal experiment showing new thermal transition (Bottom).

Having determined a method that can accurately assess the melting temperature of these adhesives, synthetic changes were needed to be completed on the polymeric backbone that would reduce the current melting temperature from ~12°C to below 0°C. The melting temperature is directly related to the ability of the polymer chains to find a conformation that is tightly packed. To reduce the ability of the polymer chains to find this, it was decided to add in another monomer that had a shorter chain length that would disrupt the ability of the polymer chains to pack together. The monomer was chosen for several reasons. The monomer contains two primary functionalities allowing for similar kinetics during polymerization as the other monomers. The monomer can be sourced from biobased sources, specifically the fermentation of corn. The monomer is financially equivalent to other monomers to ensure viability for further scale up.

The amount of monomer was then optimized by varying the amount of the new monomer that was included in the total monomer content. For instance, if the reaction required 1 mols of total monomer, a 20% loading of new monomer would be 0.20 mols and therefore an 80% loading of old monomer would be used equating to 0.80 mols. The amount of new monomer added was minimized because of its impact on the viscoelastic properties of the produced adhesive. The synthesis of these adhesives with 1new monomer was completed as described previously without any significant changes to the kinetics of the reaction. After optimization, a new monomer loading of 15% was determined as the best adhesive produced, with a melting temperature of -1.74°C (Figure 3.20).

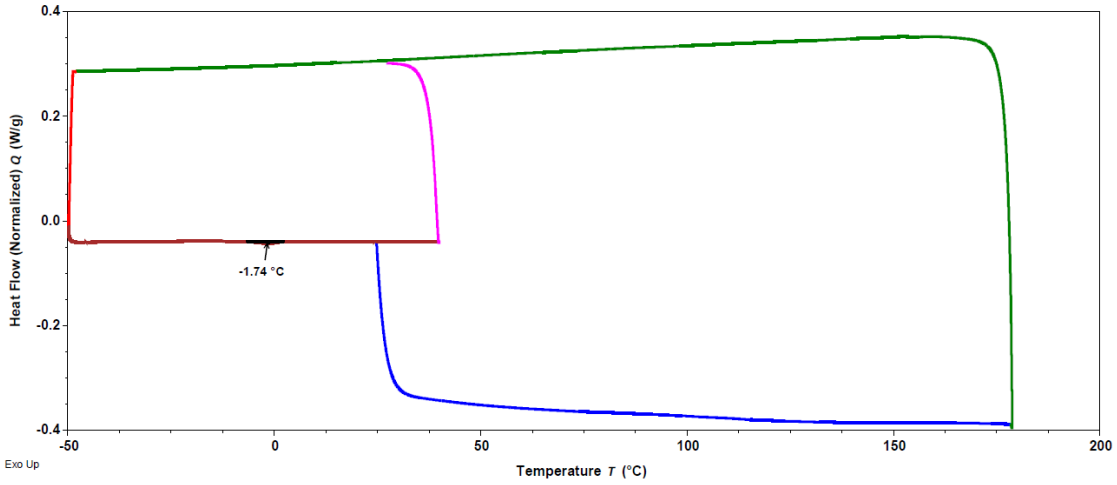

Figure 3.20 Differential scanning calorimetry of newly synthesized adhesive using new shorter chain monomer to alter melting temperature.

Having optimized the adhesive to lower the melting temperature, the new synthetic formulation needed to be characterized for its physical, chemical, and mechanical properties. The adhesive properties were also compared to current commercial adhesives (Figure 3.21).

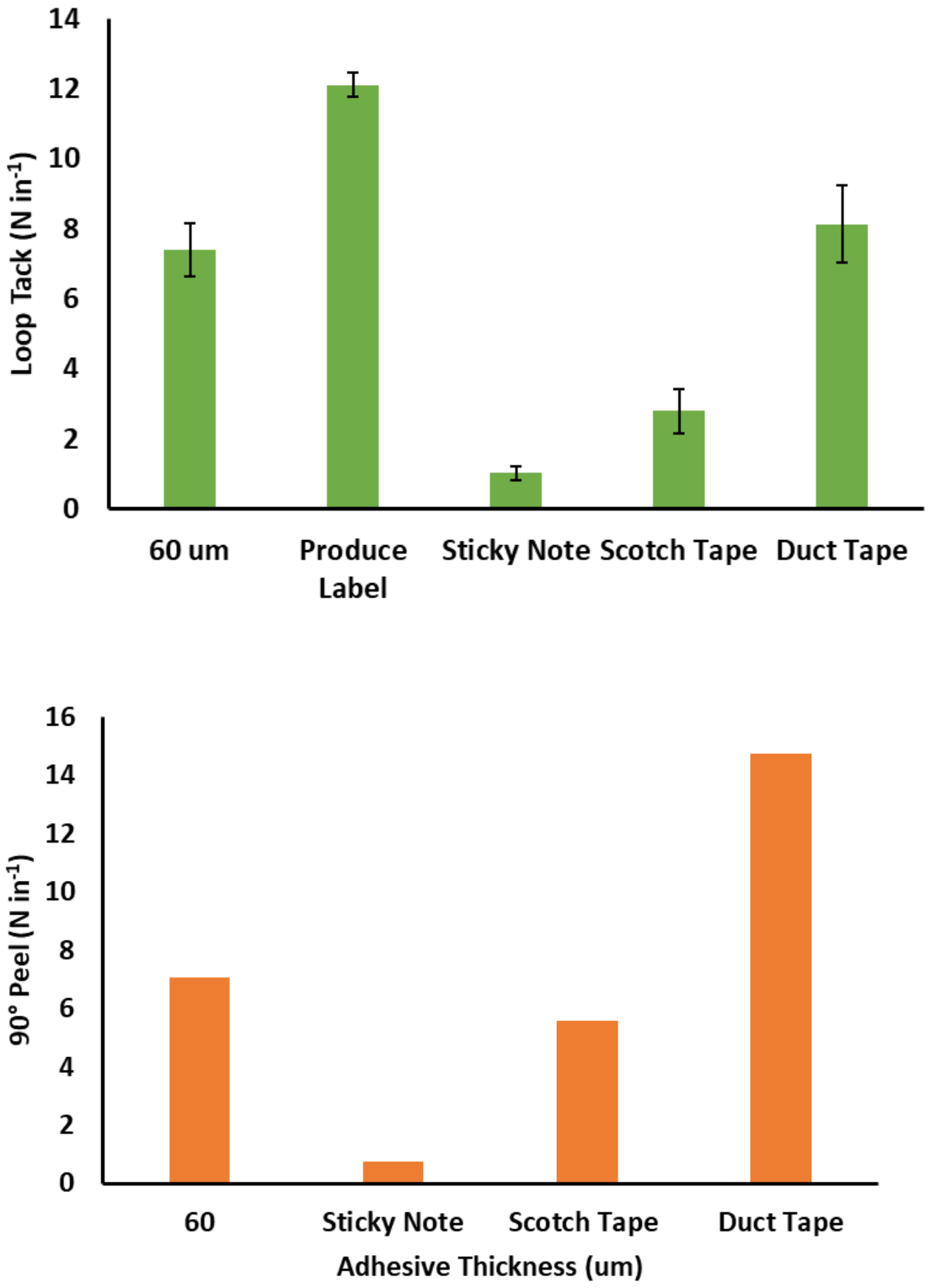

Figure 3.21 Loop tack and 90° peel values determined for produced adhesive compared to commercial adhesives.

Compounding using an extruder was completed in order to modify the physical and chemical properties of the adhesive to meet application demands. The instant tack value of the adhesive can be altered through the addition of small molecule and low molecular weight polymeric species to the bulk polymer. This was investigated to allow for the production of adhesives with varying levels of tack based upon their application. The addition of waxes, oil, and small molecules were also blended into the adhesive to change the viscosity of the adhesive. The viscosity of the base polymer is extremely high at room temperature, greater than 10 million centipoise, and still very high at elevated temperature ~100k centipoise, compared to other hot melt adhesives.

Synthetic Scale Up

The produced crosslinked adhesive was the best option to move forward for further development towards having an industrially viable product. Previous work on the small scale had created a solid outline for the scale up of this product from the lab scale to a pilot reactor with a volume of 50L. Scaling up this reaction created many issues that are not present at the small scale including the need for a completely new set up to meet the required reaction conditions.

For the scale up, a 50L glass reactor equipped with a two-part heating mantle and electronic overhead stirrer was purchased. The heating mantle has a rating up to 200°C which is right at the maximum temperature that the reaction has required at the small scale. One cause for concern is the reaction is heavily dependent on the temperature and the vacuum in the final transesterification step to reach the degree of polymerization needed for the required physical and mechanical properties from the polymer. At the larger scale as the viscosity increases the temperature gradient across the polymer mass

will be highly varied due to the decrease in mixing. Additionally, the use of a temperature probe could be problematic from a logistical issue and also from a measurement standpoint.

The reactor was also equipped with a torque controlled electronic overhead stirrer. The overhead stirrer has a speed range from 50-300 rpm allowing for precise control of the mixing of the reaction. The stir shaft provided with the reactor had a glass shaft and the stir blades were a PTFE at 35° offset. The torque control is an ideal feature for the overhead stirrer as it can be directly related to the viscosity of the polymer melt and therefore to the degree of polymerization of the polymer. Using the torque output to measure the reaction progress is a very standard method in industrial polymer synthesis. One issue that was discovered with this overhead stirrer is it has a maximum torque before it will automatically cut itself. This value is moderately low at 388 N/cm. If this torque is reached, then mixing will stop which could lead to overheating the reaction and burning the material or damaging the heating mantle. Monitoring the torque and the mixing speed will be important for ensuring repeatable reactions and products.

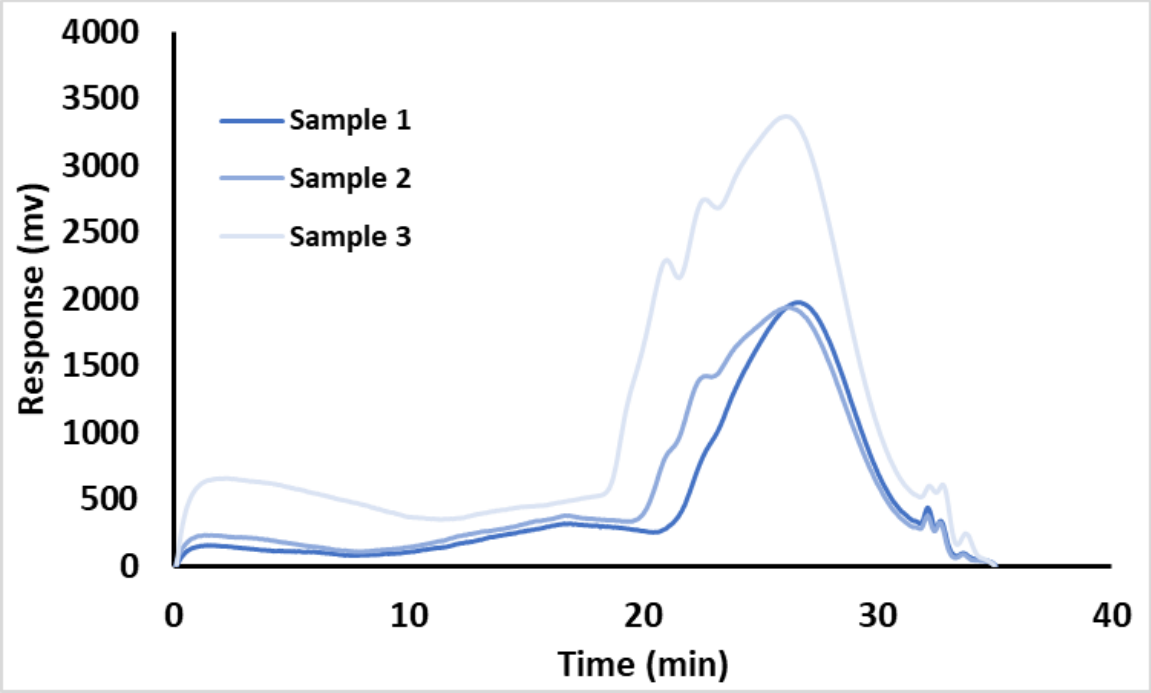

Figure 3.22 Gel permeation chromatography curves showing molecular weight changes across reaction timing of pilot scale polymerization.

Tracking the reaction completion of the pilot scale reaction was done in several ways. The polymerization progresses through the increase in molecular weight of the resulting material therefore measuring the molecular weight changes over time were completed. While this was successfully completed, as the molecular weight of the material increases the solubility of the material decreases (Figure 3.22). This makes sample preparation for gel permeation chromatography difficult. Additionally, gel permeation chromatography takes at a minimum one hour to complete and therefore would not be an ideal in process check. Tracking the change in viscosity of the polymer through the change in torque values of the is a good in process check but is not sensitive enough for ensuring full reaction completion. Instead, parallel plate rheology was applied to measure the changes in viscoelastic properties of the material as it is being produced

(Figure 3.23). This method proved to be a highly efficient and effective way to determine when to end the reaction.

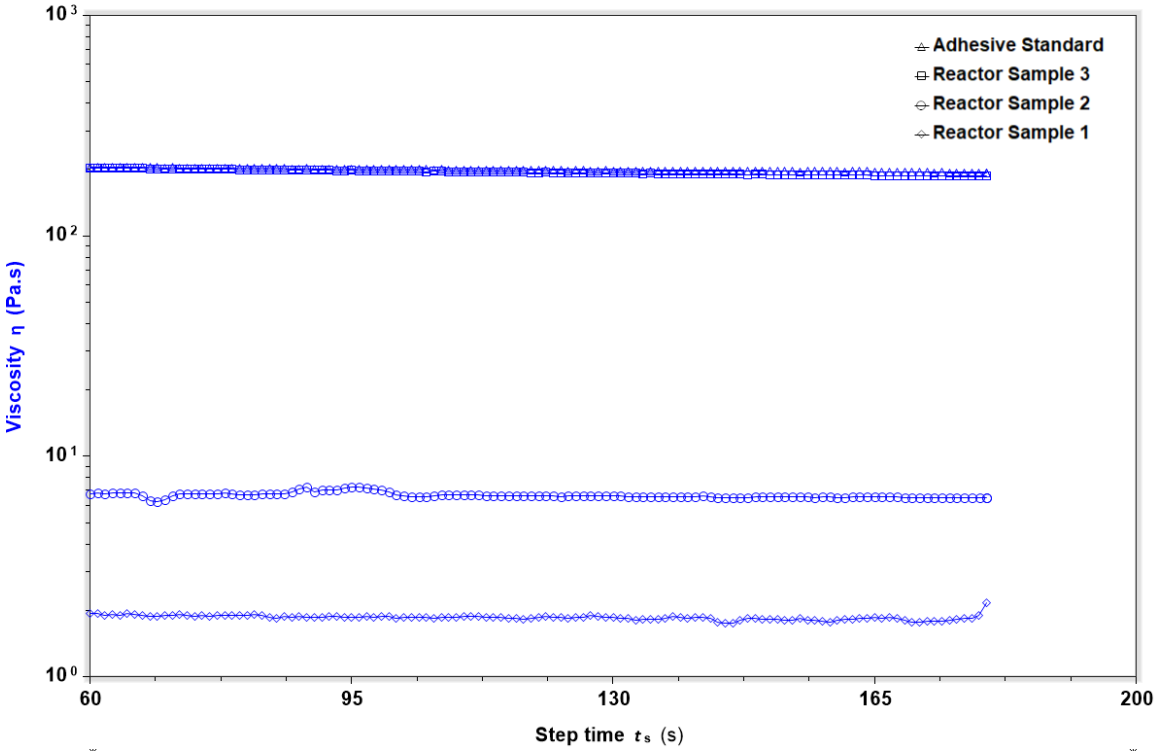

Figure 3.23 Viscosity measurements determined via parallel plate rheology tracking the reaction progression of pilot scale reaction.

Another issue to the scale up process was ensuring that multiple batches were producing similar materials. To track this over parallel plate rheology was again used to track the changes over the different batches produced (Figure 3.24). The difference between viscosity values between the four batches was very small showing good reproducibility.

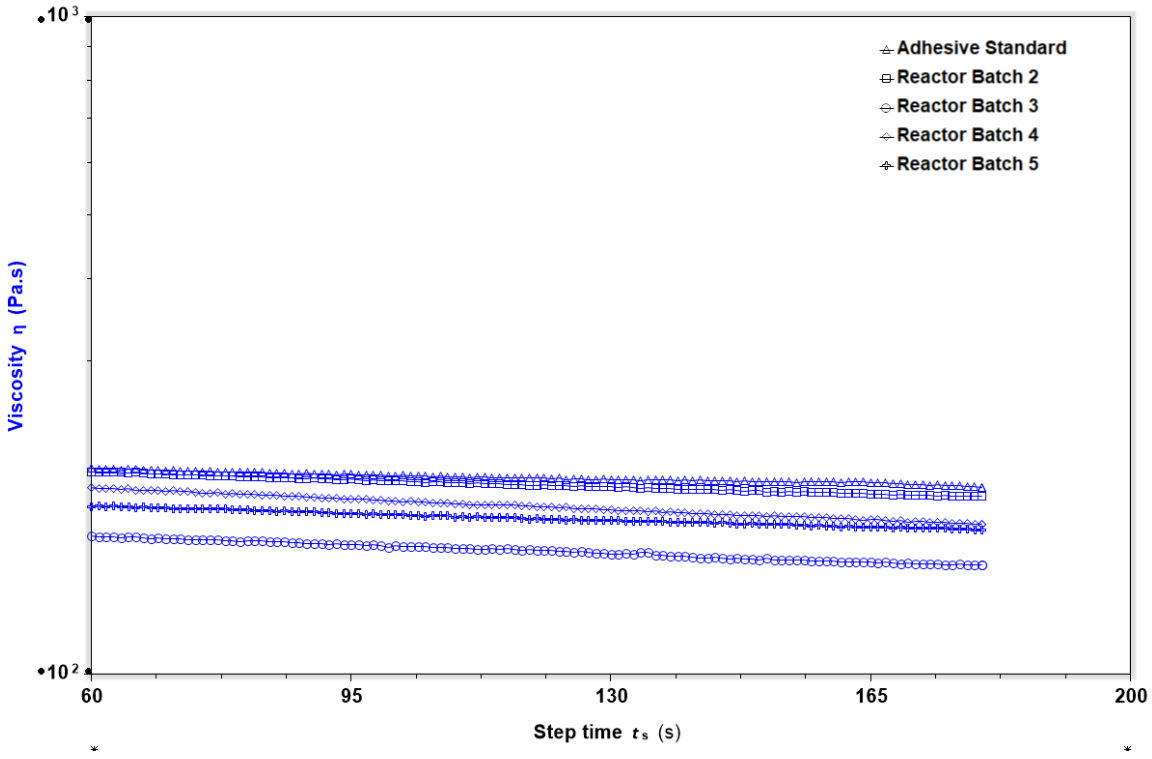

Figure 3.24 Parallel plate rheology viscosity measurements of four pilot scale reactor batches compared to a laboratory standard.

Additionally, the adhesive properties of the material are the most important facet of the material. These values were tracked across all pilot scale batches. After coating these adhesives and measuring the loop tack data it was confirmed that the between batch reproducibility of these materials was very good (Figure 3.25).

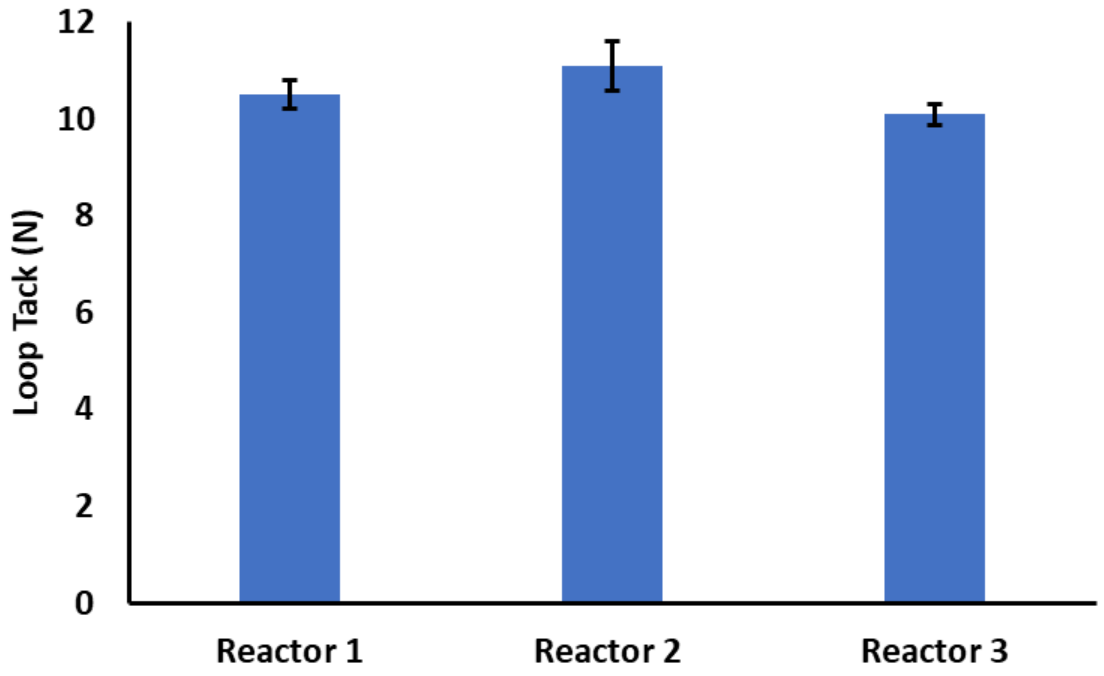

Figure 3.25 Loop tack data for three reactor batches.

Industrial Hot Melt Coating

The drum of produce adhesive was shipped to an industrial coater to coat a supplied face film and to produce rolls of coated film that can then be converted into labels. The application of the adhesive to the film was completed using a roll-to-roll hot melt coater (Figure 3.26). This method for applying the adhesive was chosen because it closely resembles the heated blade coating method that was applied within the laboratory. The adhesive is a highly viscous amorphous material at room temperature and has a significantly lower viscosity at elevated temperatures as shown above. The set up for this roll-to-roll coater starts at the drum. The drum is heated by a metal platen that is pressed down into the adhesive and is equipped with a pump that can pull the material from the drum and deposit it into a heated trough at the coating head. This heated trough is directly

situated on the doctor roll which helps to circulate the adhesive in the trough prior to coating. Once engaged, the doctor roll will transport adhesive to the applicator roll. At the interphase of these two rolls is a nip that can be varied to control the amount of adhesive that is applied to the applicator roll. The applicator roll then makes contact with the silicon release paper backer laying a controlled amount of adhesive on the backing film. At this coater, the silicon release paper is produced on site using a UV curing step immediately prior to running the material through the applicator roll. The now coated silicon backer is run through a cooling oven to reduce the temperature of the adhesive and then it is brought down and laminated onto the face film. The face film is set up on a turret unwinder and is first run through a corona treater to increase the surface energy of the film prior to coating. After lamination of the face film with the adhesive coated silicon backer the film is rolled up using a rewinder.

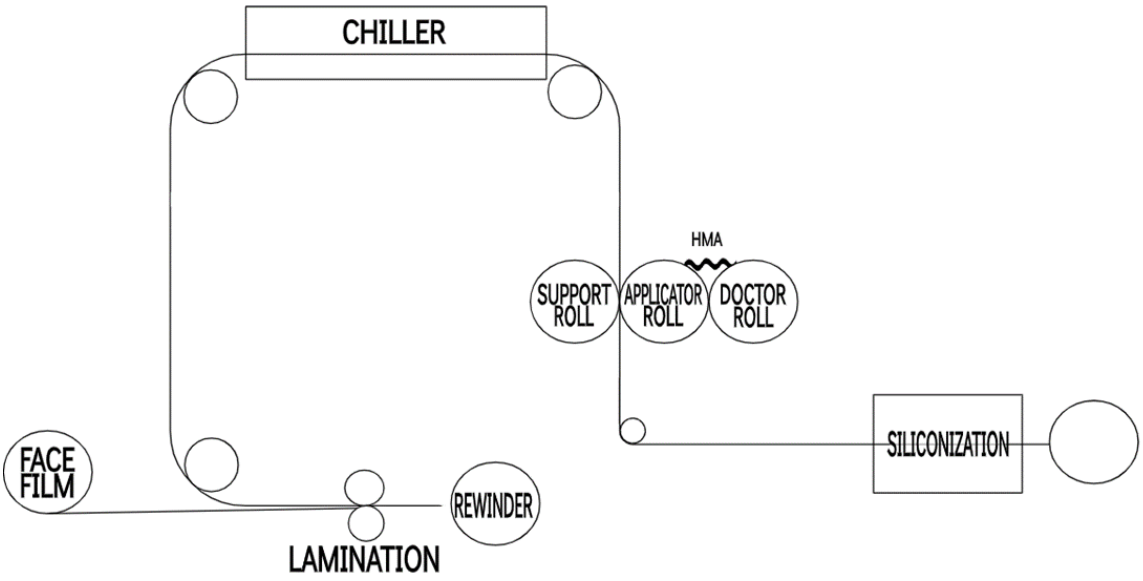

Figure 3.26 Diagram of industrial hot melt coating line used to produce three-layer coated film rolls.

As discussed above the temperature and pot stability of the adhesive was of great concern going into the trial. To work around these issues an initial temperature at the drum and at the coating head was set to 350°F. After initial set up polyethylene film was first coated to dial in different variable prior to moving to the compostable film. After running for several minutes, it was first determined that the adhesive which was being pumped into the coating head from the drum was being delivered at a temperature 25-40°F lower than the set temperature of 350°F (Figure 3.27). This was causing a temperature gradient across the coater head that was creating gaps in the adhesive curtain produced. To address this the temperature of the coating head and the drum heater was raised to 370°F, slightly below the known degradation temperature of the adhesive. After ~30 minutes of equilibration time the coating continued on polyethylene film. The curtain, thickness, and overall coating process was deemed sufficient to move to the compostable film.

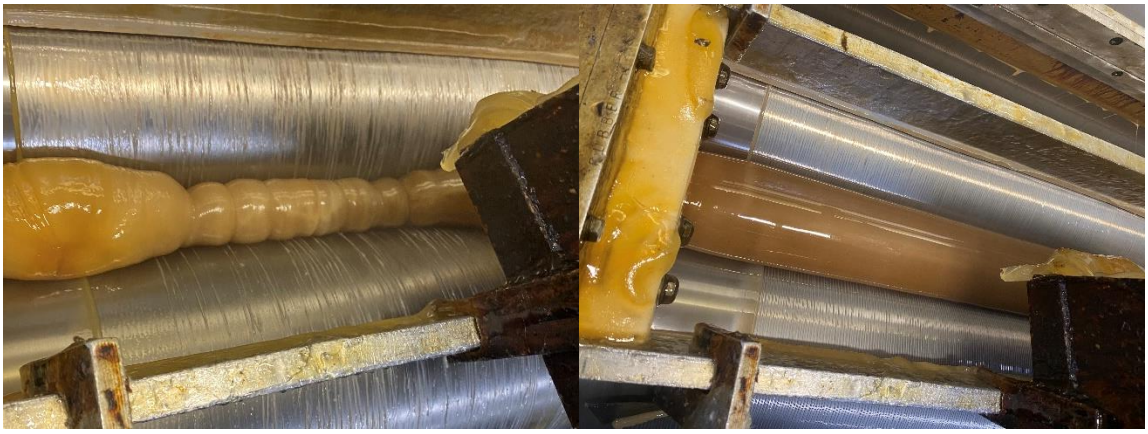

Figure 3.27 Photography showing adhesive in coating head at 350F displaying nonuniform coating of the rollers due to viscosity issues and adhesive at 370F displaying a uniform coating of the rollers.

The equipment was stopped to place the roll of compostable film onto the unwinding turret. Once the machine was back running and adhesive was being coated,

more adhesive was needed in the coater head, and it was pumped into the trough. At this point, the adhesive curtain began to be distorted in the middle. This was directly in line with where the new adhesive was being deposited into the trough (Figure 3.28). It was determined that the large difference in the temperature of the adhesive in the coating head and the newly pumped in adhesive was causing the middle of the adhesive curtain to be disturbed. To address this issue, the coating head trough was filled to max and the pump for the drum was cut off. The adhesive in the trough was allowed to equilibrate and was run until it was empty. This fix allowed for a uniform curtain to be produced and coating of the compostable film was completed.

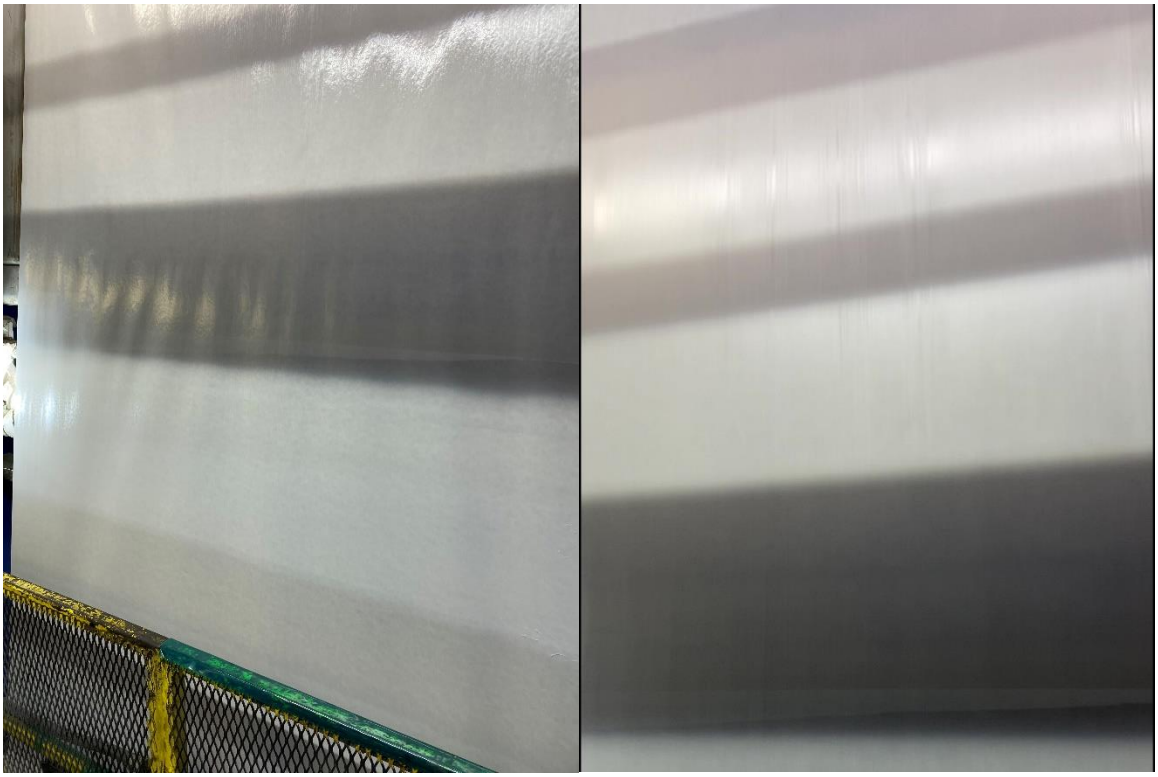

Figure 3.28 Photography showing good adhesive curtaining (left) and poor adhesive curtaining (right).

At the end of the run the coater was stopped and samples were removed and measured for coat weight, loop tack and 90° peel. The loop tack was measured following

the ATSM D6195 on a Cheminstruments loop tack tester. The value determined was an average of two replicates resulting in a loop tack value of 8.45N of force, lower than the value determined for this adhesive internally. The 90° peel was similarly determined using the ASTM standard using a Cheminstruments peel machine. The value determined was a release force of 10 g. During one of the tested samples, cohesive failure was seen during the 90° peel test. The coat weight was measured at 25 gsm, slightly higher than the target of 18 gsm. This is the high coat weight adhesive roll.

The adhesive was again filled into the trough and allowed to equilibrate to temperature prior to coating the compostable film. The goal of the second run was to reduce the coat weight of the sample to attempt to get closer to the target coat weight of 18 gsm. A lower coat weight allows for less material to be used and therefore is more financially beneficial. A balance has to be struck between lowering the coat weight, getting full adhesive coverage, and maintaining the adhesive strength required. During the process of coating this sample it was noticed that the adhesive in the trough had discolored significantly from its original color. This discoloration is directly related to the thermal degradation of the product. Along with discoloration, cohesive failure becomes the dominate failure mode for the adhesive. This shift was seen during the testing of the collected samples. The loop tack value determined was 4.89 N, the 90° peel value was 4.00N, and the coat weight was determined to be 19 gsm. During both the loop and peel measurements significant residue was observed on the glass substrate. This confirms that degradation occurred due to prolonged exposure to elevated temperatures.

Samples pulled at the coating line had a nonuniform surface which was not as expected based upon laboratory experience. This surface was documented through

photography at the time and through light microscopy the following day (Figure). The same sample was then observed one week later, and the surface was uniform in appearance under photography (Figure 3.29). The light microscopy images clearly showed that the initial surface had significant voids that occurred during the coating of the adhesive onto the face film. After one week the voids that were previously present had coalesced producing a uniform adhesive surface. This gradual adhesive flow is expected from this particular material as the rheological properties indicate that the material will continue to flow over time until a steady state is reached.

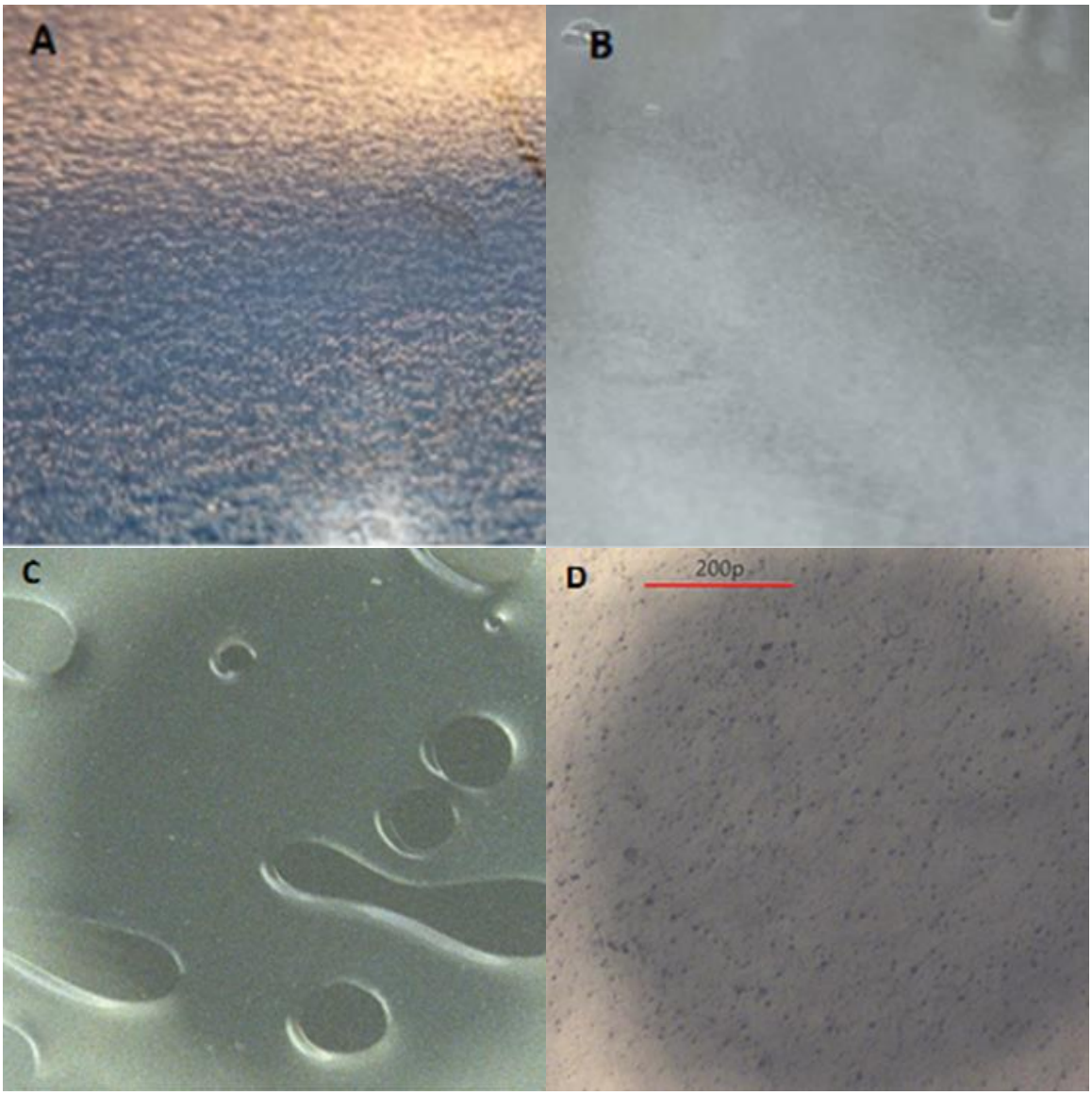

Figure 3.29 Photography images of 18 gsm coated polyethylene film immediately after coating (A) and one week after coating (B). Light microscopy images of 18 gsm coated polyethylene film 48 hours after coating (C) and one week after coating (D).

The industrial hot-melt roll-to-roll coating was successfully completed at two different coat-weights – a high coat-weight of 25 gsm and a low coat-weight of 19 gsm. Two forty-inch web-width rolls were successfully produced and then slit into four ten-inch rolls that could then be converted to labels on a printing and die-cutting press. During the coating, several issues arose that need to be addressed to improve coating

performance and commercial viability. The high viscosity of the adhesive limited its ability to be successfully pumped from the drum into the coating head and then to be coated continuously. Therefore, to meet the needs of the coating process, the viscosity of the adhesive will need to be significantly reduced at temperature through either synthetic modification or formulation changes. Additionally, the degradation determined from discoloration of the adhesive within the coater head and the shift from adhesive to cohesive failure needs to be addressed. Overall, the coating trial was a success and produced materials to move forward for label conversion and produce testing.

Label Conversion and Produce Testing

The produced rolls were shipped to a facility to complete conversion into produce labels and then label fruit using current commercial machinery. The conversion to labels followed a standard printing and dye cutting process. In this process the first stage is the turret onto which the rolls can be mounted and allows for continual feeding of the material through the machines. The material is fed first into a splicer that allows for roll-to-roll continuity so the machine will constantly be running. The material is then fed through a series of printer heads that consist of unique plaques produced that rotate into a dye bath and apply a single color to the material. After the application of the dye at each print head the material is run through a UV lamp to set the UV active ink to the face film (Figure 3.30). The material is run through as many printer heads as needed for the intricate designs demanded by the labels. After printing, the material goes through a dye cutter that is equipped with a rotating head with the label pattern that is wanted. Immediately after dye cutting the material is run through a slitter which separates the 10-inch paper into individual runs of labels. At this point, the face films that remained after

dye cutting is removed and is trashed leaving only the printed and cut label attached to the silicone release paper on each run. One unique process for certain produce labels is a non-adhesive tab to help with easier label removal. This is the final machine component that each label run is processed through prior to winding into label rolls.

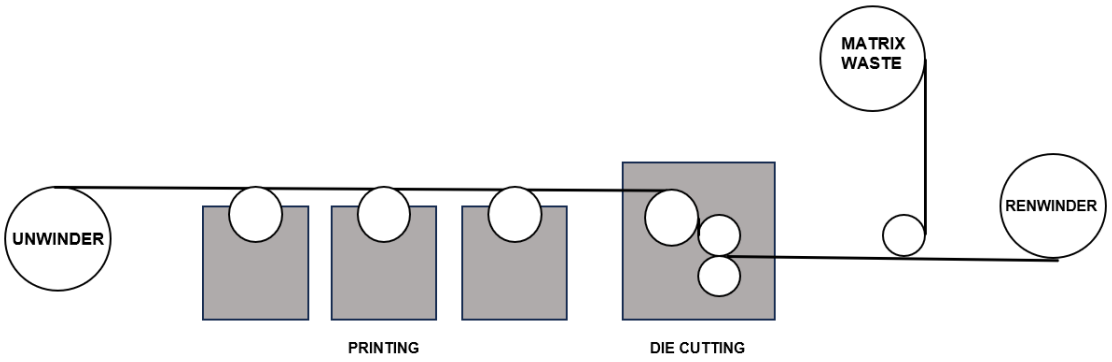

Figure 3.30 Diagram of label conversion process.

The first issue that arose during conversion was the with the 10-inch rolls that were shipped from the coater. The rolls were telescoping slightly, which is when the core of the roll and the outside layers are not perfectly inline (Figure 3.31). This telescoping is due to poor tension control during the rewinding of the rolls after slitting the 40-inch roll down. Telescoping can have an impact on roll-to-roll transitions on the conversion equipment causing downtime. For this trial conversion this had no impact on the conversion process as only one roll was converted at a time and roll to roll continuity was not needed.

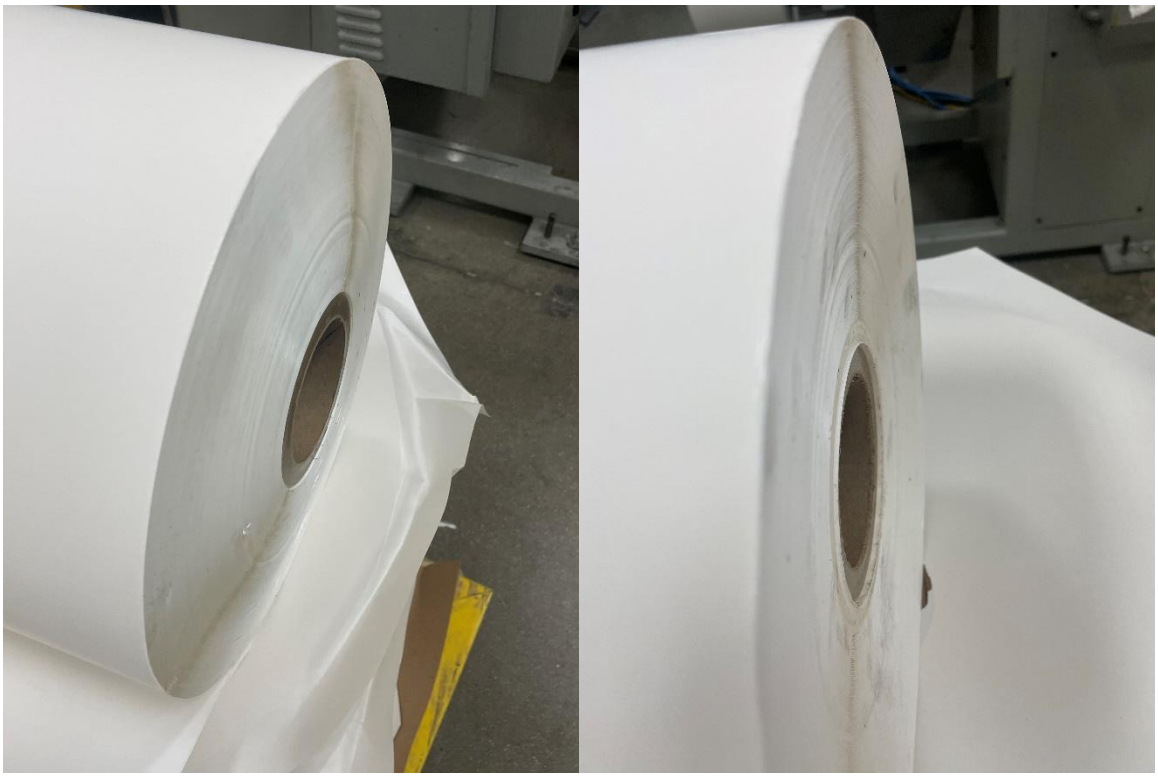

Figure 3.31 Photography images of 10-inch film rolls produced displaying telescoping defect (Left) and no telescoping (Right)

The next issue that arose was also due to problems with the 10-inch rolls. The face film with the adhesive coated widened causing the face film to overhang past the edge of the silicon backing paper (Figure 3.32). This caused the adhesive to be exposed which means it would interact with the various machine parts as it was processed through the conversion line. More importantly, it caused each layer of the rolled film to stick to each other causing difficulty when unwinding the rolls to run the film through the process. At normal processing speed, ~300 ft/min, the increased friction between the layers due to the adhesive caused the film to rip. To address this issue, the conversion equipment was significantly slowed to 100ft/min which allowed for the film to be converted into labels. It is suspected that this adhesive exposure and film expansion was due to improper

tension control during slitting at the coater. This would need to be corrected prior to commercialization of this product.

Figure 3.32 Photography images of produced film showing the expansion of the face film and the exposed adhesive (Left), and the layer-to-layer adhesion due to this defect on the unwinder.

Conversion then was completed on one roll of each of the two adhesive coat weights. After dialing in the machine settings no issues were seen with printing, dye cutting, or matrix released. The only issue seen during conversion on press was after the production of the non-adhesive release tab. This process includes physical brushing on the surface of the label (Figure 3.33). During this brushing, labels were being removed from the silicon backing paper causing the gradual buildup of labels and also blank spots within the label rolls. This problem is due to the low release values for this adhesive from the silicon release liner. Typical release values for materials that undergo the tabbing process are ~50 g/50mm while the two samples run had release values of 13.32 g/50mm

and 14.14 g/50mm. These values can be altered by changing the amount of silicon within the release paper and therefore changing the amount of adhesion to the backing paper. This is something that must be addressed at the next coating trial.

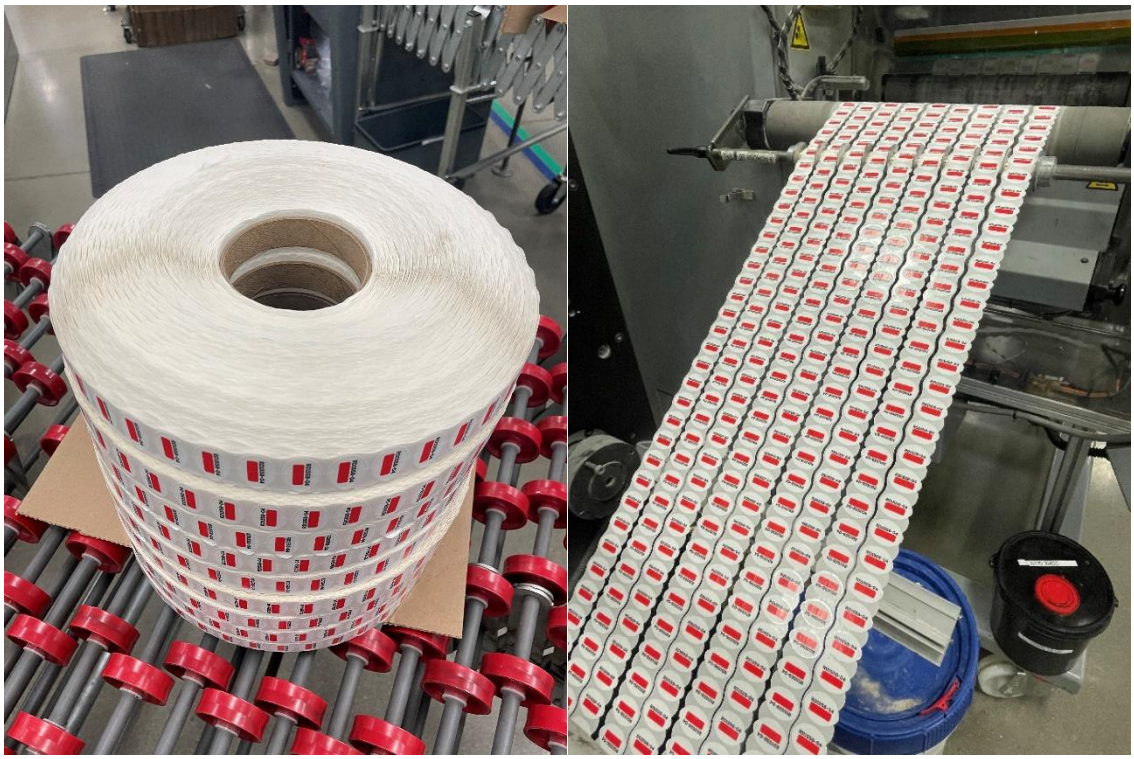

Figure 3.33 Photography images of the converted label rolls produced on the printing and dye cutting press (left) and the run of labels prior to winding on the press (right).

Overall, conversion on the press was successful in producing rolls of adhesive labels for both coat weights. These rolls were then tested using internal quality measurements to assess the printing process and also the label release using an automated labeling machine. The internal printing process check, a trade secret method, was found to be acceptable. During the label release testing, which consists of continually feeding labels through the automated labeling machine for 60 seconds found some issues with label release (Figure 3.34). Using a combination of suction and air pressure baffles grab onto a label and then deliver it to the target where it is applied. During this testing it was

seen that labels would randomly not be properly gripped by the suctioned baffle and would be sent airborne. This is potentially linked to the adhesive's low release values from the silicone release backer. This would need to be addressed prior to field trials.

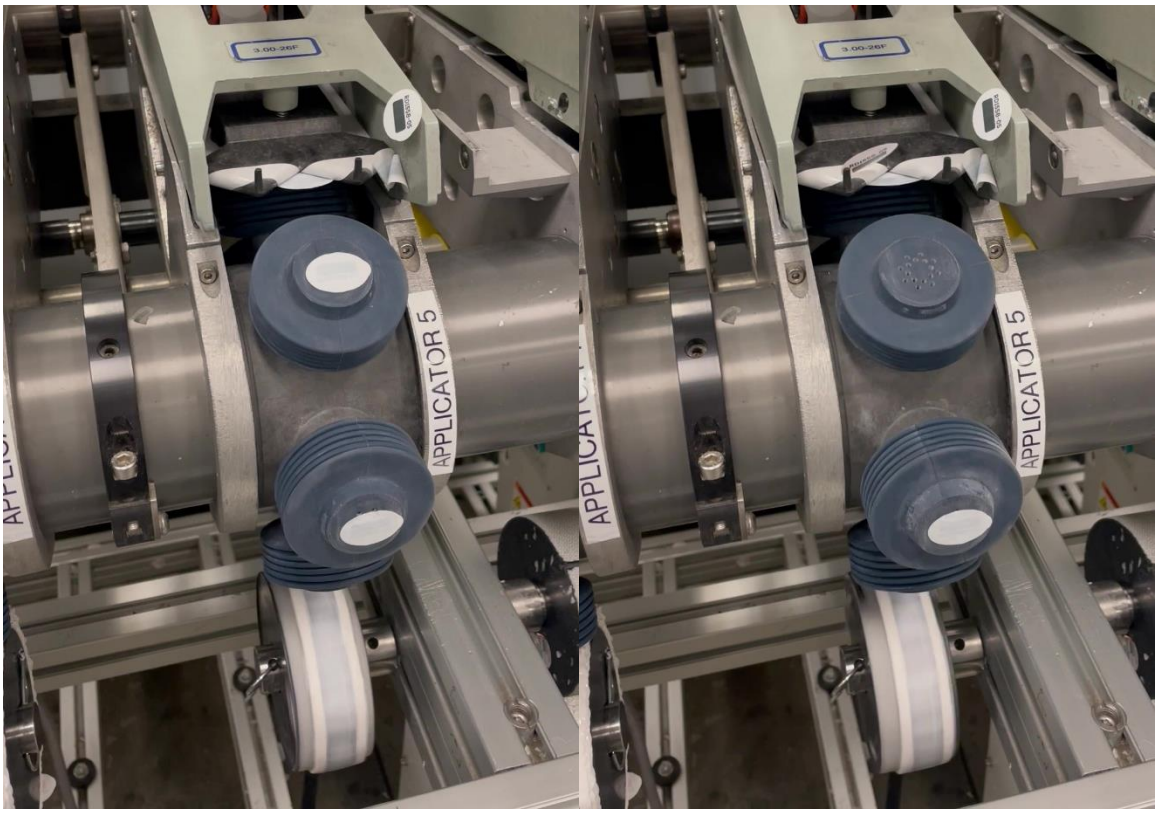

Figure 3.34 Photography images of automated labeling machine showing correct release of the label from the backer onto the baffle (left) and failure to correctly dispense labels onto the baffle (right).

Following this in lab testing, adhesive testing was completed using a pilot labeling machine and various substrates. It is important to use a pilot machine to sticker the test samples to ensure the labels are under the sample type of pressure and conditions as they would be within a packing facility. Each item was labeled ten times and scored using an internal scoring system. The items were scored at the time of labeling, and then placed into a refrigerator and scored at times 1 hour, 1 day, 1 week, and 2 weeks. This

system scores the labels lay onto the applied surface with a lower number being a more uniform label coverage. A completely conforming label would get a value of 1. A poorly adhered label would have a taco like shape where the label begins to curve away from the substrate and would be scored a value of 5. Between these two values are levels of label debonding as described in Figure 3.35. A total debonding of the label would get heavily penalized with a score of 10. A desired score would be an average of 1.5 or lower.

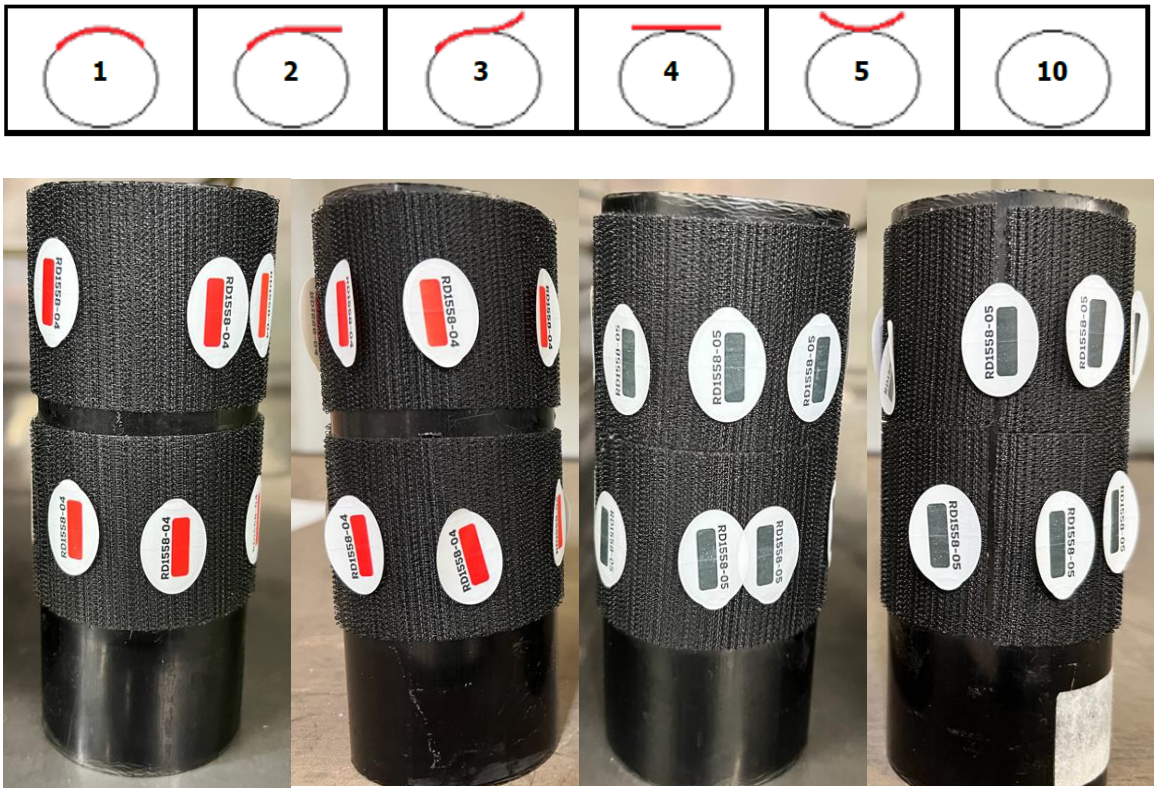

Figure 3.35 Scoring criteria for the on produce and Velcro tested showing progressive label debonding states (top). Photography images of Velcro test samples at day 0 (A) and day 14 (B) for the low coat weight sample and day 0 (C) and day 14 (D) for the high coat weight sample.

One of the in-house tests that helps to simulate difficult to label items used a PVC pipe covered in Velcro. The labels were attached to the Velcro tube using the automated labeler and measured using an internal scoring system. Both coat weights were tested

using the Velcro test and measured at time of application, 1 hour, 1 day, 1 week and 2 weeks (Table). Initially the high coat weight labels scored a moderate score of 1.4 while the low coat weight samples scored a 2.0. At the one-hour measurement time, both labels were more adhered to the Velcro with high coat weight coming in at 1.1 and the low coat weight at 1.0 (Table 3.5). Unfortunately, this level of adhesion did not last as it dropped to a score of 4.0 for the high coat weight and a 2.9 for the low coat weight at one day. These values demonstrate that the adhesive does not have the adhesive strength to maintain contact with the small surface area of the Velcro.

Table 3.5 Scoring values for the Velcro test for high and low coat weight adhesive labels over a 2-week period with samples house in refrigerated temperatures.

Time	0	1 Hour	1 Day	1 Week	2 Weeks
High Coat Weight	1.4	1.1	4	5.5	5.5
Low Coat Weight	2	1	2.9	4	4

In addition to the Velcro test, produce was also labeled with both coat weights using the automated labeling machine. The produce labeled were navel oranges, honey crisp apples, Hass avocado, Roma tomato, SunGold kiwi, green kiwi, yellow nectarine, and white peaches (Table 3.6). The two types of kiwis were chosen as hard to label produce items with green kiwi having a fury/hairy surface and the SunGold kiwi having a rusted surface. The two types of stone fruit were also chosen as hard to label produce items including the hairy white peach and the rusted yellow nectarine. The produce items were scored using the same system as described above.

Table 3.6 High and low coat weight label adherence scoring values on different produce items over 2 weeks in a refrigerated environment.

Low Coat Weight					
Time	0	1 Hour	1 Day	1 Week	2 Weeks
Navel Orange	1	1	1	1	1
Honey Crisp Apple	1	1	1	1	1
Hass Avocado	1	1	1	1	1
Roma Tomato	1	1	1	1	1.1
SunGold Kiwi	1.4	1.4	1.5	2.6	1.7
Green Kiwi	1.4	1.4	1.9	3.8	3.4
Yellow Nectarine	1.1	1.1	1.1	1.1	1.1
White Peach	2.3	2.1	1.5	2	2.4
High Coat Weight					
Time	0	1 Hour	1 Day	1 Week	2 Weeks
Navel Orange	1	1	1	1	1
Honey Crisp Apple	1	1	1	1	1
Hass Avocado	1	1	1	1.1	1.3
Roma Tomato	1	1	1	1	1.1
SunGold Kiwi	1.3	1.3	1.5	1.9	1.9
Green Kiwi	1.4	1.6	1.9	3.1	3.4
Yellow Nectarine	1.2	1.2	1.2	1.2	1.5
White Peach	1.6	1.7	2	3.3	3.1

The navel oranges, honey crisp apples, Hass avocados, Roma tomatoes, and yellow nectarines all met the internal specification of a score of 1.5 or less with both coat weight labels. The difficulty labeling white peaches was immediately apparent with the initial scoring being much lower than any other produce item. The combination of the soft skin and hairy texture made labeling the white peaches difficult. The second most difficult item to label with this adhesive was the green kiwi. This shows a trend of hairy produce items being difficult to adhere to. This also gets worse over time with the labels

slowly lifting off the surface of the fruit. From an adhesive perspective this indicates that both the instant tack and the setting adhesion strength is not high enough for these substrates.

A final test was completed with the honey crisp apples to test the ability of the adhesive to maintain adhesion upon submersion into an ice bath immediately upon labeling. This simulates the process at some produce packing facilities where the produce is labeled and immediately dunked into ice cold water for cleaning and sanitary reasons. The apples were labeled using the automated labeling machine and immediately scored (Figure 3.36). The apples were then placed into a bucket of ice for 20 minutes with the bucket being stirred once at 10 minutes. Both coat weights passed this test with no change in the label performance after the water bath test.

Figure 3.36 Photography images of apples with applied high and low coat weight labels to apples after ice bath test.

The rolls of adhesive coated film were successfully converted into labels using a commercial printing and dye cutting press. These labels were then applied to various produce and test items using an automated labeling machine. The ability of the adhesive to adhere to different surfaces was scored using an internal test method. Issues that arose during the conversion of the labels include the expansion of the face film after slitting of the original 40-inch roll into 10 inch rolls. Additionally, the low release values of the adhesive from the silicone release backer caused issues with conversion of labels with non-adhesive tabs. The application of the labels onto hairy and other hard to label produce items proved to be a challenge for this adhesive and will require additional work to improve the tack and adhesion values for future trials.

Conclusion

A pressure sensitive adhesive for the application as a produce label was produced through the application of synthetic techniques. The material was properties including strength of adhesion, viscoelasticity and thermal transitions were tailored for the application needs. The polymer was scaled to a pilot scale reactor showing considerable robustness in the synthetic process and overall material properties. The produced material was then applied in an industrial hot melt coating trail to produce three-layer adhesive rolls. These rolls were then converted into labels using a commercial printing and dye cutting press. The labels were then applied to produce and other test surfaces via an automated labeling machine and then scored for adhesive effectiveness.

References

(1) Garcia-Garcia, D.; Crespo-Amoros, J. E.; Parres, F.; Samper, M. D. Influence of Ultraviolet Radiation Exposure Time on Styrene-Ethylene-Butadiene-Styrene (SEBS) Copolymer. *Polymers* **2020**, *12* (4). DOI: 10.3390/polym12040862.

(2) Mallegol, J.; Dupont, O.; Keddie, J. L. Morphology and elasticity of waterborne acrylic pressure-sensitive adhesives investigated, with atomic force microscopy. *Journal of Adhesion Science and Technology* **2003**, *17* (2), 243-259. DOI: 10.1163/156856103762302023.

(3) Grove, G.; Houser, T.; Dove, J.; Moody, D. An objective comparison of two pulse oximetry sensors with different adhesive systems on healthy human volunteers based on biophysical assessments. *Skin Research and Technology* **2023**, *29* (1). DOI: 10.1111/srt.13212.

(4) Baek, S. S.; Jang, S. J.; Hwang, S. H. The Preparation and Adhesion Performances of Transparent Acrylic Pressure Sensitive Adhesives Containing Acrylamide Monomer for Optical Applications. *Elastomers and Composites* **2016**, *51* (3), 181-187. DOI: 10.7473/ec.2016.51.3.181.

(5) Johnsen, I. H.; Andenws, E.; Gullbrekken, L.; Kvande, T. Vapour resistance of wind barrier tape: Laboratory measurements and hygrothermal performance implications. *Journal of Building Physics* **2022**, *46* (1), 923-940. DOI: 10.1177/17442591211057188.

(6) Park, Y.; Byun, H.; Lee, J. H. Highly Stretchable and Transparent Optical Adhesive Films Using Hierarchically Structured Rigid-Flexible Dual-Stiffness Nanoparticles. *Acs Applied Materials & Interfaces* **2021**, *13* (1), 1493-1502. DOI: 10.1021/acsami.0c18488.

(7) Sundriyal, P.; Pandey, M.; Bhattacharya, S. Plasma-assisted surface alteration of industrial polymers for improved adhesive bonding. *International Journal of Adhesion and Adhesives* **2020**, *101*. DOI: 10.1016/j.ijadhadh.2020.102626.

(8) Antosik, A. K.; Bednarczyk, P.; Czech, Z. Aging of silicone pressure-sensitive adhesives. *Polymer Bulletin* **2018**, *75* (3), 1141-1147. DOI: 10.1007/s00289-017-2083-2.

(9) Droesbeke, M. A.; Aksakal, R.; Simula, A.; Asua, J. M.; Du Prez, F. E. Biobased acrylic pressure-sensitive adhesives. *Progress in Polymer Science* **2021**, *117*. DOI: 10.1016/j.progpolymsci.2021.101396.

(10) Czech, Z.; Pelech, R.; Kowalczyk, A.; Kowalski, A.; Wrobel, R. J. Electrically conductive acrylic pressure-sensitive adhesives containing carbon black. *Polish Journal of Chemical Technology* **2011**, *13* (4), 77-81. DOI: 10.2478/v10026-011-0053-2.

(11) Khan, I.; Poh, B. T. Natural Rubber-Based Pressure-Sensitive Adhesives: A Review. *Journal of Polymers and the Environment* **2011**, *19* (3), 793-811. DOI: 10.1007/s10924-011-0299-z.

(12) Lin, S. B.; Durfee, L. D.; Ekeland, R. A.; McVie, J.; Schalau, G. K. Recent advances in silicone pressure-sensitive adhesives. *Journal of Adhesion Science and Technology* **2007**, *21* (7), 605-623. DOI: 10.1163/156856107781192274.

(13) Webster, I. Recent developments in pressure-sensitive adhesives for medical applications. *International Journal of Adhesion and Adhesives* **1997**, *17* (1), 69-73. DOI: 10.1016/s0143-7496(96)00024-3.

(14) Schneiderman, D. K.; Hillmyer, M. A. 50th Anniversary Perspective: There Is a Great Future in Sustainable Polymers. *Macromolecules* **2017**, *50* (10), 3733-3749. DOI: 10.1021/acs.macromol.7b00293.

(15) Barnes, D. K. A.; Galgani, F.; Thompson, R. C.; Barlaz, M. Accumulation and fragmentation of plastic debris in global environments. *Philosophical Transactions of the Royal Society B-Biological Sciences* **2009**, *364* (1526), 1985-1998. DOI: 10.1098/rstb.2008.0205.

(16) Narayan, R. Biobased & Biodegradable Plastics: Rationale, Drivers, and Technology Exemplars. In *Degradable Polymers and Materials: Principles and Practice*, Khemani, K., Scholz, C. Eds.; ACS Symposium Series, Vol. 1114; 2012; pp 13-31.

(17) Narancic, T.; Verstichel, S.; Chaganti, S. R.; Morales-Gamez, L.; Kenny, S. T.; De Wilde, B.; Padamati, R. B.; O'Connor, K. E. Biodegradable Plastic Blends Create New Possibilities for End-of-Life Management of Plastics but They Are Not a Panacea for Plastic Pollution. *Environmental Science & Technology* **2018**, *52* (18), 10441-10452. DOI: 10.1021/acs.est.8b02963.

(18) Yang, Y.; Wang, J. L.; Xia, M. L. Biodegradation and mineralization of polystyrene by plastic-eating superworms Zophobas atratus. *Science of the Total Environment* **2020**, *708*. DOI: 10.1016/j.scitotenv.2019.135233.

(19) Taniguchi, I.; Yoshida, S.; Hiraga, K.; Miyamoto, K.; Kimura, Y.; Oda, K. Biodegradation of PET: Current Status and Application Aspects. *ACS Catalysis* **2019**, *9* (5), 4089-4105. DOI: 10.1021/acscatal.8b05171.

(20) Bartkowiak, M.; Czech, Z.; Kim, H. J.; Shim, G. S.; Nowak, M.; Antosik, A. K. Photoreactive UV-Crosslinkable Acrylic Pressure-Sensitive Adhesives (PSA) Containing Multifunctional Photoinitiators. *Polymers* **2021**, *13* (24). DOI: 10.3390/polym13244413.

(21) Creton, C. Pressure-sensitive adhesives: An introductory course. *Mrs Bulletin* **2003**, *28* (6), 434-439. DOI: 10.1557/mrs2003.124.

(22) Czech, Z.; Pelech, R. Thermal decomposition of polyurethane pressure-sensitive adhesives dispersions. *Progress in Organic Coatings* **2010**, *67* (1), 72-+. DOI: 10.1016/j.porgcoat.2009.09.019.

(23) Basile, A.; Greco, F.; Mader, A.; Carra, S.; D'Amore, A. Viscoelastic behaviour of water-based pressure sensitive adhesives (PSAs). *Plastics Rubber and Composites* **2003**, *32* (8-9), 340-344. DOI: 10.1179/146580103225004108.

(24) Hufendiek, A.; Lingier, S.; Du Prez, F. E. Thermoplastic polyacetals: chemistry from the past for a sustainable future? *Polymer Chemistry* **2019**, *10* (1), 9-33, 10.1039/C8PY01219A. DOI: 10.1039/C8PY01219A.

(25) Zink, T.; Geyer, R.; Startz, R. Toward Estimating Displaced Primary Production from Recycling A Case Study of US Aluminum. *Journal of Industrial Ecology* **2018**, *22* (2), 314-326. DOI: 10.1111/jiec.12557.

(26) Tasho, R. P.; Cho, J. Y. Veterinary antibiotics in animal waste, its distribution in soil and uptake by plants: A review. *Science of the Total Environment* **2016**, *563*, 366-376. DOI: 10.1016/j.scitotenv.2016.04.140.

(27) Mistry, A. N.; Kachenchart, B.; Pinyakong, O.; Assavalapsakul, W.; Jitpraphai, S. M.; Somwangthanaroj, A.; Luepromchai, E. Bioaugmentation with a defined bacterial

consortium: A key to degrade high molecular weight polylactic acid during traditional composting. *Bioresource Technology* **2023**, *367*. DOI: 10.1016/j.biortech.2022.128237.

(28) Mulchandani, N.; Narayan, R. Redesigning Carbon-Carbon Backbone Polymers for Biodegradability-Compostability at the End-of-Life Stage. *Molecules* **2023**, *28* (9). DOI: 10.3390/molecules28093832.

(29) Geyer, R.; Jambeck, J. R.; Law, K. L. Production, use, and fate of all plastics ever made. *Science Advances* **2017**, *3* (7). DOI: 10.1126/sciadv.1700782.

(30) Samir, A.; Ashour, F. H.; Hakim, A. A. A.; Bassyouni, M. Recent advances in biodegradable polymers for sustainable applications. *npj Materials Degradation* **2022**, *6* (1), 68. DOI: 10.1038/s41529-022-00277-7.

(31) Law, K. L.; Narayan, R. Reducing environmental plastic pollution by designing polymer materials for managed end-of-life. *Nature Reviews Materials* **2022**, *7* (2), 104-116. DOI: 10.1038/s41578-021-00382-0.

(32) Wang, H. Y.; Li, H. J.; Zhao, Y. F.; Xi, N. N. Being natural is aesthetic: the effects of "natural" labeling on lay beliefs and the purchase intention of unattractive produce. *Asia Pacific Journal of Marketing and Logistics* **2023**, *35* (7), 1759-1773. DOI: 10.1108/apjml-04-2022-0316.

(33) Chen, X. Q.; Gao, Z. F.; Swisher, M.; House, L.; Zhao, X. Eco-labeling in the Fresh Produce Market: Not All Environmentally Friendly Labels Are Equally Valued. *Ecological Economics* **2018**, *154*, 201-210. DOI: 10.1016/j.ecolecon.2018.07.014.

(34) Ulloa, R.; Villalobos, J. R. Impact of special-denomination label constraints on fresh produce supply chains. *Computers & Industrial Engineering* **2022**, *173*. DOI: 10.1016/j.cie.2022.108742.

(35) Bond, C. A.; Thilmany, D. D.; Bond, J. K. What to Choose? The Value of Label Claims to Fresh Produce Consumers. *Journal of Agricultural and Resource Economics* **2008**, *33* (3), 402-427.

CHAPTER 4

Outlook

Conclusion

This dissertation details the targeting of compostable materials through the application of different synthetic techniques to make functional polymeric materials. The production of an enzymatic degradation assay that uses a high throughput methodology was applied to polyester polyurethanes. This fluorescence assay was used as a guiding tool for the synthesis of crosslinked polyurethanes using three different biobased crosslinkers. The assay was applied to measuring the impact of crosslinker content and isocyanate indexing on the overall polymer's enzymatic degradability. These materials were then tested under industrial composting conditions, elucidating the types of crosslinker that can block biodegradation.

A home compostable pressure sensitive adhesive was also described within this dissertation. The novel adhesive was developed with the express need for a home compostable adhesive to be used in produce labeling applications. Using different synthetic techniques, the complex material requirements that accompany adhesives were navigated. The delicate balance between adhesive and cohesive failure was modulated through addition of crosslinking reactions. The produced pressure sensitive adhesive was scaled to a pilot reactor, coated on an industrial coating line, and converted into fruit labels for on produce testing.

Future Work

The fluorescence assay showed good correlation between the level of enzymatic degradation measured and the biodegradation values determined through respirometry analysis. Additional work is needed to find an enzyme cocktail that appropriately mimics the biodiversity found within composting conditions, but also to mimic other biomes where plastic degradation occurs. The fluorescence assay was applied to polyester polyurethanes, but additional chemical architectures could be tested and measured for enzymatic degradation.

The pressure sensitive adhesive was shown to have moderate natural tack and good cohesion. There are various applications for pressure sensitive adhesives where the produce material could be applied. Some material properties need to be improved depending on application and coating technology such as tack, viscosity, and degradation. Additional work is needed to move this product from the lab bench into the commercial pipeline.

Final Remarks

This work contributes to the advancement of biodegradable polymers and specifically addresses the need for additional synthetic techniques towards biobased and biodegradable polymers. The research completed has elucidated important facets of producing biodegradable materials.

Appendix

Supporting Information for Synthetically Targeting Compostability as the End-Of-Life Fate for Polymeric Materials

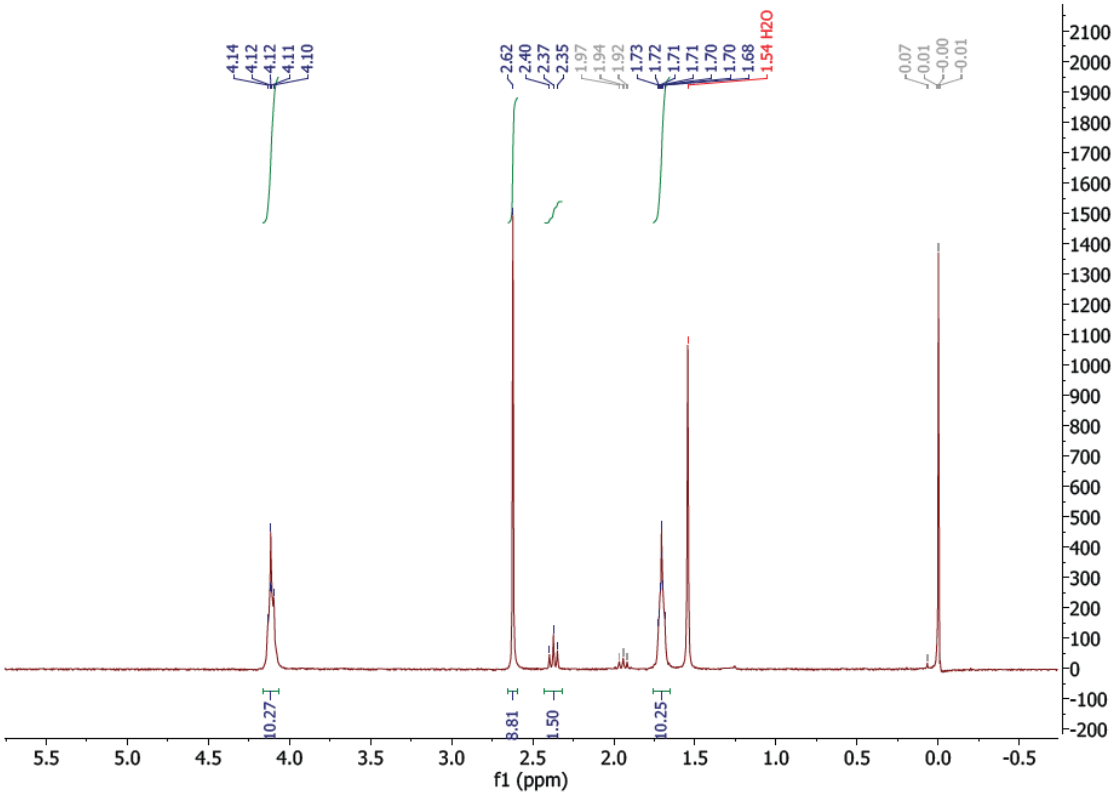

Figure A.1 ^{1}H NMR spectrum of poly(butylene glutarate-co-butylene succinate) 15:85.

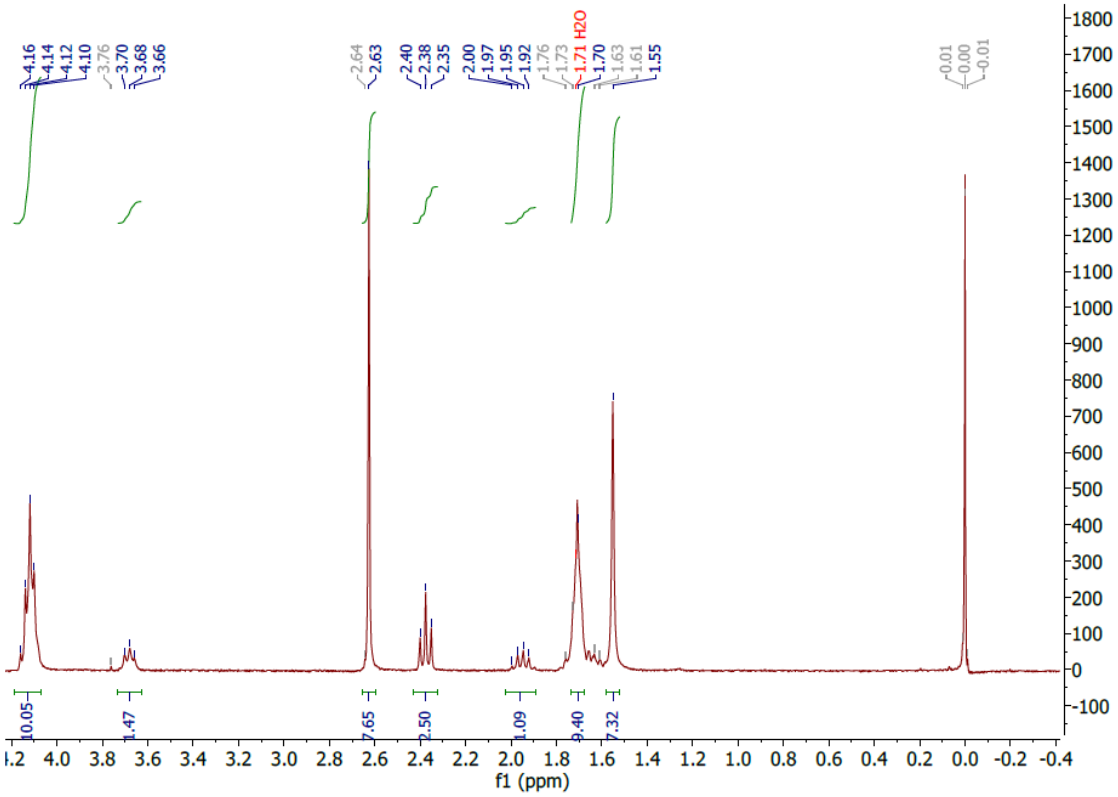

Figure A.2 ^{1}H NMR spectrum of poly(butylene glutarate-co-butylene succinate) 25:75.

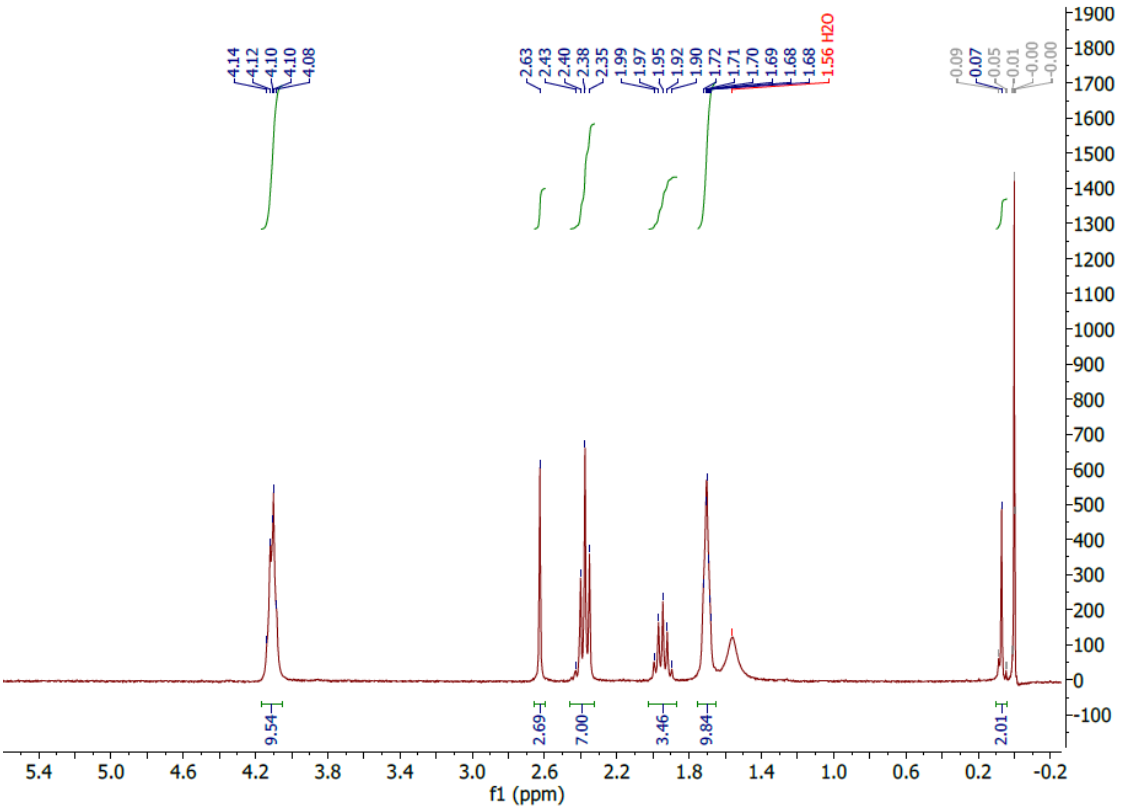

Figure A.3 ^{1}H NMR spectrum of poly(butylene glutarate-co-butylene succinate) 50:50.

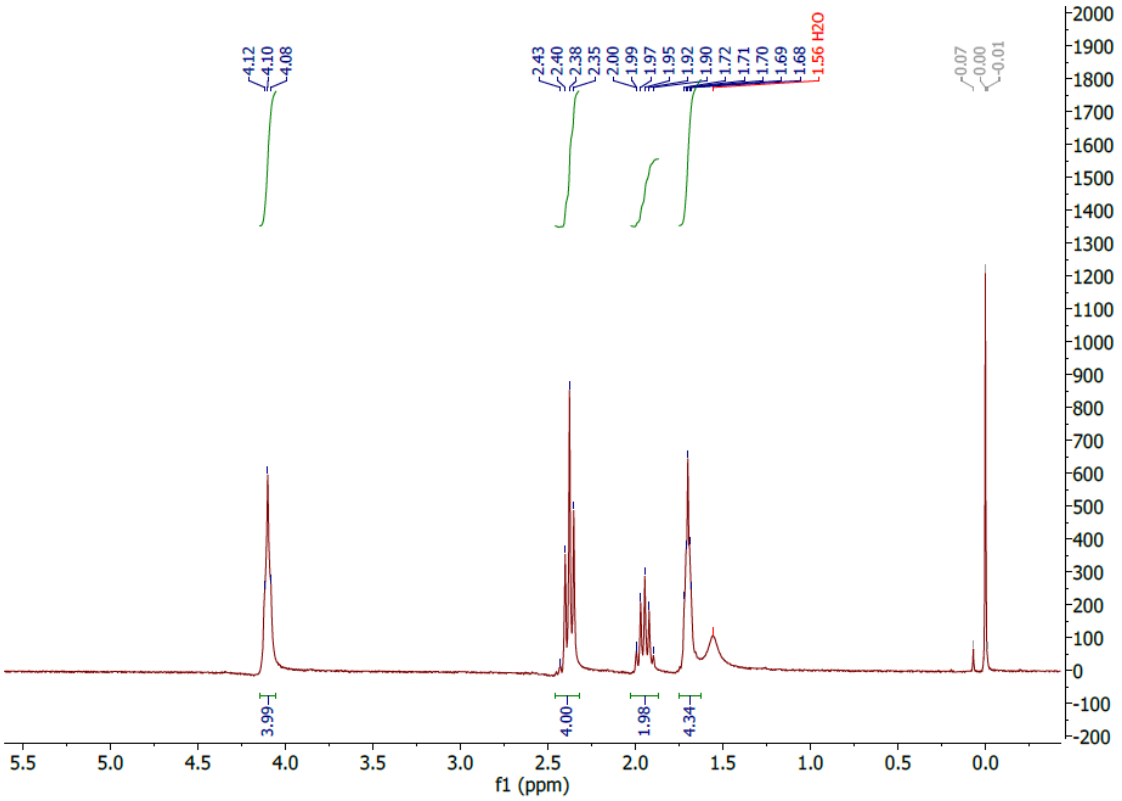

Figure A.4 ^{1}H NMR spectrum of poly(butylene glutarate-co-butylene succinate) 70:30.